

# Isolation and Characterisation of Toxic Secondary Metabolites Produced by Black Mould

by

Daniel Hudson



A thesis

submitted to Victoria University of Wellington

in fulfilment of the requirements for the degree of

Master of Science

Victoria University of Wellington

Te Whare Wānanga o te Ūpoko o te Ika a Māui

2019

## Copyright

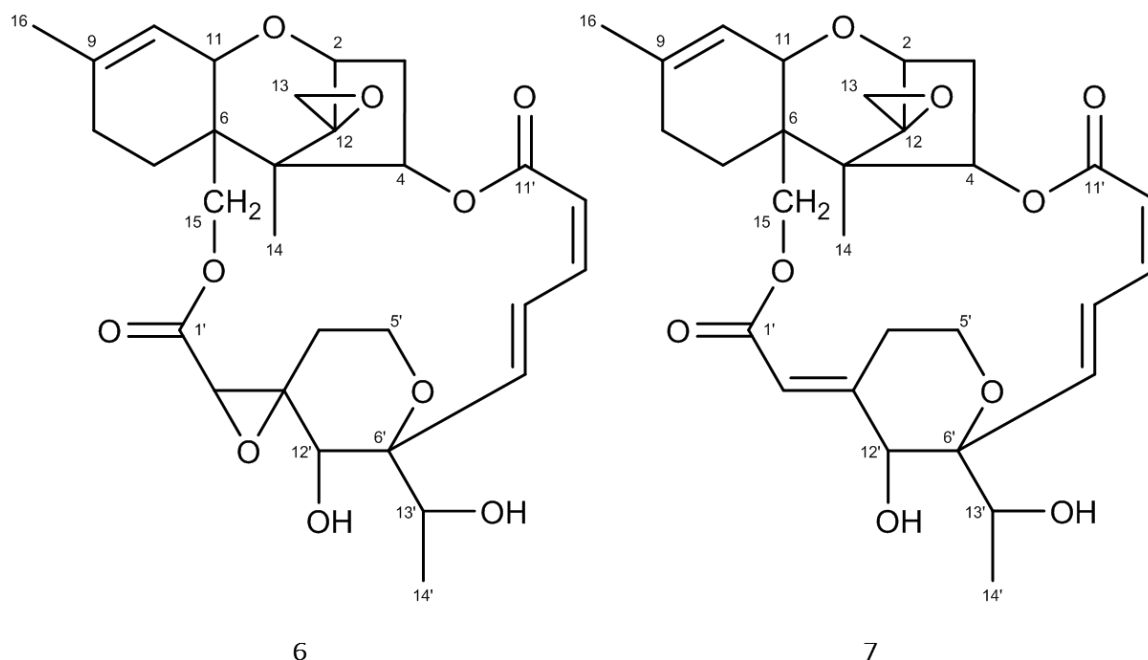
The copyright of this thesis resides with the author. The work in this thesis was completed by the author at the Ferrier Research institute, Victoria University of Wellington in conjunction with the Integrated Biotechnology Group, Callaghan Innovation. No portion of this work has been reported previously excepting:

1. “*Stachybotrys chartarum* toxins and their impact on human health”, authors (Daniel Hudson, Caroline Shorter, Michael Sulyok, Julian Crane, and Simon Hinkley), poster presentation for ACS Southwest Regional Meeting, 30<sup>th</sup> October 2017
2. “Spectral data and re-characterisation of the Satratoxins G and H”, authors (Daniel Hudson, Ameet Jonathan Singh, Andrew Lewis, Michael Sulyok, and Simon Hinkley), article in preparation for *Mag. Res. Chem.*

## Abstract

Microbial secondary metabolites, commonly called natural products, have been crucial for the progression of modern medicine. Not essential for the basic functions of life, secondary metabolites are instead produced to provide a competitive advantage in the environment. The method of action is commonly toxicity to other species in their environment, thereby harming or killing the competition. These toxic properties have allowed them to be utilised as antimicrobial and antitumor agents, however this same toxicity is able to cause detrimental health effects in humans causing symptoms ranging from minor to life threatening.

The black mould *Stachybotrys chartarum* is capable of producing very toxic secondary metabolites called macrocyclic trichothecenes. Satratoxin G (**6**) and H (**7**), are two of the most toxic naturally occurring compounds in the world. This has made *S. chartarum* a common target when adverse health has been associated with damp and mouldy dwellings. However, there is very little evidence for this link beyond its ubiquity and ability to produce the aforementioned highly toxic macrocyclic trichothecenes.



This research investigates *S. chartarum* and the toxic secondary metabolites it produces, with special emphasis on satratoxin G and H. Different culturing methods and resulting

morphology are assessed. The satratoxins were isolated from crude extracts and full characterisation by 1-D and 2-D NMR spectroscopy was done. This process revealed differences from the accepted literature, and spectra are reported herein to aid in future identification. The importance of genetics and the public health implications of mould contamination are also discussed.

## Acknowledgments

First and foremost, I would like to thank my supervisor, Simon Hinkley, for his continued support, guidance, and encouragement during my project and beyond. Thank you, Simon, for taking a chance on a biologist that wanted to dip his toes into the world of natural products chemistry and chemical biology.

Throughout my time at VUW I have enjoyed the privilege of meeting many great people who were instrumental to my success. Thank you to all the staff and students of the Ferrier Research Institute, School of Biological Sciences, and School of Chemical and Physical Sciences. In particular I must thank Jonathan Singh for all of your help with this thesis.

Thank you to all of my friends and family who helped me to get through the tough times of postgraduate study. Thank you especially to my wife Zoe Psarouthakis; you were always happy to read a new section and provide the level of feedback that I asked for.

Finally, I have to thank Benjamin Hudson, you have been the best friend anybody could ever have.

# Table of Contents

Copyright.....	ii
Abstract .....	iii
Acknowledgments .....	v
Table of Contents .....	vi
List of Figures .....	ix
List of Tables .....	xiii
Glossary .....	xiv
1. Introduction.....	1
1.1 History of Natural Products .....	1
1.2 Toxic Natural Products .....	3
1.3 Respiratory Health.....	4
1.4 <i>Stachybotrys chartarum</i> .....	5
1.4.1 Species Status .....	7
1.5 <i>Stachybotrys chartarum</i> Secondary Metabolites .....	8
1.5.1 Isolation .....	8
1.5.2 Characterisation.....	9
1.5.3 Genetics.....	10
1.6 Research Aims .....	11
2. Cultures and Isolation .....	12
2.1 <i>Stachybotrys chartarum</i> Environments.....	12
2.2 Culture Characteristics .....	14
2.3 Crude Extracts .....	17
2.4 Mass Spectrometry Analysis .....	18

2.5	Genetic Information .....	19
2.6	Metabolite Isolation .....	20
2.7	Fraction Purity .....	22
2.8	Summary .....	27
3.	NMR Characterisation.....	28
3.1	Introduction .....	28
3.2	Satratoxin G .....	29
3.3	Satratoxin H .....	40
3.4	Comparison with Literature .....	51
3.5	Related Structures.....	57
4.	Conclusion .....	59
5.	Experimental .....	61
5.1	General Experimental .....	61
5.1.1	NMR Analysis .....	61
5.1.2	Chromatography.....	61
5.2	<i>Stachybotrys chartarum</i> Strains .....	63
5.2.1	Cultures .....	63
5.2.2	Extraction of Metabolites.....	63
5.3	Purification of the Satratoxins .....	64
5.3.1	Satratoxin G.....	64
5.3.2	Satratoxin H.....	64
5.4	Genetic Analysis .....	64
5.4.1	PCR Primers.....	65
5.4.2	Analysis.....	65
	References .....	66

Appendix A	Satratoxin G NMR Data.....	73
Appendix B	Satratoxin H NMR Data.....	83



## List of Figures

Figure 1 - Structures of salicin (1), acetylsalicylic acid (2), quinine (3), and paclitaxel (4)....	2
Figure 2 - Structure of penicillin G (5) .....	3
Figure 3 - Trichothecene core.....	6
Figure 4 - Trichothecene subtypes .....	6
Figure 5 - Structures of satratoxin G (6) and satratoxin H (7) .....	8
Figure 6 - Basic principles of chromatography separation .....	9
Figure 7 - Unidentified black mould growing in a New Zealand Home .....	13
Figure 8 - Black mould growing on the backside of water damaged gypsum wall board, identified as <i>Stachybotrys chartarum</i> . Reproduced from Nelson (2001).....	13
Figure 9 - Colony characteristics of ICMP <i>Stachybotrys chartarum</i> strains.....	15
Figure 10 - ICMP <i>Stachybotrys chartarum</i> strains growing on parboiled rice.....	16
Figure 11 - A) rice cultures soaking in extraction solvent, B) concentrated crude extract	17
Figure 12 - A) original data from Hinkley, B) chromatogram generated by HPLC showing the presence of satratoxins in a crude <i>Stachybotrys chartarum</i> extract .....	18
Figure 13 - Simplified flowchart for method of satratoxin isolation, steps 3-5 can be repeated until a pure fraction is achieved .....	21
Figure 14 - TLC analysis of fractions taken during a flash chromatography separation of a semipurified crude extract sample, the solvent system in use is 30% PE in EtOAc .....	22
Figure 15 - A) A TLC plate that has been purified to the stage of containing only the satratoxins B) a TLC plate of four fractions, the first of which appears to be a pure isolate of satratoxin G as indicated by the standard running in the left most lane. The solvent system in use is 5% MeOH in DCM .....	23
Figure 16 - HPLC assessment of purity for two different fractions. Fraction 1 containing satratoxin H. Fraction 2 containing satratoxin G. In both of these fractions there is a small amount of contamination of the other satratoxin .....	23

Figure 17 - HPLC assessment of two fractions that were found to be pure and subsequently used for LCMS. Note that the RT is different from figure 10 due to these samples being run at a lower flow rate .....	24
Figure 18 - Satratoxin G LCMS data, providing chromatography and mass spectral data .	25
Figure 19 - Satratoxin H LCMS data, providing chromatography and mass spectral data .	26
Figure 20 - The tricyclic 12,13-epoxytrichothene-9-ene structure that forms the core of every trichothecene.....	28
Figure 21 - Type D trichothecenes contain a macrocyclic ring from C-4 to C-15.....	28
Figure 22 - Legend for how correlation types are represented in substructure figures ....	29
Figure 23 - COSY and HMBC correlations establishing substructure 1 of satratoxin G .....	30
Figure 24 - COSY and HMBC correlations establishing substructure 2 of satratoxin G .....	31
Figure 25 - COSY and HMBC correlations establishing substructure 3 of satratoxin G .....	31
Figure 26 - COSY and HMBC correlations establishing substructure 4 of satratoxin G .....	32
Figure 27 - COSY and HMBC correlations establishing substructure 5 of satratoxin G .....	33
Figure 28 - COSY and HMBC correlations establishing substructure 6 of satratoxin G .....	33
Figure 29 - COSY and HMBC correlations establishing substructure 7 of satratoxin G .....	34
Figure 30 - A) HMBC correlations between substructures 1-4 and isolated carbon moieties that establish the connectivity between them to form the trichothecene core of satratoxin G, B) Substructures 1-4 and isolated carbon moieties organised into the trichothecene core of satratoxin G .....	35
Figure 31 - A) HMBC correlations between substructures 5-7 and isolated carbon moieties that establish the connectivity between them to form the macrocyclic ring of satratoxin G. B) Substructures 5-7 and isolated carbon moieties organised into the macrocyclic ring of satratoxin G.....	36
Figure 32 - The completed satratoxin G structure with the HMBC correlations that link the trichothecene core and the macrocyclic ring .....	37
Figure 33 - COSY and HMBC correlations establishing substructure 1 of satratoxin H .....	41

Figure 34 - COSY and HMBC correlations establishing substructure 2 of satratoxin H .....	42
Figure 35 - COSY and HMBC correlations establishing substructure 3 of satratoxin H .....	42
Figure 35 - COSY and HMBC correlations establishing substructure 4 of satratoxin H .....	43
Figure 37 - COSY and HMBC correlations establishing substructure 5 of satratoxin H .....	44
Figure 38 - COSY and HMBC correlations establishing substructure 6 of satratoxin H .....	44
Figure 39 - COSY and HMBC correlations establishing substructure 7 of satratoxin H .....	45
Figure 40 - A) HMBC correlations between substructures 1-3 and isolated carbon moieties that establish the connectivity between them to form the trichothecene core of satratoxin G, B) Substructures 1-4 and isolated carbon moieties organised into the trichothecene core of satratoxin H .....	46
Figure 41 - A) HMBC correlations between substructures 4-6 and isolated carbon moieties that establish the connectivity between them to form the macrocyclic ring of satratoxin H. B) Substructures 4-6 and isolated carbon moieties organised into the macrocyclic ring of satratoxin H.....	47
Figure 42 - The completed satratoxin H structure with the HMBC correlation that link the trichothecene core and the macrocyclic ring .....	48
Figure 43 - Crystal structure obtained by Li, Y et al. (2017) that appears to have been mischaracterised as satratoxin G when it is myotoxin A. The circle highlights the presence of a ketone at position C-13' rather than a hydroxyl group, and the oval highlights the missing double bond at the 7' to 8' position .....	55
Figure 44 - Structure of satratoxin F ( <b>8</b> ) .....	56
Figure 45 - Structure of myotoxin A ( <b>9</b> ), the compound that Li <i>et al.</i> actually crystallised	56
Figure 46 - Structures of roridin A ( <b>10</b> ), D ( <b>11</b> ), and E ( <b>12</b> ).....	57
Figure 47 - Verrucaric acid ( <b>13</b> ).....	58
Figure 48 - <sup>1</sup> H NMR spectrum of satratoxin G ( <b>6</b> ) in CDCl <sub>3</sub> (150 MHz) .....	74
Figure 49 - <sup>13</sup> C NMR spectrum of satratoxin G ( <b>6</b> ) in CDCl <sub>3</sub> (500 MHz) .....	75
Figure 50 - COSY NMR spectrum of satratoxin G ( <b>6</b> ) in CDCl <sub>3</sub> (500 MHz) .....	76

Figure 51 - HSQC NMR spectrum of satratoxin G ( <b>6</b> ) in CDCl <sub>3</sub> (500 MHz).....	77
Figure 52 - HMBC NMR spectrum of satratoxin G ( <b>6</b> ) in CDCl <sub>3</sub> (500 MHz).....	78
Figure 53 - <sup>1</sup> H NMR spectrum of satratoxin G ( <b>6</b> ) in DMSO- <i>d</i> <sub>6</sub> (150 MHz) .....	79
Figure 54 - <sup>13</sup> C NMR spectrum of satratoxin G ( <b>6</b> ) in DMSO- <i>d</i> <sub>6</sub> (500 MHz) .....	80
Figure 55 - COSY NMR spectrum of satratoxin G ( <b>6</b> ) in DMSO- <i>d</i> <sub>6</sub> (500 MHz) .....	81
Figure 56 - HSQC NMR spectrum of satratoxin G ( <b>6</b> ) in DMSO- <i>d</i> <sub>6</sub> (500 MHz).....	82
Figure 57 - HMBC NMR spectrum of satratoxin G ( <b>6</b> ) in DMSO- <i>d</i> <sub>6</sub> (500 MHz).....	83
Figure 58 - <sup>1</sup> H NMR spectrum of satratoxin H ( <b>7</b> ) in CDCl <sub>3</sub> (150 MHz) .....	84
Figure 59 - <sup>13</sup> C NMR spectrum of satratoxin H ( <b>7</b> ) in CDCl <sub>3</sub> (500 MHz) .....	85
Figure 60 - COSY NMR spectrum of satratoxin H ( <b>7</b> ) in CDCl <sub>3</sub> (500 MHz).....	86
Figure 61 - HSQC NMR spectrum of satratoxin H ( <b>7</b> ) in CDCl <sub>3</sub> (500 MHz).....	87
Figure 62 - HMBC NMR spectrum of satratoxin H ( <b>7</b> ) in CDCl <sub>3</sub> (500 MHz).....	88
Figure 63 - <sup>1</sup> H NMR spectrum of satratoxin H ( <b>7</b> ) in DMSO- <i>d</i> <sub>6</sub> (150 MHz) .....	89
Figure 64 - <sup>13</sup> C NMR spectrum of satratoxin H ( <b>7</b> ) in DMSO- <i>d</i> <sub>6</sub> (500 MHz) .....	90
Figure 65 - COSY NMR spectrum of satratoxin H ( <b>7</b> ) in DMSO- <i>d</i> <sub>6</sub> (500 MHz) .....	91
Figure 66 - HSQC NMR spectrum of satratoxin H ( <b>7</b> ) in DMSO- <i>d</i> <sub>6</sub> (500 MHz).....	92
Figure 67 - HMBC NMR spectrum of satratoxin H ( <b>7</b> ) in DMSO- <i>d</i> <sub>6</sub> (500 MHz).....	93

## List of Tables

Table 1 - <i>Stachybotrys chartarum</i> strains used in New Zealand specific investigations.....	15
Table 2 - Mass Spectrometry metabolite data from crude extracts (< LOD = below limit of detection).....	18
Table 3 - Satratoxin G ( <b>6</b> ) NMR data in CDCl <sub>3</sub> .....	36
Table 4 - Satratoxin G ( <b>6</b> ) NMR data in DMSO- <i>d</i> <sub>6</sub> .....	39
Table 5 - Satratoxin H ( <b>7</b> ) NMR data in CDCl <sub>3</sub> .....	49
Table 6 - Satratoxin H ( <b>7</b> ) NMR data in DMSO- <i>d</i> <sub>6</sub> .....	50
Table 7 - Comparison data for satratoxin H in CDCl <sub>3</sub> .....	51
Table 8 - Comparison data for satratoxin H in DMSO- <i>d</i> <sub>6</sub> .....	52
Table 9 - Comparison data for satratoxin G in CDCl <sub>3</sub> .....	53
Table 10 - Comparison data for satratoxin G in DMSO- <i>d</i> <sub>6</sub> .....	54
Table 11 - PCR Primers. ....	65

## Glossary

$\delta$	Chemical shift (ppm)
$^{13}\text{C}$ NMR	Carbon-13 Nuclear Magnetic Resonance
$^1\text{H}$ NMR	Proton Nuclear Magnetic Resonance
ACN	Acetonitrile
BLAST	Basic Local Alignment Search Tool
$\text{CDCl}_3$	Deuterated chloroform
$\text{CHCl}_3$	Chloroform
COSY	Correlation spectroscopy
d	Doublet
dd	Doublet of doublets
ddd	Doublet of doublets of doublets
DCM	Dichloromethane
$\text{DMSO-}d_6$	Deuterated dimethyl sulfoxide
DNA	Deoxyribonucleic acid
EtOH	Ethanol
EtOAc	Ethyl acetate
HEPA	High-efficiency particulate air
HMBC	Heteronuclear Multiple Bond Correlation
HPLC	High Pressure Liquid Chromatography
HSQC	Heteronuclear Single Quantum Coherence
ICMP	International Collection of Microorganisms from Plants
ITS	Internal Transcribed Spacer
$J$	Scalar coupling constant (Hz)
LCMS	Liquid Chromatography Mass Spectrometry

LD <sub>50</sub>	Concentration at which 50% of the population will die
LOD	Limit of detection
m	Multiplet
MS	Mass Spectrometry
MeOH	Methanol
NMR	Nuclear magnetic resonance
NOESY	Nuclear Overhauser Enhancement Spectroscopy
PCR	Polymerase chain reaction
PDA	Potato Dextrose Agar
PEI	Polyethylenimine
PE	Petroleum ether
ppm	Parts per million
RNA	Ribonucleic acid
RT	Retention time
s	Singlet
SBS	Sick building syndrome
SNR	Signal-to-noise ratio
t	Triplet
td	Triplet of doublets
<i>Tri5</i>	Trichodiene synthase
TLC	Thin Layer Chromatography
UV	Ultraviolet
UV/Vis	Ultraviolet-Visible spectroscopy

# 1. Introduction

## 1.1 History of Natural Products

Throughout history mankind has utilised many resources produced by the natural world for their advancement; of particular interest is how early humans incorporated nature into their traditional medicine. While modern medicine questions the efficacy of many of these treatments<sup>1</sup> it cannot be denied that many drugs still common today have their roots in ancient practices. It is now known that many of the benefits provided by traditional treatments are from the presence of biologically active secondary metabolites; naturally produced chemical substances that are not essential for sustaining the life of an organism.

It was this understanding that began the dedicated study of secondary metabolites (also known as natural products) for therapeutic benefit in the 1800s.<sup>2</sup> Scientists developed novel scientific techniques to isolate, purify, and define these active compounds. The ability to chemically alter these compounds has unlocked their enormous potential.<sup>3</sup>

The bark from willow trees has been used for thousands of years to treat sicknesses, in 1828 the main bioactive compound, salicin (**1**), was isolated.<sup>4</sup> However, it was the derivative acetylsalicylic acid (**2**) which showed improved medicinal properties. This led to the commercialisation of aspirin in 1899.<sup>4</sup> Over 100 years later, aspirin is still widely available and used for treatment of various ailments.

The bark of the Chinchona tree has been used to treat malaria since the 1600s, and even longer by native people of South America for fever.<sup>5</sup> Quinine (**3**) was isolated and purified from Chinchona bark in 1820, and subsequently became the standard treatment for malaria for over 100 years until synthetic antimalarial compounds were shown to be more effective.<sup>5</sup>

The chemotherapeutic agent Taxol (paclitaxel) (**4**) was first isolated in 1967 from the bark of the Pacific yew tree, *Taxus brevifolia*.<sup>6</sup> Being useful in the clinical setting was a long process for Taxol; taking 21 years of development, testing and trials before the U.S Food



and Drug Administration approved the drug for clinical use. Taxol has since become an important and effective treatment for some forms of ovarian, breast, and lung cancers.<sup>6</sup>

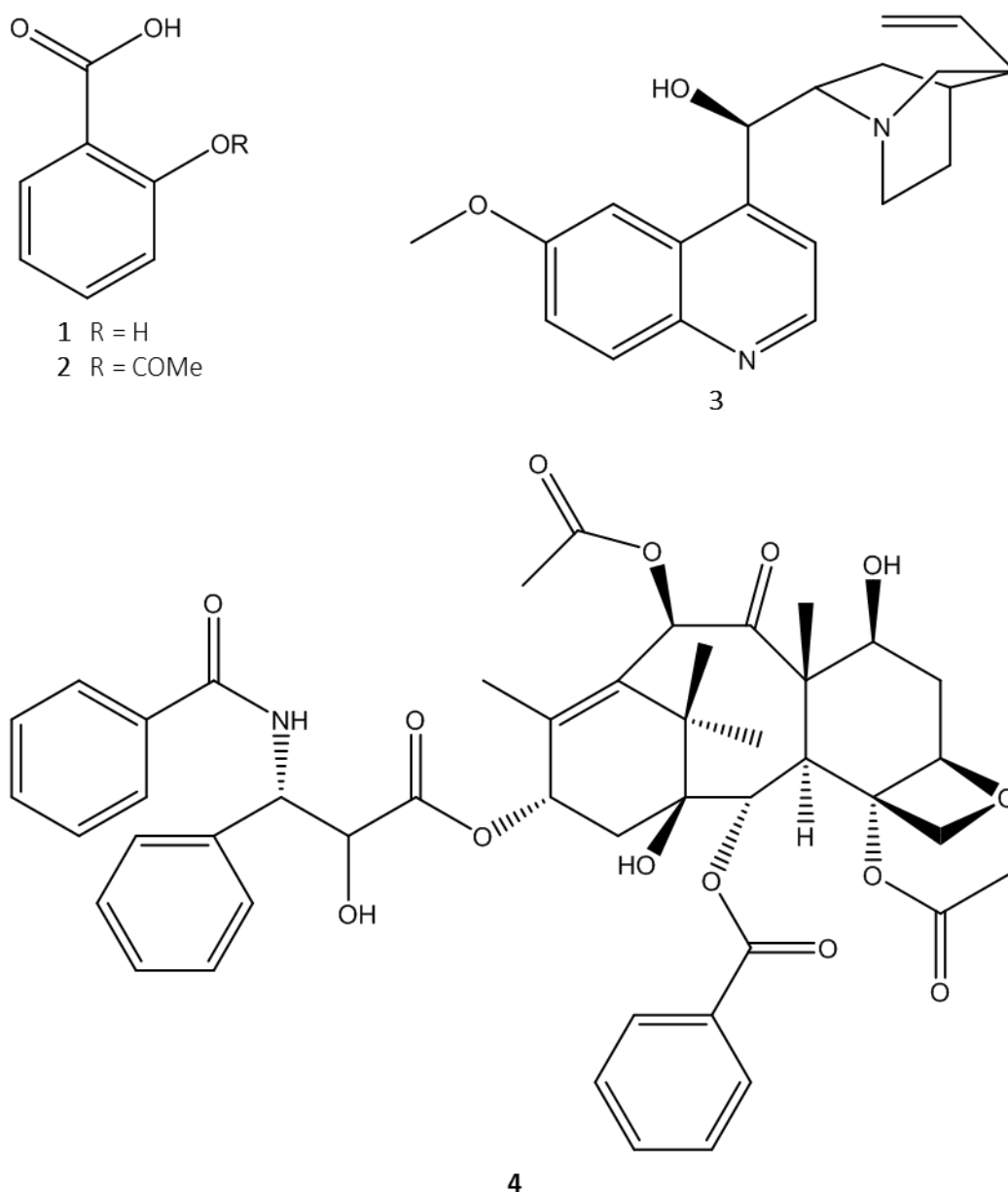


Figure 1 - Structures of salicin (1), acetylsalicylic acid (2), quinine (3), and paclitaxel (4).

Not all medicinal natural products are derived from plants; in 1929 Alexander Fleming discovered penicillin G (5) from the filamentous fungus *Penicillium notatum*.<sup>7</sup> The realisation of its broad therapeutic uses in the 1940s prompted intensive investigation of microorganisms as a source of novel bioactive natural products.<sup>8</sup> This began the “Golden

Age of Antibiotics”, which led to the discovery of many of the antibiotics (or derivatives thereof), that are still in use today for treatment of bacterial infections.<sup>9</sup>

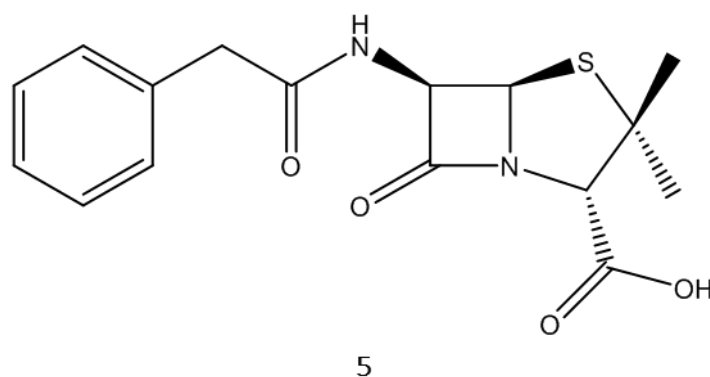


Figure 2 - Structure of penicillin G (5).

Natural products still play an important role in drug development. A 2016 review covering the sources of new drugs between 1981 and 2014 shows that at least 51.6% of all new drugs in this period were natural products or naturally derived in some way.<sup>10</sup> Naturally derived compounds include those that are natural product “botanical drug” derivatives, synthetic compounds based on a natural product pharmacophore, and synthetic compounds that are classed as being natural product mimics. This study and others do note that natural products are not often used as drugs in their directly isolated form, instead they serve as lead compounds resulting in the development of analogues with optimised pharmacological properties.<sup>2, 10</sup>

## 1.2 Toxic Natural Products

The dedicated research into natural products chemistry and the resulting plant and microbial derived drugs played a crucial role in the improvements seen in the medical field during the 20<sup>th</sup> century.<sup>8</sup> A common method of action for secondary metabolites is through some form of toxicity that harms or kills their targets. For example the antibiotic penicillin works by weakening the cell walls of dividing bacteria, causing them to break apart under stress and thereby killing the target.<sup>11</sup> This worked well for *P. notatum*, giving it a survival advantage in its environment and it worked well for humans when leveraged to treat

bacterial infections. These toxic properties are what enable secondary metabolites to be utilised as antimicrobial and antitumor agents.

The toxicity of some secondary metabolites can also affect humans, causing adverse health effects that can range from minor to life threatening.<sup>12</sup> The consequences of some toxic metabolites have been known for a long time. Ancient tribes used plants containing toxic secondary metabolites to increase the effectiveness of their weapons.<sup>13</sup> Metabolites from bacteria and fungi are responsible for food poisoning.<sup>14-16</sup> Exposure to toxins can normally be avoided through sufficient preparation and mitigation techniques, but some exposures can only be avoided through drastic changes to circumstance and behaviours.

One of these scenarios is environmental exposure, people being exposed to toxic metabolites where they live and work. The nature of the built environment means that at any time there are many different conditions appropriate for microbes to flourish.<sup>17</sup> The most readily identifiable indoor contaminant is black mould. Black mould is a blanket term for a variety of fungal species that grow in indoor environments and have a predominantly black appearance. One species in particular is capable of producing toxic secondary metabolites, *Stachybotrys chartarum*.<sup>18</sup>

### 1.3 Respiratory Health

There is accumulating evidence that indoor mould and moisture contribute to poor respiratory health.<sup>19-21</sup> Built structures contain complex microbiomes the entirety of which may be contributing to the adverse effects on respiratory health and to a condition known as sick building syndrome (SBS).<sup>17, 22</sup> SBS is a loosely defined term for the variety of adverse health effects associated with living or working in cold and damp buildings. Mechanisms explaining the association between mould and adverse health effects remain unknown, but fungal fragments, spores, cell wall components, volatile organic compounds, and secondary microbial metabolites, including mycotoxins, have all been suggested.<sup>23</sup>

New Zealand has very high levels of respiratory illnesses,<sup>24</sup> and with the prevalence of low quality buildings that are frequently water-damaged<sup>25</sup> it is logical to draw a link between exposure to mould and these respiratory disorders. A recent report commissioned by the New Zealand Foundation for Asthma calculated that the annual cost of respiratory

disorders to New Zealand is greater than 6 billion dollars,<sup>24</sup> meaning that investigations into the cause of these effects are urgently needed.

This study concentrated on isolating and characterising the key toxic metabolites produced by *S. chartarum* because they have been observed in New Zealand environments and can produce high levels of extremely toxic compounds. Information gathered from assessing samples from the New Zealand environment will be used to investigate the hypothesis that adverse respiratory symptoms are being caused by chronic low-level exposure to the toxic metabolites produced by *S. chartarum*.

#### **1.4 *Stachybotrys chartarum***

*S. chartarum* is an infamous black mould,<sup>26, 27</sup> it produces a variety of toxic secondary metabolites capable of causing mycotoxicosis in animals and humans.<sup>28</sup> Most importantly it has the ability to produce highly toxic trichothecenes. Found in moisture rich environments, it is one of the major species occurring on cellulose-based building materials experiencing long-term indoor water damage. *S. chartarum* has repeatedly been associated with SBS.<sup>29-32</sup>

The widespread interest in *S. chartarum* began after it was attributed as the causative factor in several cases of acute pulmonary haemorrhage in infants during the early 1990s.<sup>33</sup> Another study reported a high prevalence of pulmonary diseases among office workers of Florida court buildings following prolonged indoor exposure to *S. chartarum* and *Aspergillus versicolor*.<sup>34</sup> Substantial evidence in these cases showing if moulds are the actual causative agent for these complaints or whether they are merely a result of the environment of these buildings is lacking. Newer studies are beginning to provide evidence that an increase in respiratory disorders is associated with fungal contamination in homes.<sup>19, 30, 35</sup>

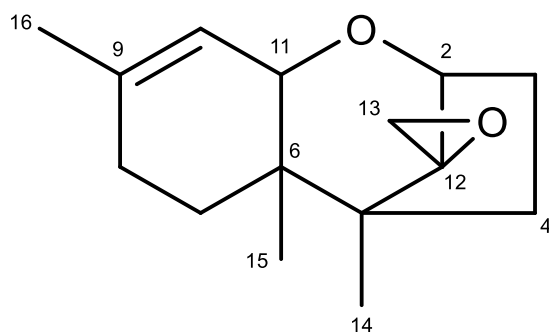


Figure 3 - Trichothecene core.

The trichothecenes, which are produced by many fungi species, are characterised by the presence of a tricyclic 12,13-epoxytrichothene-9-ene core structure known as the trichothecene core (Figure 3).<sup>36</sup> There are five potential variable sites,  $R_1$  to  $R_5$ , and the trichothecenes are grouped into four subtypes, A-D, depending upon what functional groups are found at these variable sites (Figure 4). *S. chartarum* is able to produce both simple trichothecenes, types A-C, and the very toxic macrocyclic trichothecenes, type D.

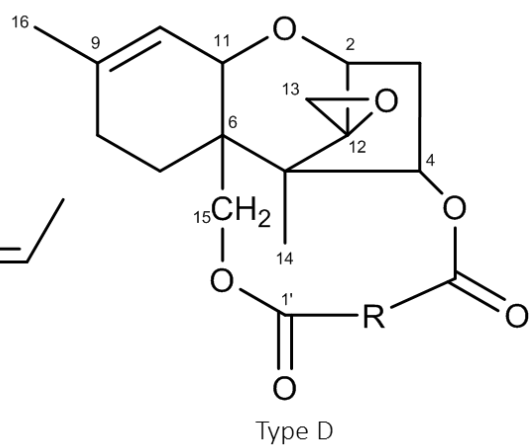
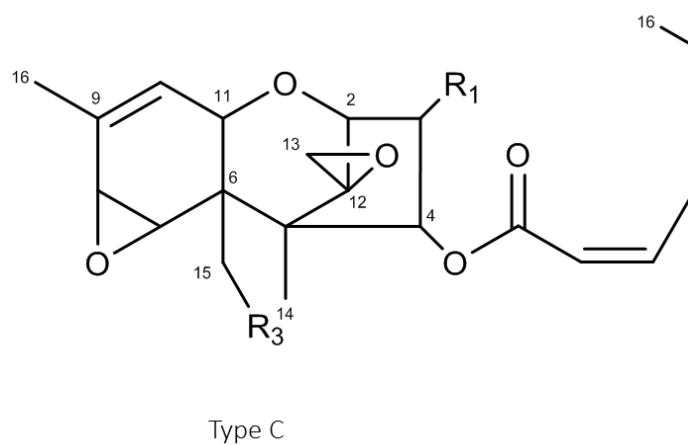
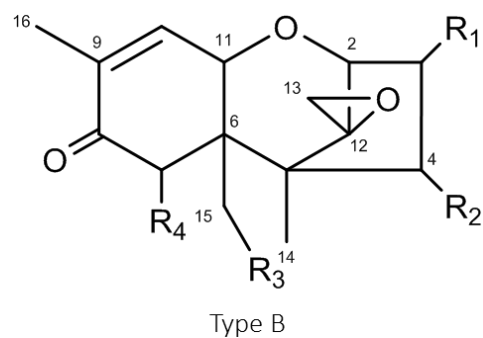
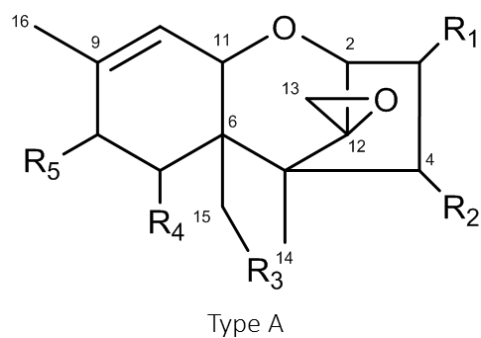


Figure 4 - Trichothecene subtypes.

The toxic profile of any given microbe is an important consideration when investigating it for adverse health effects. Research has shown that *S. chartarum* exists as two main chemotypes, one capable of producing the highly toxic macrocyclic trichothecenes, chemotype S, while the other produces the less toxic atranones, chemotype A.<sup>18, 37</sup> It is important to note that chemotype A is still capable of producing the simple trichothecenes that form the beginning of the macrocyclic trichothecene biosynthesis pathway.<sup>38</sup> The high prevalence of *S. chartarum* and the toxic metabolites it is capable of producing make it a good candidate as a causative agent responsible for adverse health effects.<sup>35</sup>

#### 1.4.1 Species Status

Fungal species were traditionally differentiated based upon morphology and other observable characteristics. In the past few decades, with the ease of genetic sequencing, this has given way to identification by sequencing the Internal Transcribed Spacer (ITS) regions.<sup>39, 40</sup> The ITS region refers to the spacer deoxyribose nucleic acid (DNA) situated between the small subunit ribosomal ribose nucleic acid (rRNA) and large-subunit rRNA genes. This has led to new understanding of how different fungi are related at the genus, species, and sub-species level, and has rewritten the relationships between many fungal groups that were originally grouped or separated based on morphological characteristics.<sup>41</sup> These recent changes exemplify the differences that can occur within a species; which are commonly due to having distinct sexual stages and pleomorphic changes in response to environmental conditions.

The term black mould covers a general indoor fungal contamination linked together by being similar in appearance. This means that *S. chartarum* and black mould or toxic black mould are not necessarily synonyms. Identifying information on *S. chartarum* is further complicated by the confusion surrounding species and subspecies categorisation, throughout the years it has been known by several names, including *Stachybotrys atra*.<sup>35, 42</sup> Recent research has suggested that the *Memnoniella* genus and *Stachybotrys* should be merged.<sup>28</sup> These inconsistencies appear less frequently with newer research, but they complicate the search for evidence in older literature.

## 1.5 *Stachybotrys chartarum* Secondary Metabolites

The *S. chartarum* chemotype that produces macrocyclic trichothecenes is of primary interest for investigating potential adverse health effects. The macrocyclic trichothecene class are highly cytotoxic and have been implicated in a general mycotoxicosis.<sup>28</sup> The most toxic of these are satratoxins G (**6**) and H (**7**) (Figure 5), which have been shown to be highly potent cytotoxins, with a lethal dose (LD<sub>50</sub>) of 1 mg/kg or less.<sup>43, 44</sup>

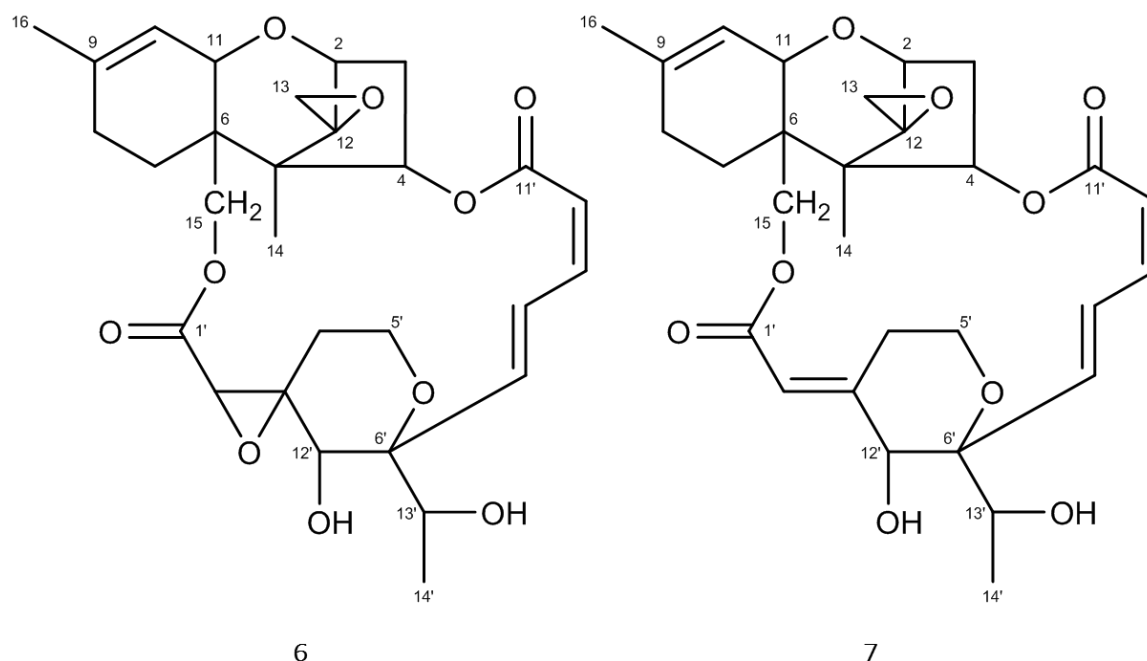


Figure 5 - Structures of satratoxin G (**6**) and satratoxin H (**7**).

Secondary metabolites are not essential for the basic functioning of an organism, this has made understanding why, when, and how they are produced sometimes difficult to determine. Recent research has investigated the effect of different growth conditions and environments on the production of *S. chartarum* toxins,<sup>45</sup> and comparative genome sequencing has revealed chemotype-specific gene clusters.<sup>38</sup>

### 1.5.1 Isolation

*S. chartarum* produces many other secondary metabolites, including several other macrocyclic trichothecenes,<sup>43</sup> this impedes efforts to isolate these compounds at sufficient quantities for characterisation. Quantifying the presence of these compounds in the

environment is made even more difficult by the fact that many other fungal species and sub-species will coexist in the same environment making a variety of metabolites that will obscure the signal during analysis.

Isolation is achieved with chromatography techniques. A process that separates based upon molecular size and charge. For different stages of isolation different techniques and systems are necessary. Figure 6 shows a basic demonstration of how chromatography separates two components from a sample.

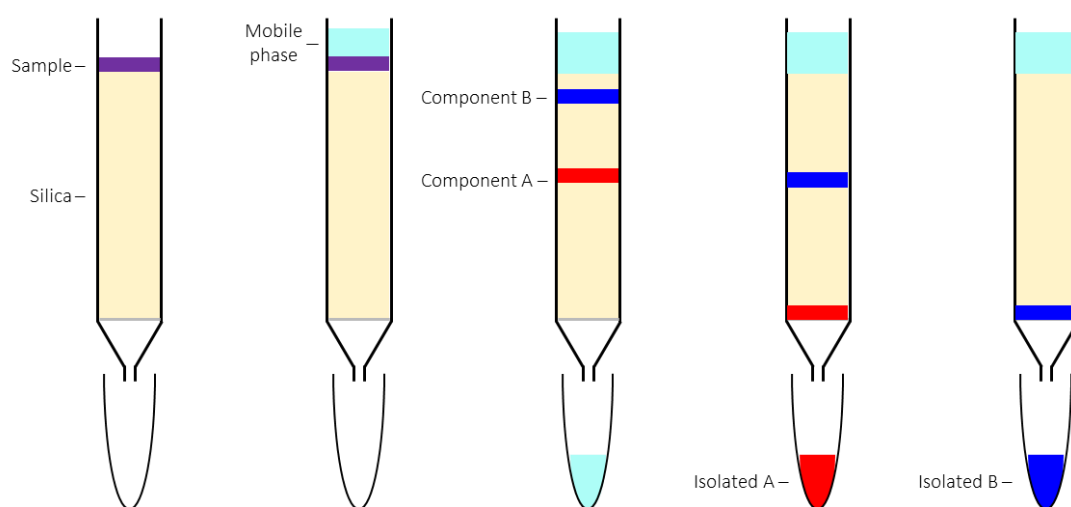


Figure 6 - Basic principle of chromatography separation.

### 1.5.2 Characterisation

Published data and nuclear magnetic resonance (NMR) spectra for these hard to isolate compounds is uncommon. Since the original characterisation of the satratoxins, H in 1977<sup>46</sup> and G in 1980,<sup>47</sup> there have been very few reports. A recent article has shown that with modern techniques and equipment there are discrepancies with the original spectral data and characterisation of Roridin E, another macrocyclic trichothecene produced by *S. chartarum*.<sup>48</sup> This report has since been used by a different group to aid in their identification of isolated molecules.<sup>49</sup> This shows that it is important to keep the literature up to date using modern NMR experimentation.



Updated NMR data for the satratoxins was recently published, as well as a crystal structure for satratoxin G.<sup>50</sup> However, that study used deuterated dimethyl sulfoxide (DMSO-*d*<sub>6</sub>) as the solvent and only reported the raw data, providing no images of the spectra. Because the majority of NMR studies performed with trichothecenes have used deuterated chloroform (CDCl<sub>3</sub>),<sup>51</sup> we chose to provide characterisations of the satratoxins in CDCl<sub>3</sub>, with supporting DMSO-*d*<sub>6</sub> data, and include updated spectral information which are entirely absent from peer reviewed, easily accessible literature.

### 1.5.3 Genetics

An organism can survive without the ability to produce secondary metabolites, especially when being cultured in a lab which inherently removes competition from its environment. This is the key reason that inhibits understanding the genetics of secondary metabolism. Genes often cannot be identified from basic knockout studies, the traditional method for identifying gene function.<sup>52</sup> The existence of large multigene cassettes and complicated biosynthetic pathways means that any knockout that does produce an effect may not be directly related to the metabolite of interest.<sup>53</sup>

Despite this the field of secondary metabolite genetics is progressing, aided by new techniques such as CRISPR,<sup>54</sup> and RNA-seq.<sup>55, 56</sup> There are now many published reports detailing the genetic and biosynthetic pathways of secondary metabolites, including that of simple trichothecenes.<sup>57, 58</sup> The two chemotypes of *S. chartarum* have now been proven to be the result of varying gene sequence within the *Stachybotrys* genus.<sup>38</sup>

Knowing the genetics of your targeted metabolites can be helpful at even a basic level. Anderson et al.<sup>18</sup> showed that just 35% of their *S. chartarum* isolates produced satratoxins, the rest produced other macrocyclic trichothecenes or atranones. Understanding how to identify chemotype based upon genetic sequence can prevent time consuming work growing cultures that may not produce the desired metabolites.

## 1.6 Research Aims

The aim of this research was to isolate and characterise the *S. chartarum* secondary metabolites G and H. Isolation and identification was undertaken using crude extracts and specimens collected from New Zealand environments. Genotyping experiments were planned to check their species and subspecies status as well as their chemotype specific genes. Crude samples from the New Zealand specimens were also analysed for the presence of toxic metabolites other than the satratoxins.

This project aims to provide starting blocks to investigate the hypothesis that respiratory issues in affected buildings are the result of key microbial toxins. With modern analytical chemical methodology, we propose the isolation and characterisation will enable detection of toxic substances in the environment even at very low levels.

## 2. Cultures and Isolation

### 2.1 *Stachybotrys chartarum* Environments

The environment where *S. chartarum* can proliferate ranges from animal feed<sup>59</sup> and soil<sup>60</sup> to damp buildings.<sup>61</sup> Figure 7 shows an unidentified black mould growing on the window frame of a New Zealand home (Wilton, Wellington, 5 April 2018). Black mould is found everywhere in the world, and when present it is likely that *S. chartarum* is a major component. What is less well known is how different environments and substrates might affect its toxic profile; the distribution and concentrations of toxic metabolites. Recent research, by Aleksic *et al.* (2016), has aimed to answer this question by quantifying production of the highly toxic macrocyclic trichothecenes during growth on different types of building materials.<sup>45</sup> It was found that the nature of a building material strongly influenced the levels of macrocyclic trichothecenes produced. Standard wallpaper appeared to be the most favourable to both fungal development and production of the four toxins measured, whereas on vinyl wallpaper there was minimal fungal growth, and no toxins were produced. *S. chartarum* is a cellulolytic fungus so it is expected that growth will be improved on substrates that are cellulose-based materials.

A building material not investigated in the Aleksic *et al.* study, that is very popular in modern homes, is gypsum-based wallboards, known as drywall and plasterboard. Another study, by Anderson *et al.* (2017), investigated whether this material was pre-contaminated with fungi species because it had been observed that it was frequently overgrown with mould following water damage.<sup>62</sup> The Anderson *et al.* study found that their samples of gypsum-based wallboard were already infected with fungal spores before the panels reach their end-users. This has important implications for the safety of using these materials in a moisture prone environment. The authors of the study recommend that manufacturers undertake stricter quality control of their raw materials and finished products. Figure 8 provides an example of *S. chartarum* growing on a gypsum wall board, reproduced from Nelson (2001).<sup>63</sup>

Black mould can be easily controlled if a building has adequate ventilation, which serves to lower the levels of moisture in the air. Unfortunately, during the rapid construction of offices and houses in the 1990s and early 2000s there were fundamental flaws in the

building practices and materials being used. This led to a large number of moisture prone buildings being built in this time period. These buildings are now known as leaky homes.<sup>64</sup> This has caused ongoing issues regarding the best way to remediate these leaky homes that were prone to dampness and subsequent contamination from the beginning.



*Figure 7 - Unidentified black mould growing in a New Zealand home.*

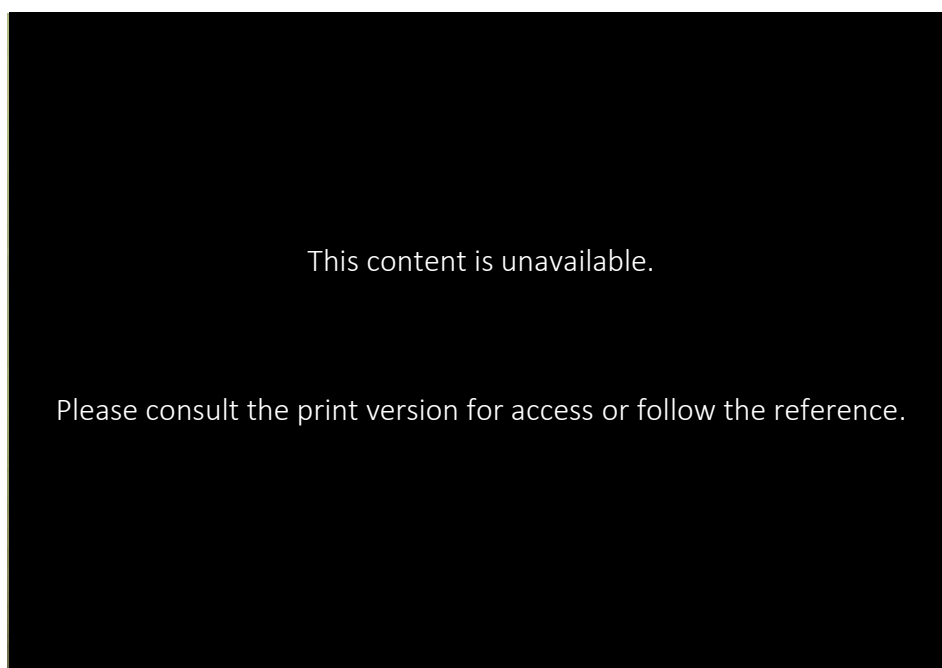


*Figure 8 - Black mould growing on the backside of water damaged gypsum wall board, identified as *Stachybotrys chartarum*. Reproduced from Nelson (2001).<sup>63</sup>*

The New Zealand company BRANZ Ltd, an independent research and testing company for the construction industry, produce publications and guidelines for the current best practices for building remediation. In their remediation details for mould they state that *S. chartarum* is a toxic mould and as such they provide the following guidelines:

*“If mould is covering a significant area of the building, a specialist contractor should be employed to carry out the removal. Small areas may be done without using a specialist contractor, but precautions must be taken. Wear a respirator with a P1 filter (these filters 80% of airborne particles and is considered minimum protection) and wear protective clothing that is disposable or can easily be washed. Before beginning work seal off the space from other parts of the building by taping up all openings. Remove all materials from which the mould cannot be removed such as wallpaper, timber products, ceiling tiles, gypsum board, drapes, furniture. Place all removed materials in plastic bags that can be sealed. Clean the affected area of materials such as glass, plastic and metal from which the mould can be removed using hot water and chlorine bleach. Use a stiff brush on rough or uneven surfaces. Vacuum all surfaces of the sealed area thoroughly using a vacuum with a high-efficiency particulate air (HEPA) filter.”<sup>65</sup>*

## 2.2 Culture Characteristics

To investigate the characteristics of New Zealand *S. chartarum* strains four specimens were purchased from the Landcare Research International Collection of Microorganisms from Plants (ICMP) repository (Table 1). Note that although ICMP 13983 has been listed as *S. atra* it is now accepted that this is the same species as *S. chartarum* (as discussed in section 1.3.1).

Slants of these species were supplied growing on Potato Dextrose Agar (PDA); therefore, PDA was selected as the growth medium for plate-based colonies. PDA has been used frequently in previous research so there was a high level of confidence that it would be suitable.<sup>38, 44, 50</sup> The *S. chartarum* isolates were grown on agar plates for observation of differences in morphology between strains and production of spores to inoculate rice. The four different cultures, despite being the same species, all displayed significantly different

morphology and growth characteristics (Figure 9). The vastly different growth characteristics again highlights the importance of ITS sequencing for proper fungal identification.

Table 1 - *Stachybotrys chartarum* strains used in New Zealand specific investigations.

Identifier	Strain	Isolated From	Isolation Date
ICMP 13983	<i>Stachybotrys atra</i> Corda	Unknown	January 1999
ICMP 14263	<i>Stachybotrys chartarum</i> (Ehrenb.) S. Hughes	Auckland, NZ	April 2001
ICMP 20761	<i>Stachybotrys chartarum</i> (Ehrenb.) S. Hughes	Waiheke, NZ	August 2014
ICMP 20762	<i>Stachybotrys chartarum</i> (Ehrenb.) S. Hughes	Auckland, NZ	August 2014

The plates were used to inoculate rice cultures for metabolite production (Figure 10). Parboiled rice introduced as the optimal media by Jarvis *et. al.*<sup>66</sup> was used for larger scale growth when production of secondary metabolites was the goal. Previous literature reports have shown success with this method.<sup>43, 67</sup> Liquid cultures were not used because some researchers report that this method of culturing does not produce macrocyclic trichothecenes.<sup>68, 69</sup>



ICMP Strain	13983	ICMP Strain	14263
Form	Irregular	Form	Irregular
Margin	Filiform	Margin	Filiform
Surface	Rough	Surface	Smooth
Colour	Black, white sporulation	Colour	Brown, grey hyphae
			

Figure 9 - Colony characteristics of ICMP *Stachybotrys chartarum* strains. Continued next page.

ICMP Strain	20761	ICMP Strain	20762
Form	Irregular	Form	Filamentous
Margin	Irregular	Margin	Filiform
Surface	Rough	Surface	Fuzzy
Colour	Grey and black	Colour	Black

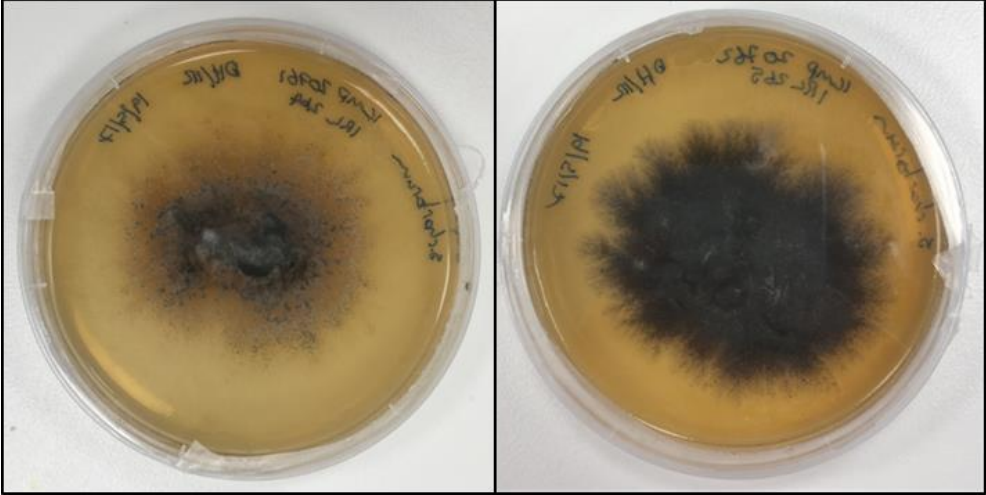


Figure 9 Continued - Colony characteristics of ICMP *Stachybotrys chartarum* strains.



Figure 10 - ICMP *Stachybotrys chartarum* strains growing on parboiled rice.



## 2.3 Crude Extracts

Crude extracts of the New Zealand strains were generated from the extraction of rice cultures, the cultures were incubated for a minimum of two weeks. Extraction of the cultures was achieved by an overnight soak in a 1:1 chloroform:methanol mixture and filtration (Whatman filter paper) to separate from rice. This extraction yielded a dark solution. The process was repeated, and the extracts were combined (Figure 11).

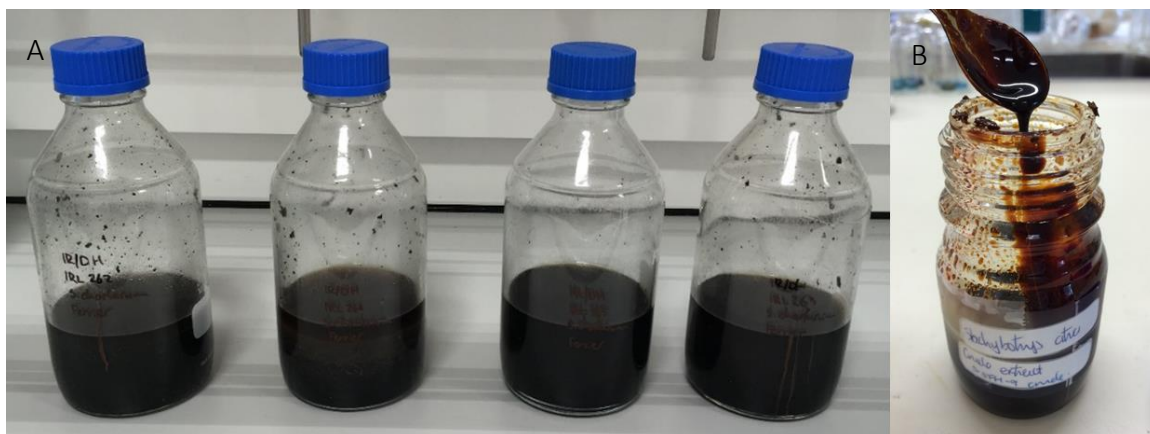


Figure 11 - A) rice cultures soaking in extraction solvent, B) concentrated crude extract.

Presence of the satratoxins was verified by following the method of high performance liquid chromatography (HPLC) analysis detailed by Hinkley (2001).<sup>43</sup> This method provided a reference for the expected retention time (RT) of the satratoxins and other *S. chartarum* toxins. The HPLC method used a 100 x 3 mm reversed-phase C18 column with a flow rate of 0.2 mL/min, running conditions were a gradient of increasing ACN in deionised water, 25% to 80% over 30 minutes, followed by an increase from 80% to 100% over 1 minute where it was held for a further 9 minutes before returning to starting mixture for equilibrium, signals were detected with UV/Vis at 225, 260, 280, and 300 nm wavelengths. Figure 12A shows a reproduction of an original figure from the original article. Figure 12B shows the HPLC chromatogram of a *S. chartarum* crude extract where key peaks have been labelled.



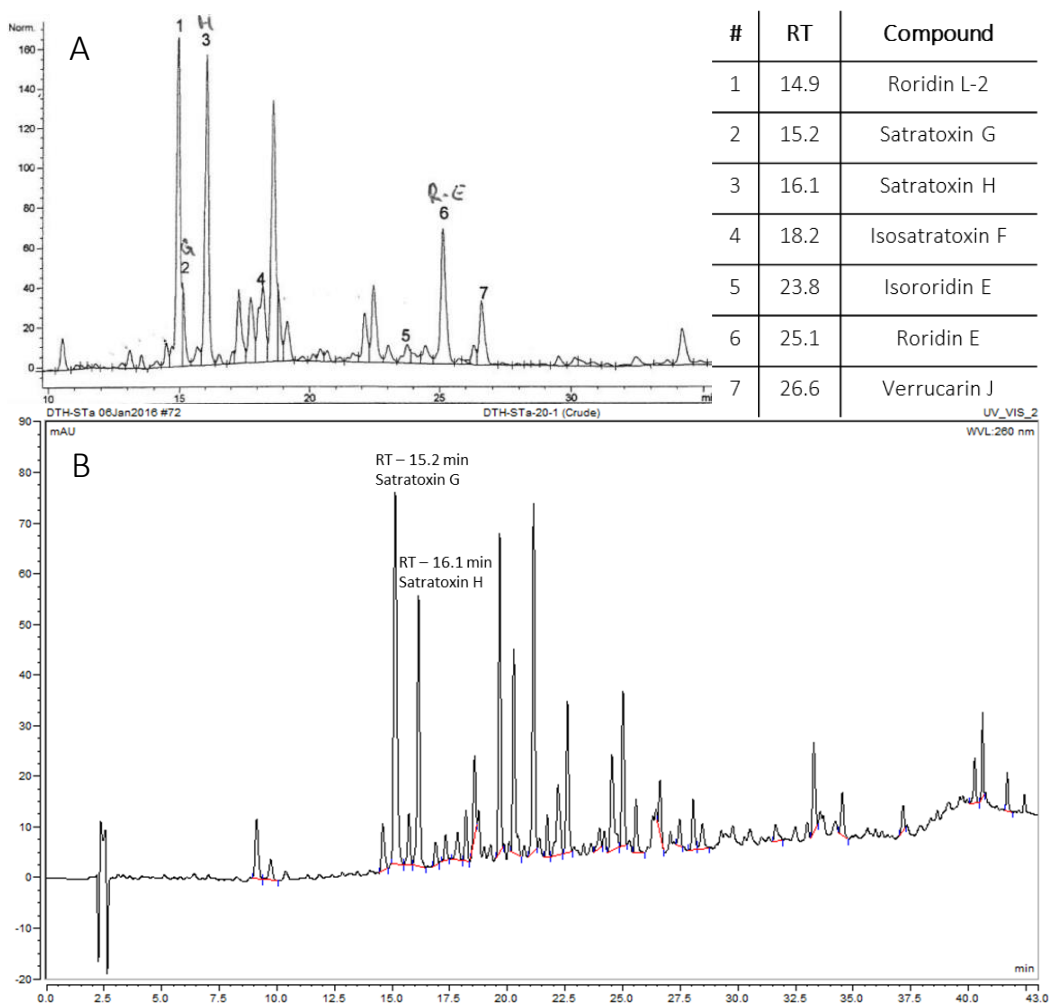


Figure 12 - A) original data from Hinkley, B) chromatogram generated by HPLC showing the presence of satratoxins in a crude *Stachybotrys chartarum* extract. HPLC conditions were an increasing gradient of ACN in deionised water using a C18 reversed-phase column and a UV/Vis detector.

## 2.4 Mass Spectrometry Analysis

After confirming the likelihood of satratoxins being present in the crude extract samples they were sent to a collaborators laboratory, Michael Sulyok from the University of Natural Resources and Life Sciences Vienna, for analysis with a tandem mass spectrometry (MS) array. Extracts were complete with no further purification steps excepting filtration to remove particulates.

The salient metabolites detected in this analysis were; satratoxin G, satratoxin H, stachybotryamide, stachybotrylactam, and trichodermin. The metabolites

stachybotryamide and stachybotrylactam are produced by all *Stachybotrys* species. Trichodermin is a simple trichothecene produced by both *S. chartarum* chemotypes.

The data obtained from the tandem MS analysis (Table 2) shows that two of the New Zealand strains, ICMP 14263 and ICMP 20761, are producing satratoxins G and H. Interestingly, the strain ICMP 13983, which was deposited as a satratoxin G producer, was not found to be producing any satratoxins. However, the regulation of metabolite production is complicated and the fact that it is also not producing trichodermin indicates that the trichothecene pathway may have been turned off in this culture at the time of extraction.

This showcases the strength of modern analytical tests. Purified samples only need to be isolated if they are going to be used in assays or if structural elucidation is desired. We will attempt this method in the future to allow rapid identification of metabolites in the environment.

Table 2 - Mass Spectrometry metabolite data from crude extracts (< LOD = below limit of detection), values are ng of metabolite per mg of sample supplied.

Strain	Metabolites found in <i>Stachybotrys chartarum</i> crude extracts (ng/mg)				
	Satratoxin G	Satratoxin H	Stachybotryamide	Stachybotrylactam	Trichodermin
ICMP 13983	< LOD	< LOD	1165.6	205.4	< LOD
ICMP 14263	329.7	460.2	1238.4	2360.4	478.8
ICMP 20761	11.2	48.4	980.0	2372.4	3.1
ICMP 20762	< LOD	< LOD	2750.0	2302.0	0.8

## 2.5 Genetic Information

The goal was to extract DNA from the ICMP strains and use it to confirm species status and investigate their chemotypes, using ITS and Tri5 respectively. Unfortunately, due to unforeseen complications this was not possible, however, some conclusions can be drawn from the information contained within the ICMP database and from the MS results.

First, all strains were confirmed as *Stachybotrys spp.* due to their ability to produce the *Stachybotrys* metabolites stachybotryamide and stachybotrylactam.<sup>70, 71</sup> Following this all strains were confirmed as *S. chartarum*. ICMP 20761 and ICMP 20762 were deposited into the ICMP database after being identified with ITS sequencing. A BRANZ report that is co-authored by the original contributor of these strains (Nick Waipara), shows that his lab uses

standardised ITS identification.<sup>64</sup> This provides a high level of confidence that the identification is correct. ICMP 13983 was deposited into the ICMP database after being identified based upon morphology and its ability to produce satratoxin G. *S. chartarum* is the only mould species reported to produce satratoxins<sup>35, 72</sup> so again there is a high level of confidence in the identification. The identification of ICMP 14263 prior to being deposited into the ICMP database was based solely on morphology; as discussed identification based upon morphology is no longer the accepted way of identification. This strain produced both satratoxin G and H in our cultures meaning we are confident it can be identified as *S. chartarum*.

In addition to confirming these strains as *S. chartarum*, genotyping was going to provide information on the chemotype. However, from the ICMP database information and MSMS data the strains ICMP 13983, 14263, and 20761 can be designated as chemotype S due to reported or measured production of satratoxins. The chemotype of ICMP 20762 cannot be identified from the MSMS data without the genetic information or by measuring if it has the ability to produce atranones. (Figure 5)

## 2.6 Metabolite Isolation

HPLC and MSMS analysis confirmed the presence of satratoxins in the crude extracts. A combination of regular and polyethylenimine (PEI) silica-based flash chromatography was used to purify the crude extract and isolate the satratoxins. The use of PEI silica for fractioning macrocyclic trichothecenes was first described by Jarvis in 1992.<sup>73</sup> This method was further developed by Hinkley in 2001.<sup>43</sup> Two methods are described; 1) PEI absorption and 2) direct application. The direct application method was used throughout metabolite isolation because Hinkley states that some trichothecenes may irreversibly bind to the PEI silica when the absorption method is used. Due to the potential of eventually using this process for low level environmental isolations it was decided that this loss was not acceptable.

Using PEI has the advantage of quickly separating metabolites based upon compound class, but it is not suitable for separating between compounds of the same class. Regular silica-based chromatography with a variety of solvent systems was used to isolate the satratoxins

into pure fractions. The solvent systems used were developed following experimentation with thin layer chromatography (TLC), changing solvents and gradients dependent upon how they affected the separation of crude extracts. The solvents used included: methanol (MeOH), dichloromethane (DCM), petroleum ether (PE), and ethyl acetate (EtOAc). Three different systems used for flash chromatography were developed:

1. Increasing concentrations of MeOH in DCM, from 0 to 15%
2. Increasing concentrations of MeOH in 5% PE and DCM, from 0 to 15%
3. Decreasing concentrations of PE in EtOAc, from 50 to 10%.

Satratoxin G was the first to elute and was much easier to isolate in a fraction of high purity. Satratoxin H was more difficult to isolate, and chromatography steps often had to be repeated with fractions being recombined to obtain fractions of sufficient purity and amount. Figure 13 shows a simplified flowchart of satratoxin isolation, with an arrow indicating that steps 3-5 are repeated until sufficient purity is obtained.

The contents of fractions and their purity was measured during flash chromatography by TLC. Figure 14 shows a TLC plate that was used to measure what fractions the satratoxins eluted into during a flash chromatography experiment using a semi-purified sample. The marked areas indicate which fractions were combined into new samples. In this instance

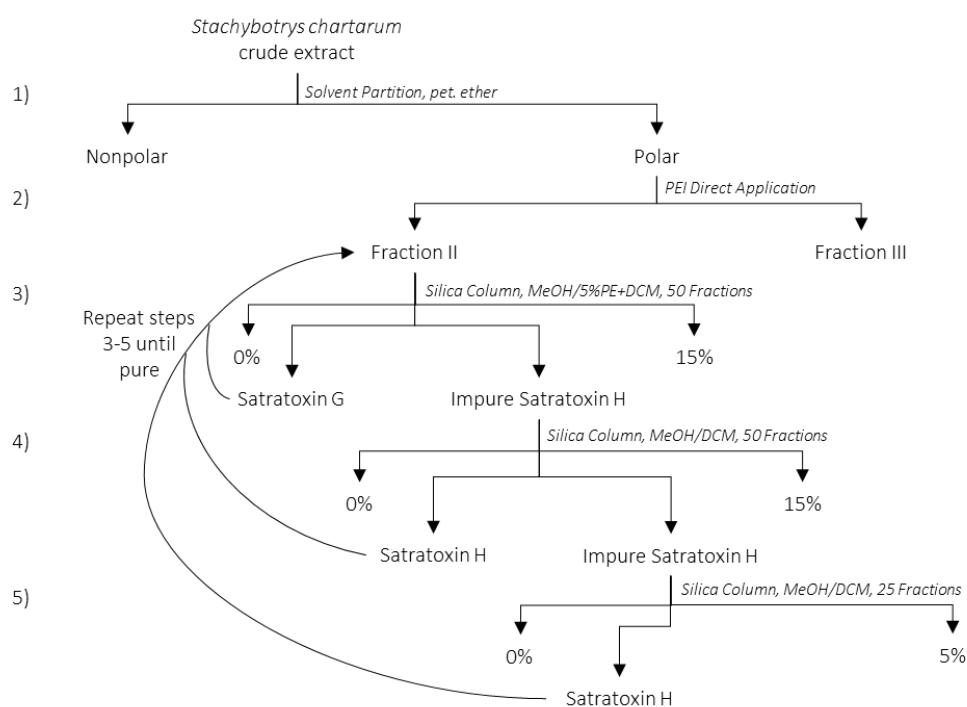


Figure 13 - Simplified flowchart for method of satratoxin isolation, steps 3-5 were repeated until a pure fraction was achieved.

group 5 shows a good presence of satratoxin G, indicated by the satratoxin G standard that was used in the leftmost lane.

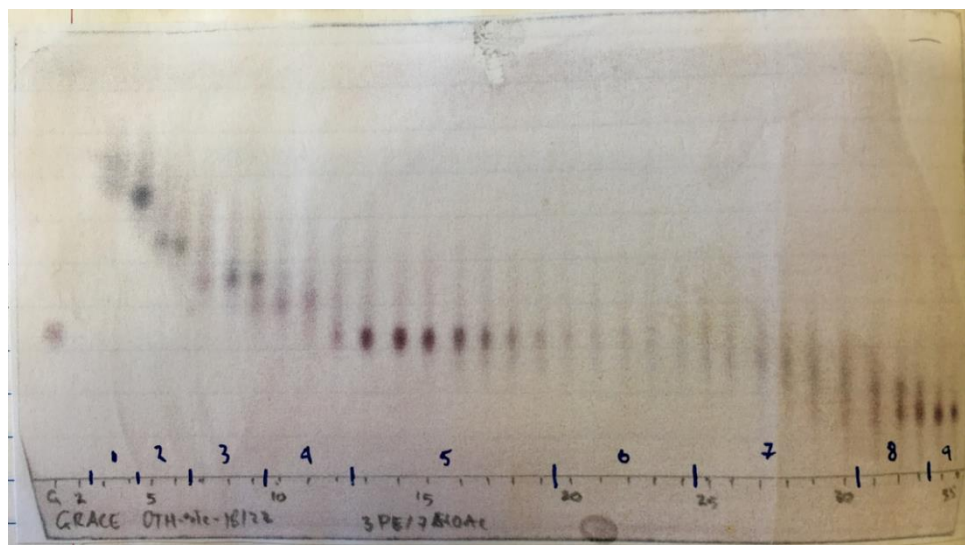


Figure 14 - TLC analysis of fractions taken during a flash chromatography separation of a semi-purified crude extract sample. A satratoxin G standard was run in the leftmost lane, the solvent system in use is 30% PE in EtOAc, visualisation was with a vanillin staining solution.

## 2.7 Fraction Purity

The purity of an isolate was assessed with three methods:

1. TLC - used to provide a rapid indication of fraction purity
2. HPLC - provided chromatograms that can be compared to literature
3. Liquid chromatography mass spectrometry (LCMS) - a sensitive technique combining liquid chromatography and mass spectrometry.

The first step used for identifying the purity of samples was by TLC. This provides a rapid method for identifying the presence or absence of the metabolites of interest when paired with a standard. Figure 15A shows a TLC plate with fractions that are almost purified, it also demonstrates how closely the satratoxins G and H elute and why there was difficulty separating them. Figure 15B shows a TLC plate with four fractions from a flash chromatography run, the first of which appears to be pure satratoxin G.

Once a fraction was indicated as pure from TLC analysis HPLC was used to give a more precise measure of purity. HPLC analysis used the same Hinkley method used in section 2.3,<sup>43</sup> except the flow rate was set to 0.4 or 0.5 mL/min dependent on pressure and the

gradient from 25% to 80% over 15 min, this was done to increase throughput. Figure 16 is a HPLC chromatogram of two fractions that were shown to be pure from TLC analysis, however, they were both found to contain trace amounts of the opposing satratoxin.

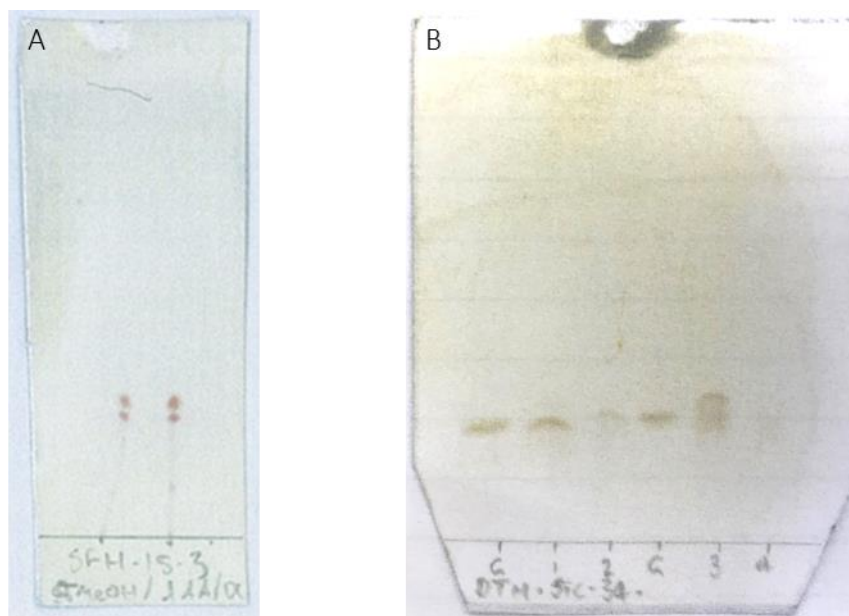


Figure 15 - A) A TLC plate that has been purified to the stage of containing only the satratoxins B) a TLC plate of four fractions, the first of which appears to be a pure isolate of satratoxin G as indicated by the standard running in the left most lane. The solvent system in use is 5% MeOH in DCM, visualisation was with a vanillin staining solution.

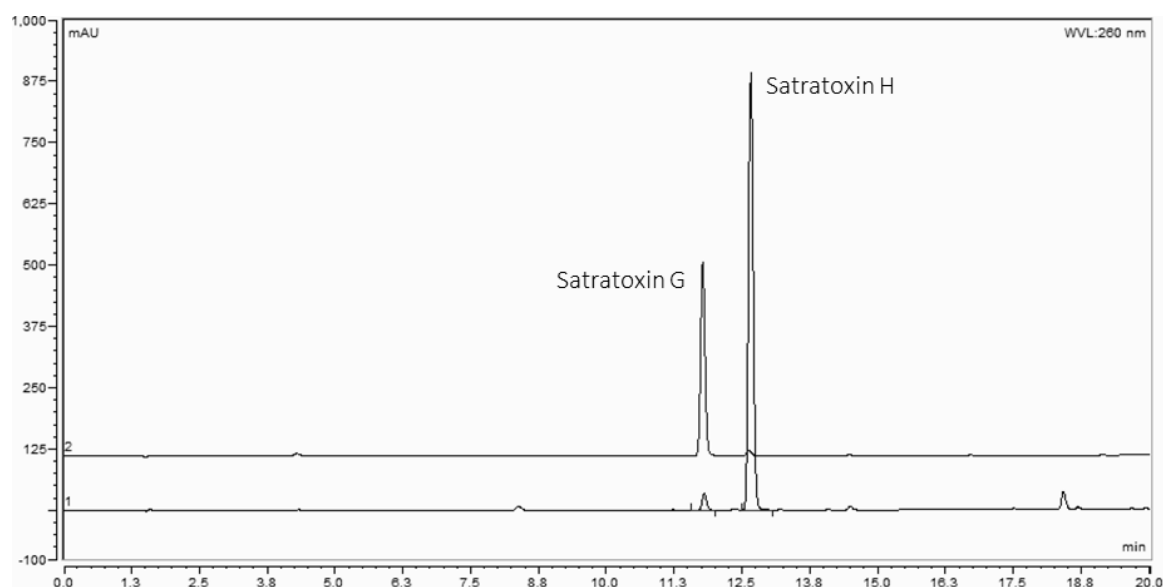
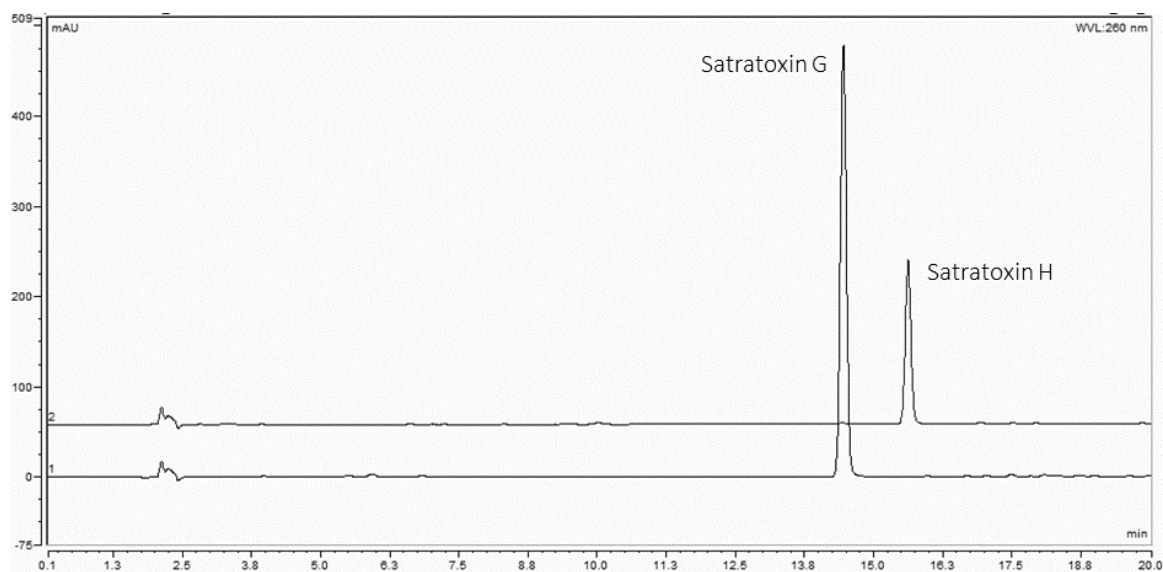


Figure 16 - HPLC assessment of purity for two different fractions. Fraction 1 containing satratoxin H. Fraction 2 containing satratoxin G. In both of these fractions there is a small amount of contamination of the other satratoxin. HPLC conditions were an increasing gradient of ACN in deionised water using a C18 reversed-phase column and a UV/Vis detector.

Figure 17 is a HPLC chromatogram of the two fractions from Figure 16 that have undergone further purification to remove the opposite satratoxin contamination. This level of purity made the samples suitable for the final measure of purity by LCMS.

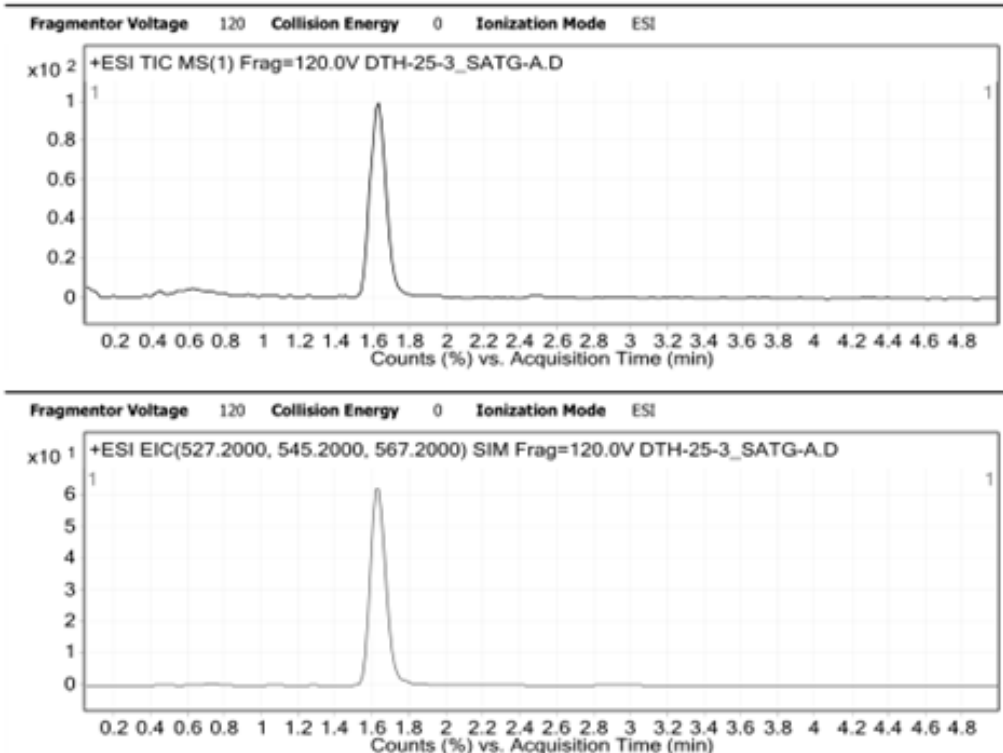


*Figure 17 - HPLC assessment of two fractions that have gone through further round of purification to remove trace amounts of contamination. These two fractions were subsequently used for LCMS and NMR. HPLC conditions were an increasing gradient of ACN in deionised water using a C18 reversed-phase column and a UV/Vis detector.*

Following the verification of the HPLC method and a suitable level of fraction purity was achieved a much quicker LCMS method was developed. The LCMS method used a 50 x 3 mm reversed-phase C18 column with a flow rate of 0.5 mL/min, running conditions were 45% deionised water with 55% MeOH for 10 minutes, signals were detected with UV/Vis at 225, 260, and 300 nm wavelengths, Single Ion Monitoring recorded for protonated, sodiated, and loss of water species. The LCMS platform provides both chromatograms and mass spectra. This method enables confirmation that the fractions contain purified satratoxins due to the chemical formula that is derived from the MS data.

Figure 18 shows the LCMS data for satratoxin G. The chromatograms show the purity of the satratoxin G sample. The MS data provides a  $m/z$  value of 545.2, consistent with a  $[M + H]^+$  pseudomolecular ion based upon the molecular formula found in the literature. Figure 19 shows the LCMS data for satratoxin H. The chromatograms show the purity of the satratoxin H sample. The MS data provides a  $m/z$  value of 529.2, consistent with a  $[M + H]^+$  pseudomolecular ion based upon the molecular formula found in the literature. In both Figure 18 and 19 sodium adducts can be observed in the LCMS chromatograms.

## User Chromatograms



## User Spectra

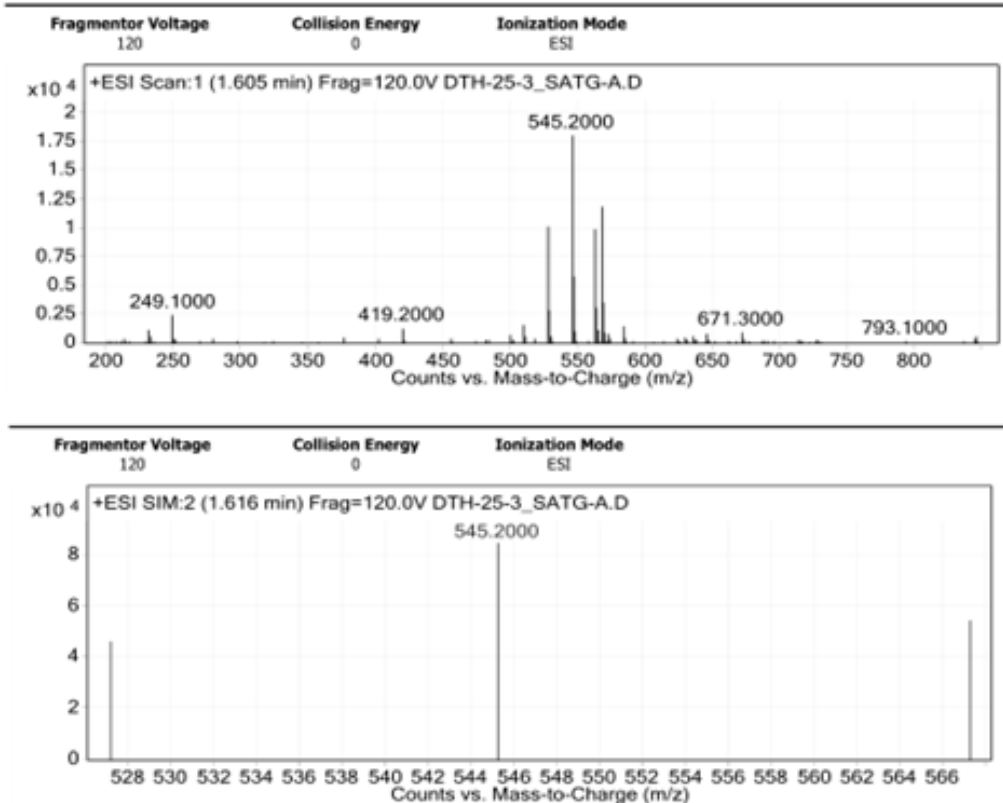
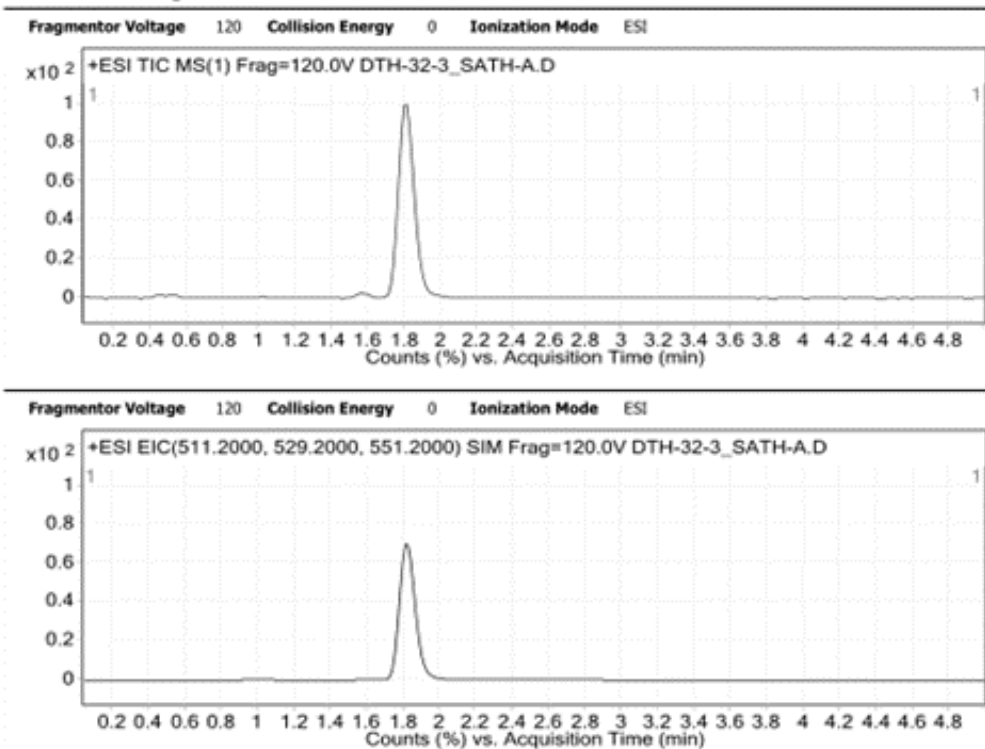


Figure 18 - Satratoxin G LCMS data, providing chromatography and mass spectral data. LCMS conditions was an isocratic run of 45% deionised water with 55% MeOH, using a reversed-phase C18 column, UV/Vis detection, and Single Ion Monitoring.



## User Chromatograms



## User Spectra

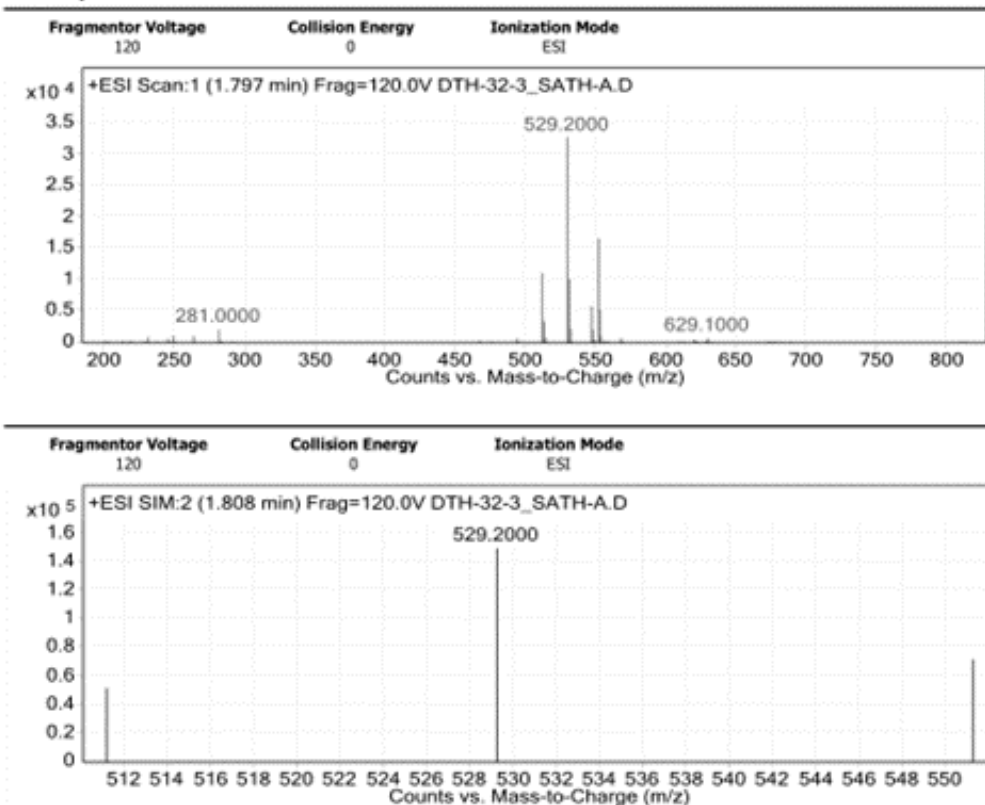


Figure 19 - Satratoxin H LCMS data, providing chromatography and mass spectral data. LCMS conditions was an isocratic run of 45% deionised water with 55% MeOH, using a reversed-phase C18 column, UV/Vis detection, and Single Ion Monitoring.

## 2.8 Summary

This study of New Zealand strains of *S. chartarum* and the metabolites contained within crude extracts was undertaken to identify their characteristics and determine if they contained the metabolites of interest, namely the satratoxins G and H. Although only four strains were used they were isolated from different locations and at different times, this was judged to be suitable for an initial screening with further testing being done on samples obtained directly from the environment.

Despite the absence of a genetic screen some conclusions can be drawn from the information provided by the ICMP database and from what was found from the MSMS analysis. Notably, it means we can confirm that strains capable of producing satratoxins and other toxic metabolites are present in New Zealand. This also provides a reason to begin sampling the environments of people suffering from adverse respiratory symptoms for these metabolites.

The secondary goal of isolating the satratoxins into purified fractions was also successful. The purified satratoxin fractions enabled full NMR spectral information to be obtained for characterisation. This is discussed in the next chapter.

### 3. NMR Characterisation

#### 3.1 Introduction

The data presented in section 2.7 confirmed that the purified samples were the satratoxins G and H making them suitable for NMR characterisation. As stated previously satratoxins are part of the trichothecene family. A large group of over 200 toxic metabolites identified by the presence of the trichothecene core, a tricyclic 12,13-epoxytrichothene-9-ene structure (Figure 20).<sup>36</sup> Trichothecenes are differentiated into four types, A-D, based upon the substitution pattern. Macrocyclic trichothecenes, such as the satratoxins, are known as type D trichothecenes with a macrocyclic ring structure linking C-4 to C-15 (Figure 21).

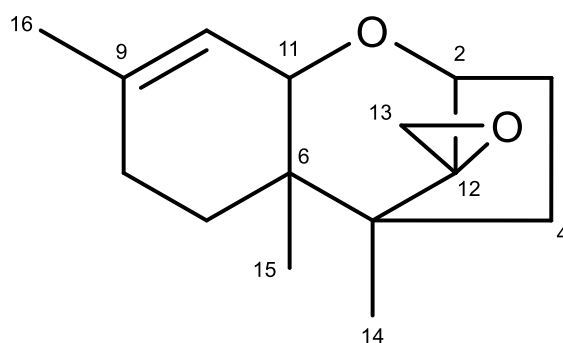


Figure 20 - The tricyclic 12,13-epoxytrichothene-9-ene structure that forms the core of every trichothecene.

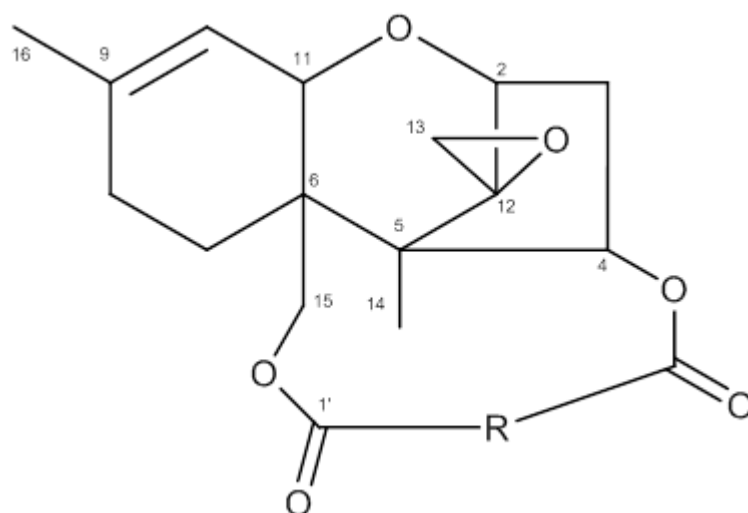


Figure 21 - Type D trichothecenes contain a macrocyclic ring from C-4 to C-15.

For the full NMR characterisation proton, carbon, DEPT, COSY, HSQC, and HMBC spectra were obtained. Preliminary analysis of the satratoxin  $^{13}\text{C}$  and  $^1\text{H}$   $\text{CDCl}_3$  NMR spectra showed strong similarities to the values reported by Eppley et. al. in 1977,<sup>46</sup> and 1980.<sup>47</sup> These articles report the molecular formulas of satratoxins G and H as  $\text{C}_{29}\text{H}_{36}\text{O}_{10}$  and  $\text{C}_{29}\text{H}_{36}\text{O}_9$ , respectively.

Throughout this chapter correlations from NMR analysis from both  $\text{CDCl}_3$  and  $\text{DMSO}-d_6$  are used. To represent different correlations the following system is used; COSY correlations are represented by a bold bond, HMBC correlations are represented by arrows. The colours of the bonds and arrows change depending upon the solvent that the correlation is from (Figure 22). Correlations come from NMR analysis done in  $\text{CDCl}_3$  unless stated otherwise.

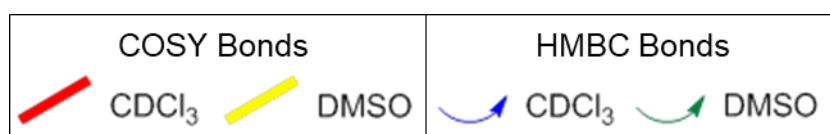


Figure 22 - Legend for how correlation types are represented in substructure figures.

## 3.2 Satratoxin G

Mass spectrometry data provided a  $[\text{M} + \text{Na}]^+$  pseudomolecular ion of  $m/z$  567.2205, revealing a molecular formula of  $\text{C}_{29}\text{H}_{36}\text{O}_{10}$  for satratoxin G, this is consistent with both the  $^{13}\text{C}$  and  $^1\text{H}$  NMR spectra and the information found in literature.

All 29 carbon resonances of satratoxin G were identified through interpretation of the  $^{13}\text{C}$ , DEPT, and HSQC NMR spectra; three methyl groups ( $\delta_{\text{C}}$  8.0; 16.0; 23.3), four methylene groups ( $\delta_{\text{C}}$  20.1; 22.6; 27.5; 34.4), three oxymethylene groups ( $\delta_{\text{C}}$  48.1; 60.1; 64.9), five methine groups ( $\delta_{\text{C}}$  118.7; 119.9; 131.5; 131.9; 144.2), six oxymethine groups ( $\delta_{\text{C}}$  61.0; 68.1; 70.0; 72.4; 73.7; 79.2), and eight non-protonated groups ( $\delta_{\text{C}}$  43.2; 49.2; 65.7; 65.4; 81.2; 140.4; 166.9; 166.9).

The  $^1\text{H}$  and HSQC NMR spectra of satratoxin G showed that 34 of the 36 protons were bonded to carbon, meaning the other two protons were bonded to oxygens. Detailed analysis of the COSY and HMBC NMR data of satratoxin G revealed seven substructures.

The first substructure (Figure 23) consisted of a three-carbon unit consisting of a methylene CH<sub>2</sub>-3 ( $\delta_{\text{H}}$  2.44, 2.20;  $\delta_{\text{C}}$  34.4), and two oxymethines CH-2 ( $\delta_{\text{H}}$  3.83;  $\delta_{\text{C}}$  79.2) and CH-4 ( $\delta_{\text{H}}$  5.91;  $\delta_{\text{C}}$  73.7).

The bonds between these three carbons were established by the COSY correlations between H-2 and H-3b and H-4 and H<sub>2</sub>-3. HMBC correlations from H-2 to C-4, H-3a to C-2, H-3b to C-2, and H-3b to C-4 confirmed the connectivity of these three carbons. Of further interest with this substructure is that the chemical shift value of CH-4 is in the range of esters, the macrocyclic trichothecenes have ester linkages between the trichothecene core and the macrocyclic ring. Substructure 1 is shown in Figure 3 with the proposed ester linkage. HMBC correlations from H-4 to C-11' ( $\delta_{\text{C}}$  166.9) provided a link to the other side of the ester linkage.

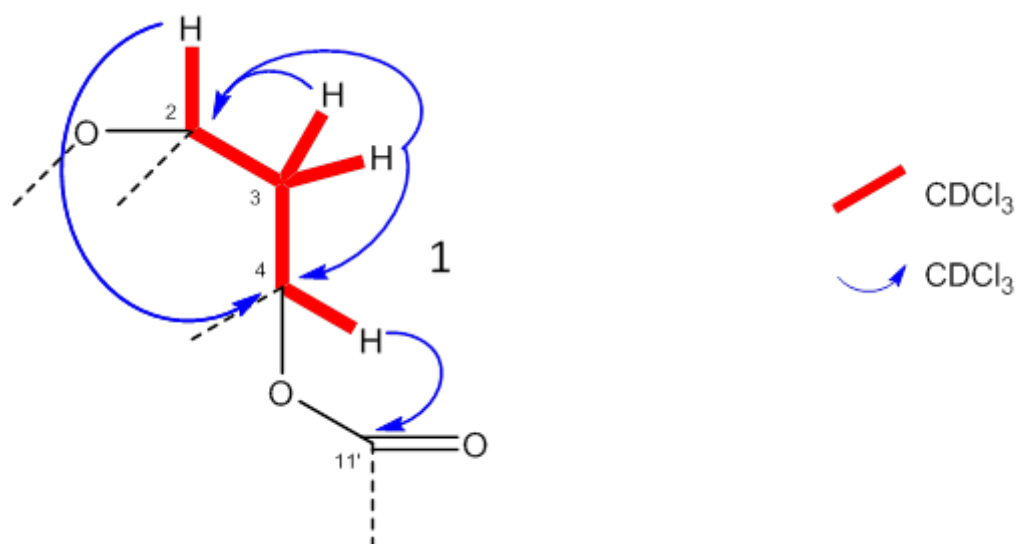


Figure 23 - COSY and HMBC correlations establishing substructure 1 of satratoxin G.

The second substructure (Figure 24) consisted of a six-carbon unit consisting of a methyl CH<sub>3</sub>-16 ( $\delta_{\text{H}}$  1.71;  $\delta_{\text{C}}$  23.3), two methylenes CH<sub>2</sub>-8 ( $\delta_{\text{H}}$  2.04, 2.00;  $\delta_{\text{C}}$  27.5) and CH<sub>2</sub>-7 ( $\delta_{\text{H}}$  1.87;  $\delta_{\text{C}}$  20.1), an oxymethine CH-11 ( $\delta_{\text{H}}$  3.58;  $\delta_{\text{C}}$  68.1), a methine CH-10 ( $\delta_{\text{H}}$  5.42;  $\delta_{\text{C}}$  118.7), and a quaternary carbon C-9 ( $\delta_{\text{C}}$  144.2).

COSY correlations revealed two sequences, a) between H-10 and H-11, H-10 and H-16 (long range), H-11 and H-16 (long range), and b) between H<sub>2</sub>-8 and H<sub>2</sub>-7. The HMBC correlations H-10 to C-16, H-11 to C-9, H-11 to C-10, and H<sub>2</sub>-7 to C-8 support the order of carbons in these sequences.

The protons on CH<sub>3</sub>-16 provided characteristically strong HMBC correlations to three resonances, establishing links between H-16 to C-9, H-16 to C-10, and H-16 to C-8. The HMBC correlations from H-8a to C-9 and H-16 to C-8 link the two COSY fragments together. Finally, there is an HMBC correlation from H-11 to C-7. This correlation would be much weaker than the observed strength of it if substructure 2 is linear as shown in Figure 24, suggesting some other form of link between the two carbons.

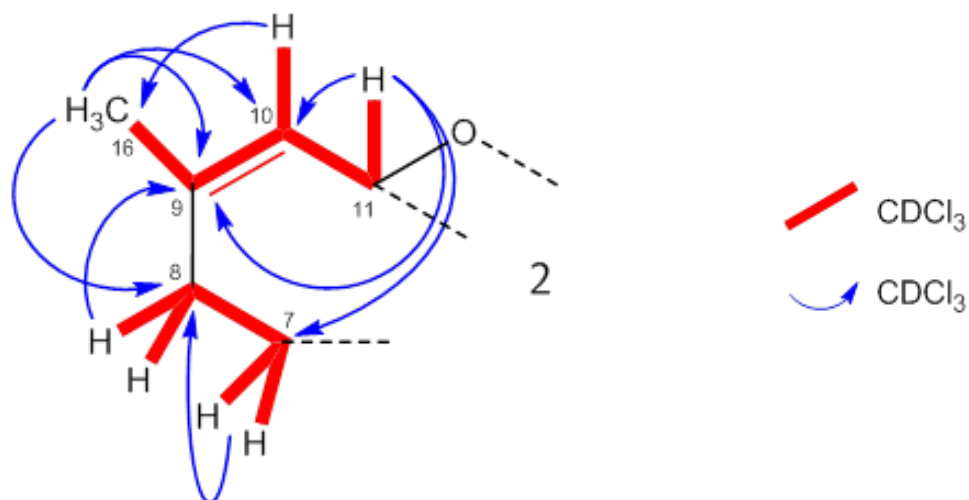


Figure 24 - COSY and HMBC correlations establishing substructure 2 of satratoxin G.

The third substructure (Figure 25) was a singular oxymethylene CH<sub>2</sub>-13 ( $\delta_{\text{H}}$  3.13, 2.81;  $\delta_{\text{C}}$  48.1), and a quaternary carbon C-12 ( $\delta_{\text{C}}$  65.4). The observed COSY correlation is between the hydrogens both linked to the same carbon, H-13a and H-13b. HMBC correlations from DMSO-*d*<sub>6</sub> data link H<sub>2</sub>-13 to C-12.

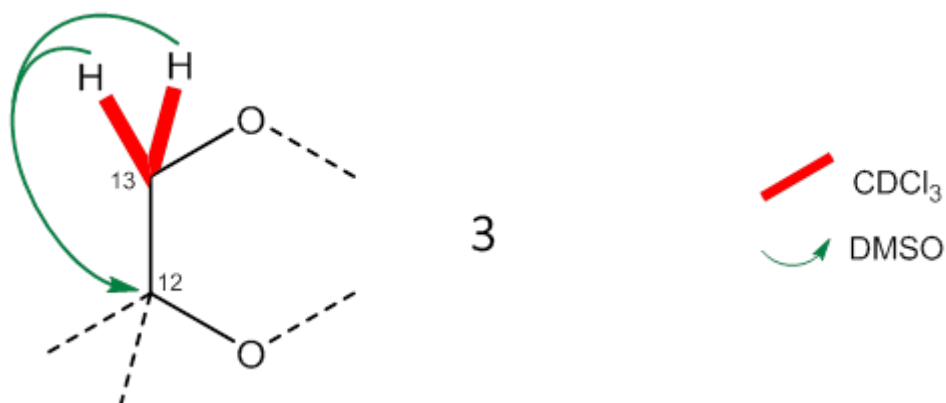


Figure 25 - COSY and HMBC correlations establishing substructure 3 of satratoxin G.

Similar to substructure 3 the fourth substructure (Figure 26) begins with a singular oxymethylene CH<sub>2</sub>-15 ( $\delta_{\text{H}}$  4.38, 4.11;  $\delta_{\text{C}}$  64.9). The observed COSY correlation is between the hydrogens both linked to the same carbon, H-15a and H-15b. The chemical shift value of CH<sub>2</sub>-15 is in the range of an oxymethylene that is part of an ester, the macrocyclic trichothecenes have ester linkages between the trichothecene core and the macrocyclic ring. Substructure 4 is shown in Figure 6 with HMBC correlations from H<sub>2</sub>-15 to C-1' ( $\delta_{\text{C}}$  166.9) providing a link to the other side of the ester linkage.



Figure 26 - COSY and HMBC correlations establishing substructure 4 of satratoxin G.

The fifth substructure (Figure 27) consisted of a five-carbon unit consisting of an oxymethylene CH<sub>2</sub>-5' ( $\delta_{\text{H}}$  3.99, 3.93;  $\delta_{\text{C}}$  60.1), a methylene and CH<sub>2</sub>-4' ( $\delta_{\text{H}}$  2.42;  $\delta_{\text{C}}$  22.63), two oxymethines CH-2' ( $\delta_{\text{H}}$  3.41;  $\delta_{\text{C}}$  61.0) and CH-12' ( $\delta_{\text{H}}$  3.26;  $\delta_{\text{C}}$  72.4), a quaternary carbon C-3' ( $\delta_{\text{C}}$  65.4), and from the DMSO-*d*<sub>6</sub> data a hydroxyl proton ( $\delta_{\text{H}}$  4.28).

The COSY correlations between H-12' and H<sub>2</sub>-4', H-5a' and H-5b', H-5a' and H<sub>2</sub>-4' provide evidence for the carbons C-12', C-5', and C-4' to be linked. Substructure 5 (Figure 7) shows the link between H-12' and H<sub>2</sub>-4' via C-3', this linkage is supported by the varying strength of the HMBC correlations observed between H-12' to C-3', H-12' to C-4', H-5a' to C-3', H-5b' to C-4', H<sub>2</sub>-5' to C-3', H<sub>2</sub>-5' to C-4', H<sub>2</sub>-4' to C-12'. The position of C-2' is established by the HMBC correlations from H-2' to C-3', H-2' to C-12', H<sub>2</sub>-4' to C-2', and H-12' to C-2'. Finally, from the DMSO-*d*<sub>6</sub> data there is a COSY correlation from the hydroxyl proton on C-12' linking the OH to H-12', and there is a HMBC correlation from the OH to C-12'.

The sixth substructure (Figure 28) consisted of a five-carbon unit consisting of four methenes CH-9' ( $\delta_{\text{H}}$  6.65;  $\delta_{\text{C}}$  144.2), CH-7' ( $\delta_{\text{H}}$  5.88;  $\delta_{\text{C}}$  131.9), CH-8' ( $\delta_{\text{H}}$  6.95;  $\delta_{\text{C}}$  131.5) and CH-10' ( $\delta_{\text{H}}$  5.90;  $\delta_{\text{C}}$  119.9), and a quaternary carbon C-11' ( $\delta_{\text{C}}$  166.9).

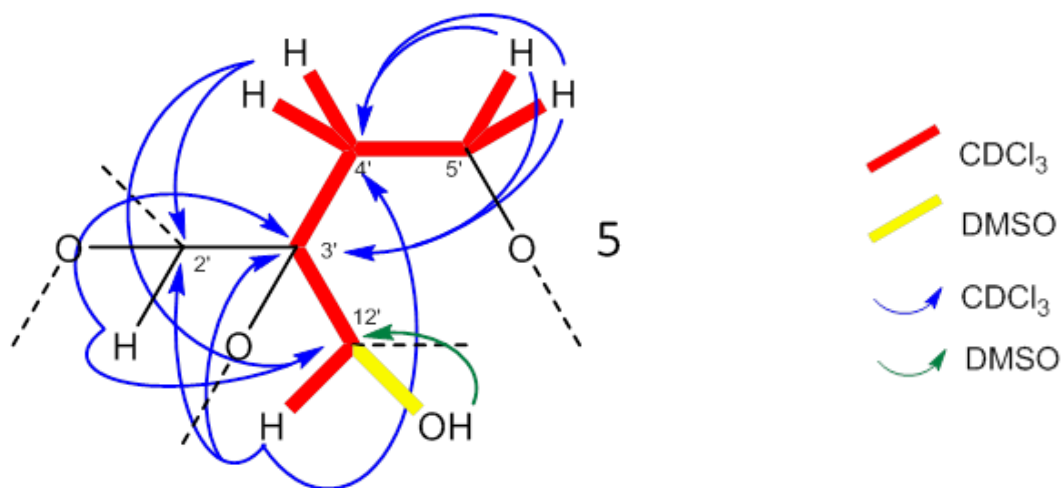


Figure 27 - COSY and HMBC correlations establishing substructure 5 of satratoxin G.

The COSY correlations between H-9' and H-8', H-9' and H-10', H-7' and H-8' provided evidence for the carbons C-10', C-9', C-8' and C-7' to be linked in a linear sequence. HMBC correlations from H-9' to C-11' and H-10' to C-11' provide evidence for the placement of C-11'. The very high  $^{13}\text{C}$  chemical shift of C-11' is typical of an ester, C-11' is shown as an ester in substructure 6. The remaining HMBC correlations from H-9' to C-7', H-7', to C-9', H-8' to C-10', H-10' to C-9' further support the connectivity and order of the carbons in this substructure.

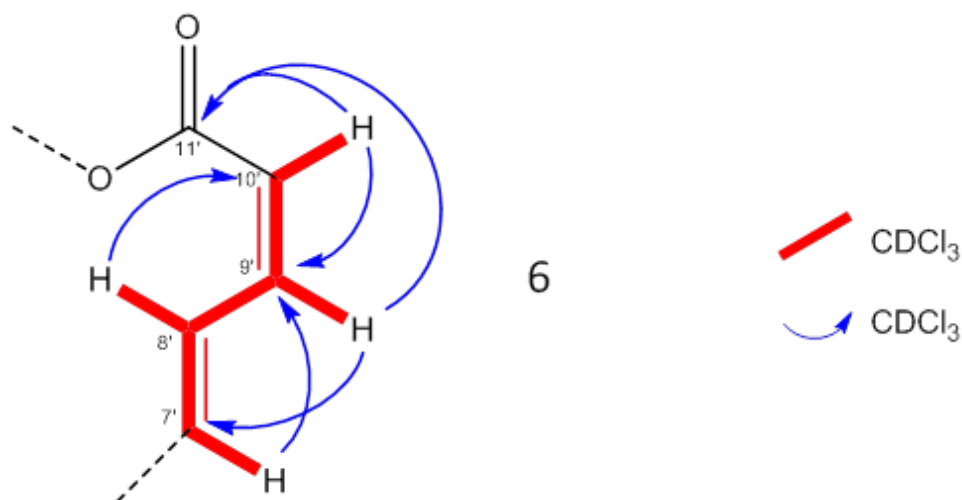


Figure 28 - COSY and HMBC correlations establishing substructure 6 of satratoxin G.



The seventh substructure (Figure 29) consisted of a three-carbon unit consisting of a methyl CH<sub>3</sub>-14' ( $\delta_{\text{H}}$  1.10;  $\delta_{\text{C}}$  16.0), an oxymethine CH-13' ( $\delta_{\text{H}}$  4.35;  $\delta_{\text{C}}$  70.0), a quaternary carbon C-6' ( $\delta_{\text{C}}$  81.4), and from the DMSO-*d*<sub>6</sub> data a hydroxyl proton ( $\delta_{\text{H}}$  5.29). A COSY correlation between H-13' and H-14' provided evidence for the connectivity between C-13' and C-14', while an HMBC correlation from H<sub>3</sub>-14' to C-13' and C-6' strengthened this relationship and extended the substructure further. Lastly from the DMSO-*d*<sub>6</sub> data there is a COSY correlation from the hydroxyl proton on C-13' linking the OH to H-13', and there is a HMBC correlation from the OH to C-13'.

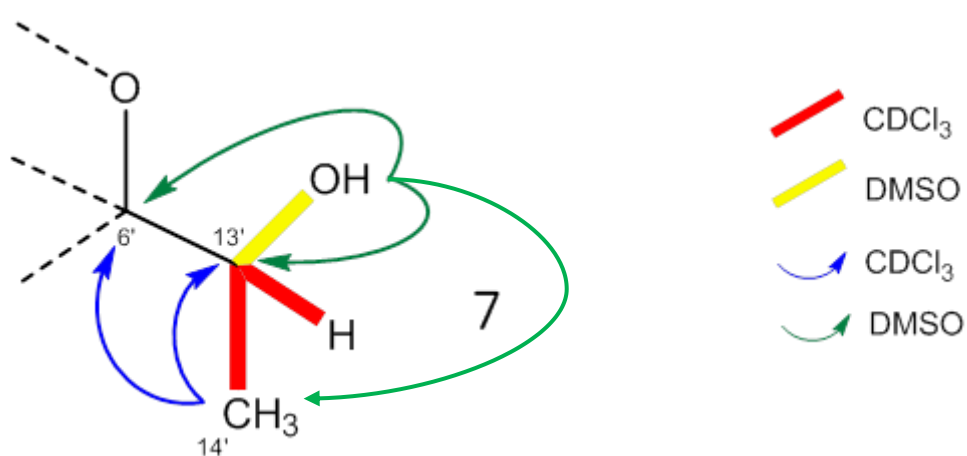


Figure 29 - COSY and HMBC correlations establishing substructure 7 of satratoxin G.

The substructures 1-4 can be linked through HMBC correlations between them, these correlations in addition to HMBC correlations from isolated carbon moieties that could not be linked into substructures enabled these fragments to be assembled into the trichothecene core (Figure 30).

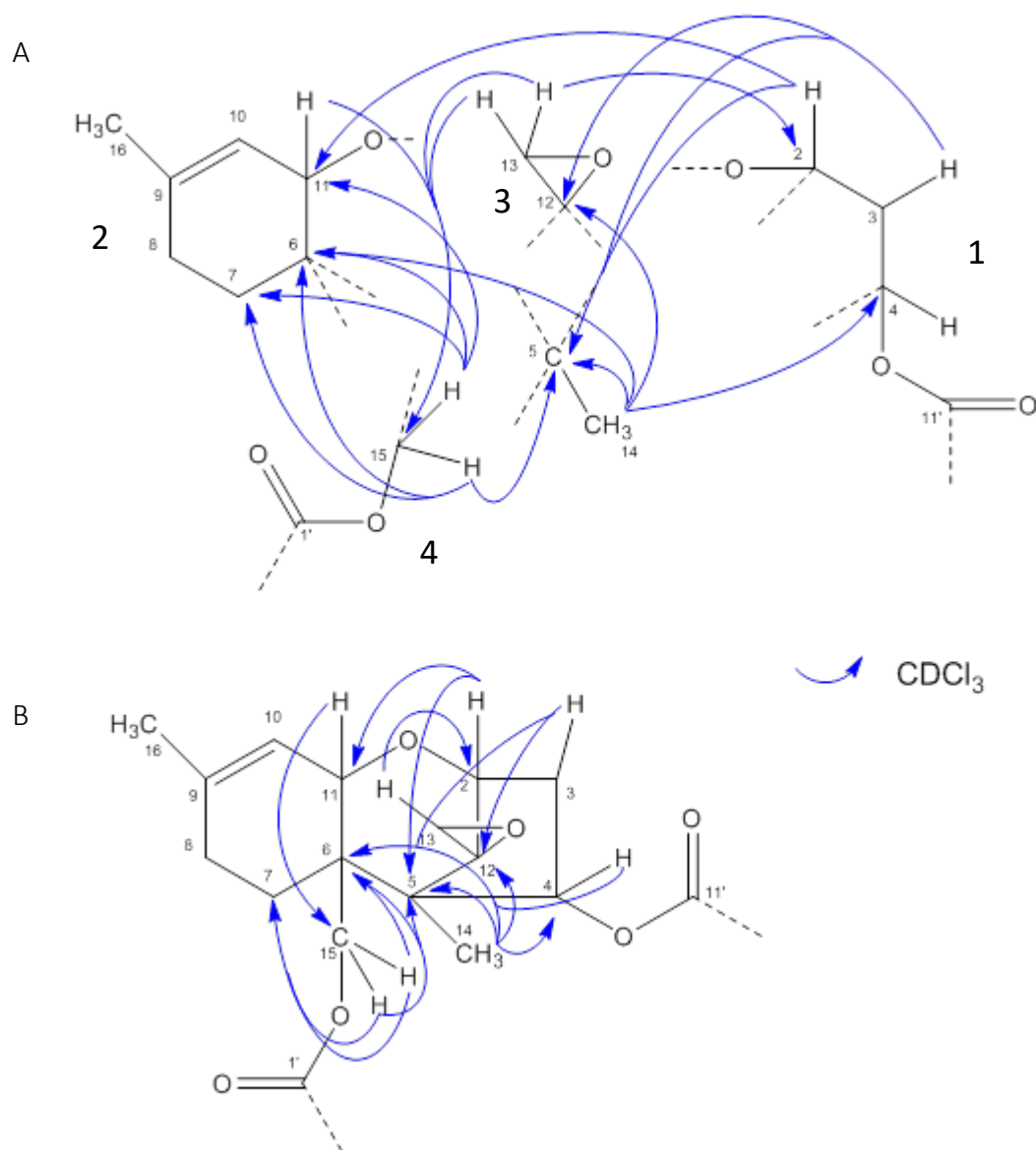


Figure 30 - A) HMBC correlations between substructures 1-4 and isolated carbon moieties that establish the connectivity between them to form the trichothecene core of satratoxin G, B) Substructures 1-4 and isolated carbon moieties organised into the trichothecene core of satratoxin G.

Substructures 5-7 can be linked through HMBC correlations between them, these correlations in addition to HMBC correlations from isolated carbon moieties that could not be linked into substructures enabled these fragments to be assembled into the macrocyclic ring of satratoxin G (Figure 31).

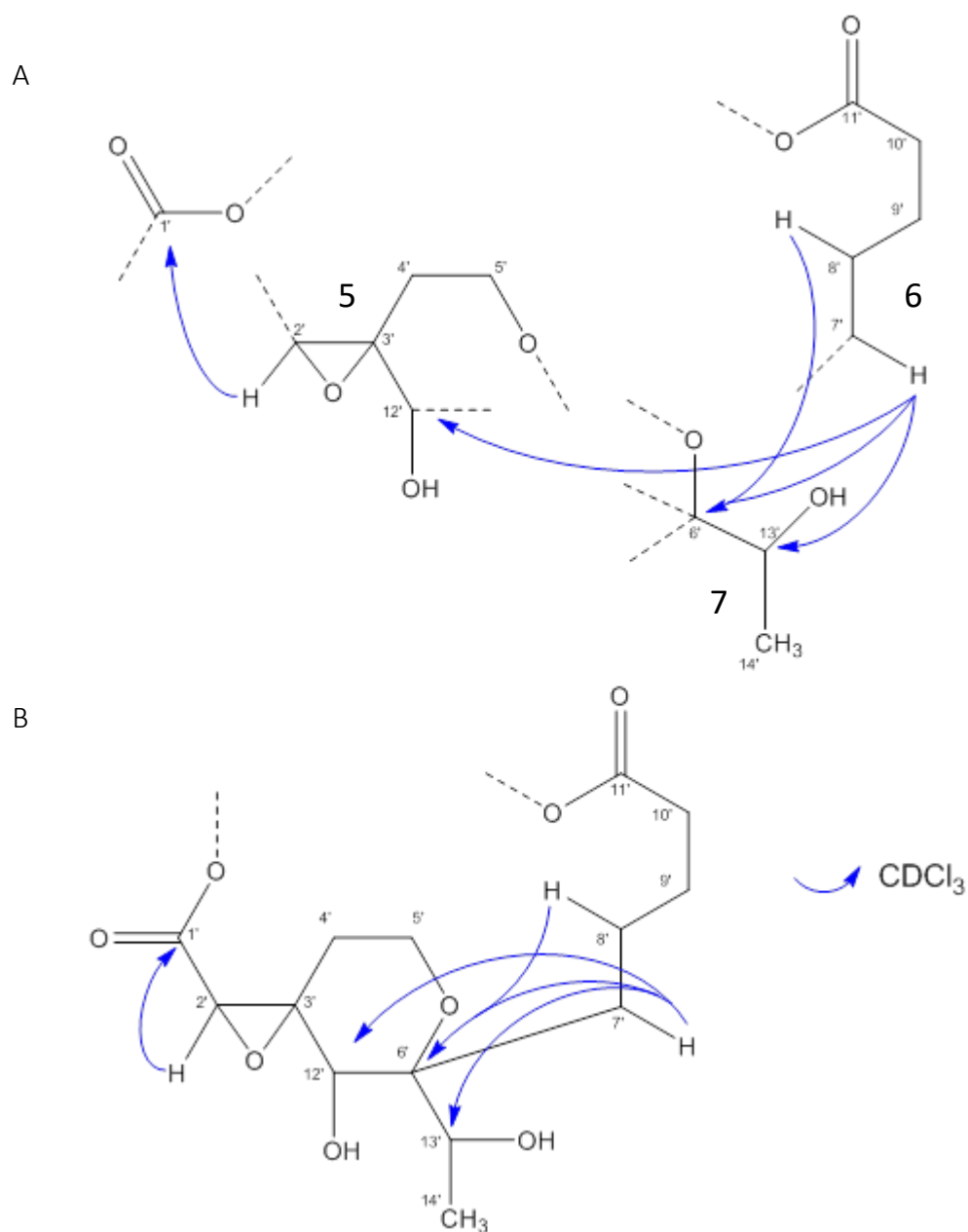


Figure 31 - A) HMBC correlations between substructures 5-7 and isolated carbon moieties that establish the connectivity between them to form the macrocyclic ring of satratoxin G. B) Substructures 5-7 and isolated carbon moieties organised into the macrocyclic ring of satratoxin G.

The HMBC correlations between H<sub>2</sub>-15 to C-1', and H-4 to C-11' provide the link between the trichothecene core and the macrocyclic ring through the esters forming the complete satratoxin G structure (Figure 32).

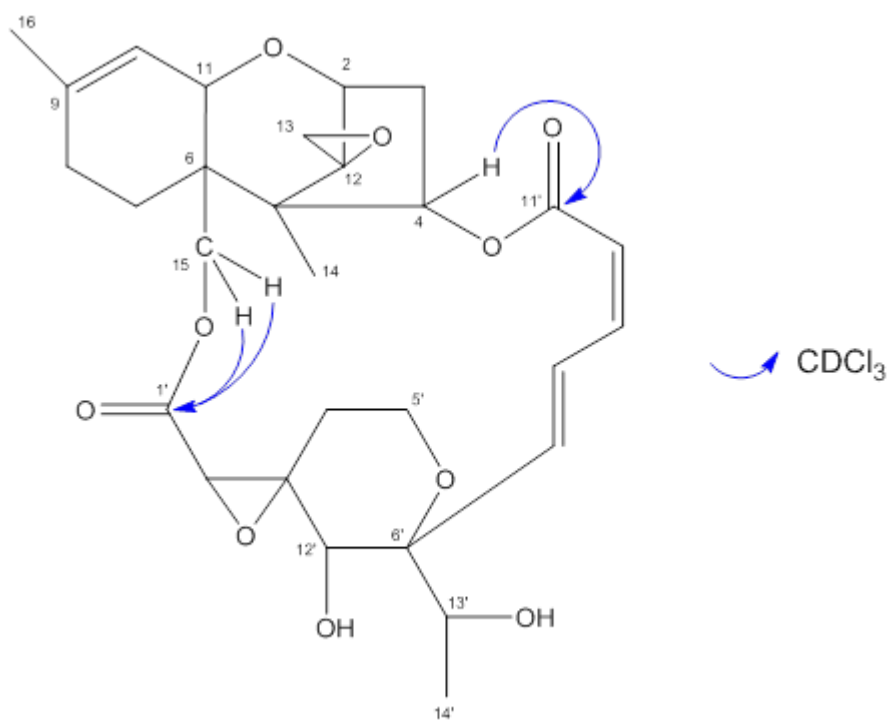


Figure 32 - The completed satratoxin G structure with the HMBC correlations that link the trichothecene core and the macrocyclic ring.

Table 3 - Satratoxin G (6) NMR data in CDCl<sub>3</sub>.

Satratoxin G - CDCl <sub>3</sub>								
Position	<sup>13</sup> C	DEPT	HSQC	<sup>1</sup> H Peak	<i>J</i> = Hz	<i>n</i> H	HMBC	COSY
2	79.2	CH	3.83	d	(4.9)	1	C-4, C-5, C-11	H-3b
3	34.4	CH <sub>2</sub>	2.44	dd	(15.2, 8.6)	1	C-5, C-12	H-3b, H-4
			2.20	dt	(15.1, 5.0)	1	C-2, C-4	H-2, H-3a, H-4
4	73.7	CH	5.91	dd	(8.7, 5.3)	1	C-6, C-11'	H <sub>2</sub> -3
5	49.2	C						
6	43.2	C						
7	20.1	CH <sub>2</sub>	1.87	m		2	C-8	H <sub>2</sub> -8
8	27.5	CH <sub>2</sub>	2.04	m		1	C-9	H <sub>2</sub> -7, H-8b
			2.00	m		1		H <sub>2</sub> -7, H-8a
9	140.4	C						
10	118.7	CH	5.42	d	(4.6)	1	C-16	H-11, H-16
11	68.1	CH	3.58	d	(5.1)	1	C-7, C-9, C-10, C-15	H-10, H-16
12	65.4	C						
13	48.1	CH <sub>2</sub>	3.13	d	(4.0)	1	C-2, C-15	H-13b
			2.81	d	(4.0)	1	C-15	H-13a
14	8.0	CH <sub>3</sub>	0.83	s		2	C-4, C-5, C-6, C-12	
15	64.9	CH <sub>2</sub>	4.38	d	(12.6)	1	C-6, C-7, C-11, C-1'	H-15b
			4.11	d	(12.6)	1	C-5, C-6, C-7, C-1'	H-15a
16	23.3	CH <sub>3</sub>	1.71	s		3	C-8, C-9, C-10	H-10, H-11
1'	166.9	C						
2'	61.0	CH	3.41	s		1	C-1', C-3', C-12'	
3'	65.4	C						
4'	22.6	CH <sub>2</sub>	2.42	m		2	C-2', C-12'	H <sub>2</sub> -5', H-12'
5'	60.1	CH <sub>2</sub>	3.99	ddd	(12.0, 10.3, 4.8)	1	C-3', C-4'	H <sub>2</sub> -4', H-5'b
			3.93	ddd	(12.3, 4.6, 3.2)	1	C-3', C-4'	H <sub>2</sub> -4', H-5'a
6'	81.4	C						
7'	131.9	CH	5.88	dd	(16.7, 2.1)	1	C-6', C-9', C-12', C-13'	H-8'
8'	131.5	CH	6.95	ddd	(16.9, 8.1, 1.3)	1	C-6', C-8', C-10'	H-7', H-9'
9'	144.2	CH	6.65	ddd	(11.2, 8.1, 1.3)	1	C-7', C-11'	H-8', H-10'
10'	119.9	CH	5.90	dd	(11.3, 1.9)	1	C-9', C-11'	H-9'
11'	166.9	C						
12'	72.4	CH	3.26	s		1	C-2', C-3', C-4'	H <sub>2</sub> -4'
13'	70.0	CH	4.35	q	(6.5)	1		H-14'
14'	16.0	CH <sub>3</sub>	1.10	d	(6.5)	3	C-6', C-13'	H-13'

Table 4 - Satratoxin G NMR (6) data in DMSO-*d*<sub>6</sub>.

Satratoxin G - DMSO - <i>d</i> <sub>6</sub>								
Position	<sup>13</sup> C	DEPT	HSQC	<sup>1</sup> H Peak	<i>J</i> = Hz	<i>n</i> H	HMBC	COSY
2	78.1	CH	3.70	d	5.0	1	C-4, C-5, C-11, C-12	H-3b
3	34.0	CH <sub>2</sub>	2.44	dd	(14.8, 8.4)	1	C-2, C-12	H-4
			1.96	m		1		
4	73.6	CH	5.95	dd	(8.4, 4.9)	1	C-6, C-12	H-3, H-11
5	48.7	C						
6	42.6	C						
7	19.4	CH <sub>2</sub>	1.76	m		2		H <sub>2</sub> -8
8	26.8	CH <sub>2</sub>	1.97	m		2		H <sub>2</sub> -7
9	138.4	C						
10	119.2	CH	5.32	d	(5.4)	1		H-11, H-16
11	66.8	CH	3.73	m		1	C-9, C-10	H-10
12	65.4	C						
13	47.2	CH <sub>2</sub>	3.07	dd	(4.0)	1	C-2, C-12	H-13b
			2.80	dd	(4.0)	1	C-12	H-13a
14	7.9	CH <sub>3</sub>	0.77	s		3	C-4, C-5, C-6, C-12	
15	64.4	CH <sub>2</sub>	4.26	m		1	C-6, C-7	H-15b
			3.96	dd	(12.5)	1	C-5, C-6, C-1'	H-15a
16	22.7	CH <sub>3</sub>	1.66	s		3	C-8, C-9, C-10	H-10, H-11
1'	167.6	C						
2'	58.3	CH	3.58	s		1	C-1', C-3'	
3'	64.6	C						
4'	22.8	CH <sub>2</sub>	2.27	td	(13.6, 5.9)	1		H-4b, H <sub>2</sub> -5'
			2.04	dt	(13.8, 2.7)	1		H-4a, H <sub>2</sub> -5'
5'	59.2	CH <sub>2</sub>	3.81	dd	(12.0, 2.6)	1		H <sub>2</sub> -4', H-5'b
			3.77	m		1	C-3'	H <sub>2</sub> -4', H-5'a
6'	82.2	C						
7'	132.8	CH	5.84	m		1	C-6', C-9', C-11', C-13'	H-8', H-9'
8'	130.2	CH	6.78	m		1	C-6', C-7', C-10', C-11'	H-7', H-10'
9'	145.2	CH	6.78	m		1	C-6', C-7', C-10', C-11'	H-7', H-10'
10'	118.8	CH	5.89	m		1	C-8'	H-8', H-9'
11'	166.2	C						
12'	68.7	CH	3.21	dd	(5.7)	1	C-3', C-5'	12'-OH
13'	70.9	CH	4.09	qd	(6.5, 4.5)	1	C-6', C-7', C-14'	H-14', 13'-OH
14'	17.3	CH <sub>3</sub>	0.92	d	(6.5)	3	C-12', C-6'	H-12'
12'-OH			4.28	d	(4.3)	1	C-12', C-14'	H-12'
13'-OH			5.29	d	(5.7)	1	C-6', C-13'	H-13'

### 3.3 Satratoxin H

Mass spectrometry data provided a  $[M + Na]^+$  pseudomolecular ion of  $m/z$  551.2256, revealing a molecular formula of  $C_{29}H_{36}O_9$  for satratoxin H, this is consistent with both the  $^{13}C$  and  $^1H$  NMR spectra and the information found in literature.

All 29 carbon resonances of satratoxin H were identified through interpretation of the  $^{13}C$ , DEPT, and HSQC NMR spectra; three methyl groups ( $\delta_C$  7.6; 15.7; 23.3), four methylene groups ( $\delta_C$  20.3; 25.3; 27.6; 34.4), three oxymethylene ( $\delta_C$  48.1; 60.5; 64.2), six methine groups ( $\delta_C$  118.9; 119.1; 120.4; 132.0; 134.2; 142.9), five oxymethine ( $\delta_C$  68.2; 69.7; 73.6; 74.1; 79.1), eight quaternary carbons ( $\delta_C$  43.4; 48.9; 64.5; 81.3; 140.3; 154.9; 166.2; 167.1).

The  $^1H$  and HSQC NMR spectra of satratoxin H showed that 34 of the 36 protons were bonded to carbons, meaning the other two protons were bonded to oxygens. Detailed analysis of the COSY and HMBC NMR data of satratoxin H revealed seven substructures, many of which were very similar to the substructures of satratoxin G.

The first substructure (Figure 33) consisted of a three-carbon unit consisting of a methylene  $CH_2$ -3 ( $\delta_H$  2.42, 2.16;  $\delta_C$  34.4), and two oxymethines  $CH$ -2 ( $\delta_H$  3.82;  $\delta_C$  79.1) and  $CH$ -4 ( $\delta_H$  5.88;  $\delta_C$  74.1).

The bonds between these three carbons were established by the COSY correlations between H-2 and H-3b, H<sub>2</sub>-3 and H-4. HMBC correlations from H-2 to C-4, H-3a to C-2, H-3b to C-4 confirmed the connectivity of these three carbons.

The chemical shift of CH-4 is in the range of a methine linked to an ester, the macrocyclic trichothecenes have ester linkages between the trichothecene core and the macrocyclic ring. Substructure 1 is shown in Figure 33 with the proposed ester linkage, comparison with satratoxin G would suggest that C-4 is linked to C-11' through this ester but without the HMBC correlation from H-4 to C-11' that was observed in the satratoxin G data the carbon is currently unassigned.

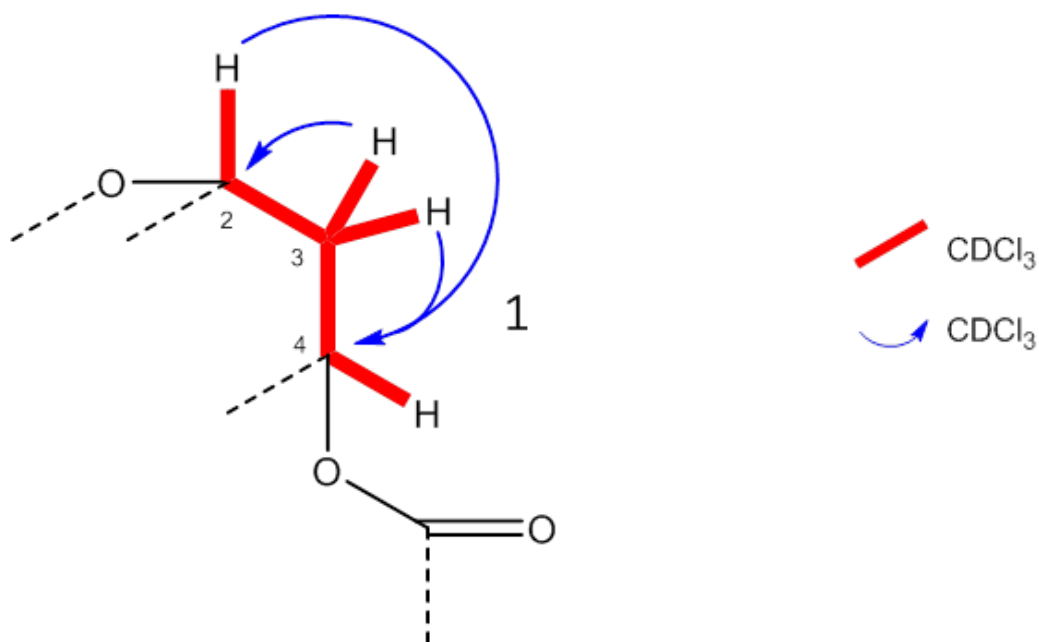


Figure 33 - COSY and HMBC correlations establishing substructure 1 of satratoxin H.

The second substructure (Figure 34) consisted of a six-carbon unit consisting of a methyl CH<sub>3</sub>-16 ( $\delta_{\text{H}}$  1.70;  $\delta_{\text{C}}$  23.3), two methylenes CH<sub>2</sub>-8 ( $\delta_{\text{H}}$  2.02, 1.91;  $\delta_{\text{C}}$  27.6) and CH<sub>2</sub>-7 ( $\delta_{\text{H}}$  1.87;  $\delta_{\text{C}}$  20.3), an oxymethine CH-11 ( $\delta_{\text{H}}$  3.58;  $\delta_{\text{C}}$  68.2), a methine CH-10 ( $\delta_{\text{H}}$  5.42;  $\delta_{\text{C}}$  118.9) and a quaternary carbon C-9 ( $\delta_{\text{C}}$  140.3).

COSY correlations between H-10 and H-11, H-10 and H-16, H-11 and H-16, H-8a and H-8b, H-8a and H-16, H-8a and H<sub>2</sub>-7 linked all 6 carbons. The hydrogens on CH<sub>3</sub>-16 provided characteristically strong HMBC correlations to three resonances, establishing links between H-16 to C-9, H-16 to C-10, and H-16 to C-8. The HMBC correlations from H<sub>2</sub>-7 to C-6, H-10 to C-6, H-10 to C-8, H-10 to C-16, H-11 to C-7, H-11 to C-9, H-11 to C-10, H-8a to C-9, H-8a to C-7 further support the linking of these carbons.

The HMBC correlations from H-10 to C-6 and H-11 to C-7 would require too many bonds for this substructure to be linear, strongly suggesting that substructure 2 forms a ring structure.



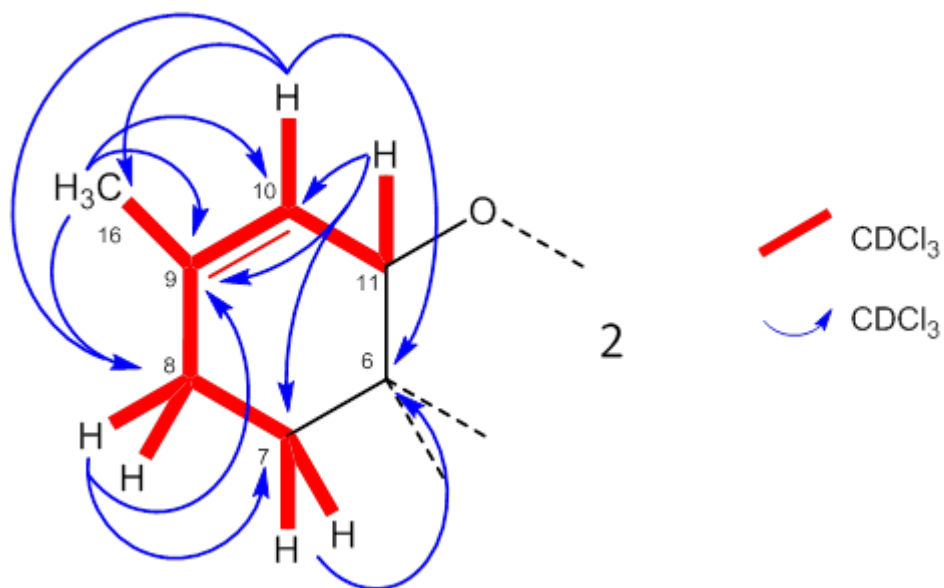


Figure 34 - COSY and HMBC correlations establishing substructure 2 of satratoxin H.

The third substructure (Figure 35) was not revealed until correlations from the DMSO- $d_6$  data were analysed. It consisted of a singular oxymethylene  $\text{CH}_2$ -13 ( $\delta_{\text{H}}$  3.13, 2.81;  $\delta_{\text{C}}$  48.1), and a quaternary carbon C-12 ( $\delta_{\text{C}}$  65.4). The substructure was established by a COSY correlation between H-13a and H-13b, and a HMBC correlation from  $\text{H}_2$ -13 to C-12.

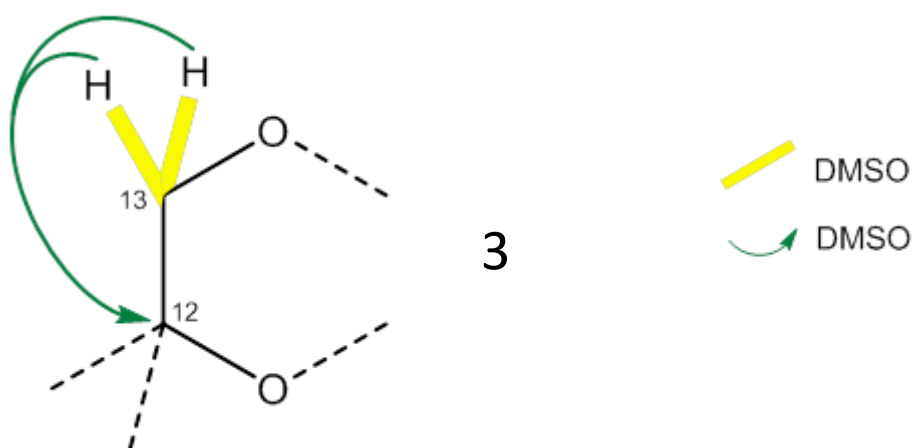


Figure 35 - COSY and HMBC correlations establishing substructure 3 of satratoxin H.

The fourth substructure (Figure 36) is a singular oxymethylene  $\text{CH}_2$ -15 ( $\delta_{\text{H}}$  4.55, 3.84;  $\delta_{\text{C}}$  64.2). The observed COSY correlation is between the hydrogens both linked to the same carbon, H-15a and H-15b. The chemical shift value of  $\text{CH}_2$ -15 is in the range of a oxymethylene that is part of an ester, the macrocyclic trichothecenes has ester linkages between the trichothecene core and the macrocyclic ring, substructure 3 is with the

proposed ester linkage. HMBC correlations from H-15a to C-1' ( $\delta_c$  166.2) provided a link to the other side of the ester linkage.

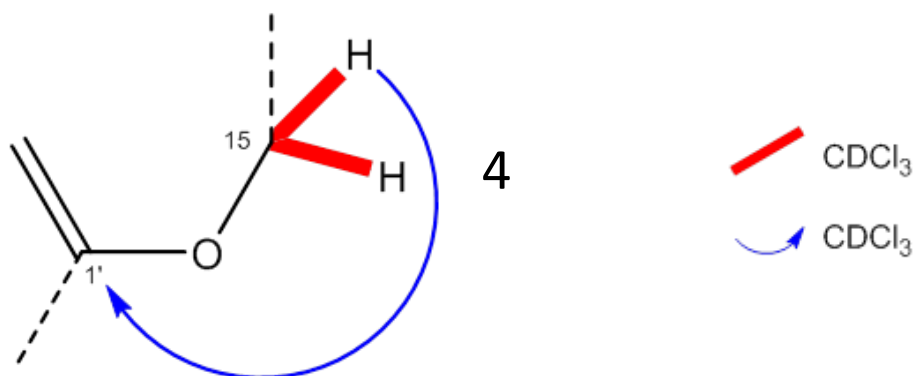


Figure 36 - COSY and HMBC correlations establishing substructure 4 of satratoxin H.

The fifth substructure (Figure 37) consisted of a five-carbon unit forming a ring structure that consists of an oxymethylene  $\text{CH}_2$ -5' ( $\delta_H$  3.88, 3.73;  $\delta_c$  60.5), a methyl  $\text{CH}_2$ -4' ( $\delta_H$  3.86, 2.64;  $\delta_c$  25.3), an oxymethine  $\text{CH}$ -12' ( $\delta_H$  3.96;  $\delta_c$  73.6), a methine  $\text{CH}$ -2' ( $\delta_H$  5.82;  $\delta_c$  119.1), two quaternary carbons C-3' ( $\delta_c$  154.9) and C-6' ( $\delta_c$  81.3), and from the  $\text{DMSO}-d_6$  data a hydroxyl proton ( $\delta_H$  5.32).

There are COSY correlations between H-5a' and H-5b', H-4a' and H-4b', H<sub>2</sub>-5' and H<sub>2</sub>-4'. The HMBC correlations from H-5a' to C-4', H-4b' to C-5' strengthen this relationship. The rest of the ring structure proposed for substructure 4 is proposed through the strength of HMBC correlations. There are HMBC correlations from H1-4' to C-3', H2-4' to C-3', H1-5' to C-6', H-12' to C3', and H-12' to C-4'.

The position of C-2' is established by the HMBC correlations from H-2' to C-4', H-2' to C-12', H-4a' to C-2', and H-12' to C-2'. From the  $\text{DMSO}-d_6$  data there is a COSY correlation from H-2' to H-4'b. Lastly there is a COSY correlation from the hydroxyl proton on C-12' linking the OH to H-12', and HMBC correlations from the OH to C-6', and OH to C-12'.

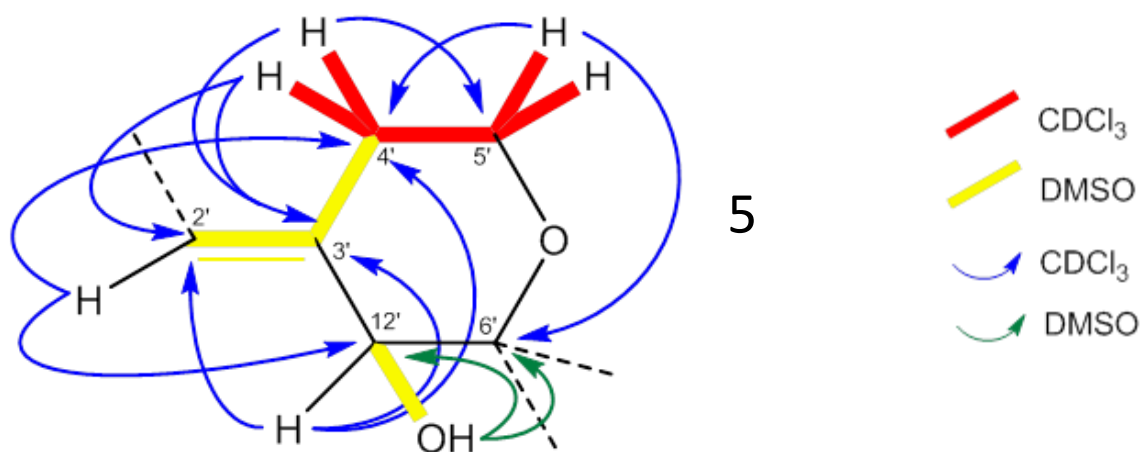


Figure 37 - COSY and HMBC correlations establishing substructure 5 of satratoxin H.

The sixth substructure (Figure 38) consisted of a five-carbon unit consisting of four methines, CH-9' ( $\delta_{\text{H}}$  6.58;  $\delta_{\text{C}}$  142.9), CH-8' ( $\delta_{\text{H}}$  7.32;  $\delta_{\text{C}}$  134.2), CH-7' ( $\delta_{\text{H}}$  6.05;  $\delta_{\text{C}}$  132.0) and CH-10' ( $\delta_{\text{H}}$  5.87;  $\delta_{\text{C}}$  120.4), and a C-11' ( $\delta_{\text{C}}$  167.1).

The COSY correlations between H-9' and H-8', H-9' and H-10', H-8' and H-7' provide evidence for the carbons C-10', C-9', C-8' and C-7' to be linked in a linear structure. HMBC correlations from H-9' to C-11' and H-10' to C-11' provide evidence for the position of C-11'. In substructure 6 C-11' is reported as being part of an ester, evidence for this is provided by the very high  $^{13}\text{C}$  chemical shift of C-11'. The remaining HMBC correlations from H-10' to C-8', H-9' to C-7', H-7' to C-9', H-7' to C-8', H-8' to C-10' and H-8' to C-9', further support the connectivity and order of the carbons in this substructure.

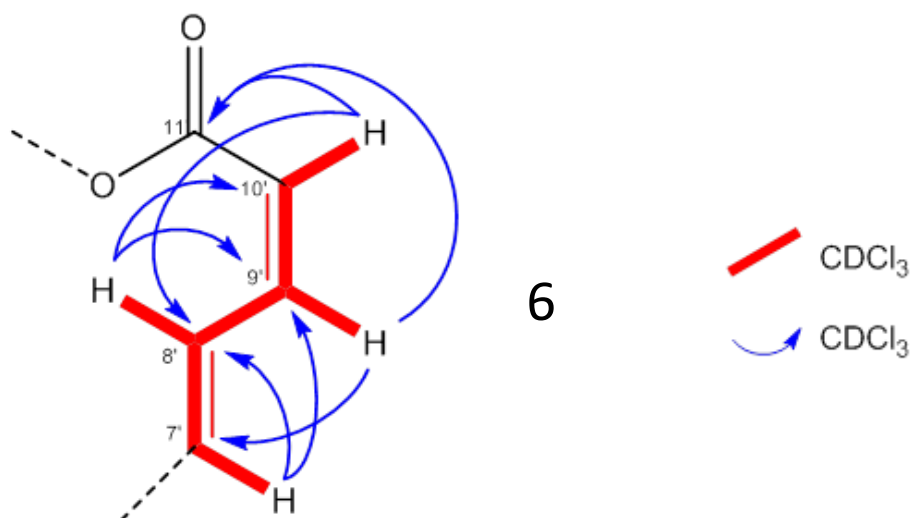


Figure 38 - COSY and HMBC correlations establishing substructure 6 of satratoxin H.

The seventh substructure (Figure 39) consisted of a two-carbon unit consisting of a methyl  $\text{CH}_3\text{-14'}$  ( $\delta_{\text{H}}$  1.14;  $\delta_{\text{C}}$  15.7), an oxymethine  $\text{CH-13'}$  ( $\delta_{\text{H}}$  4.33;  $\delta_{\text{C}}$  69.7), and from the  $\text{DMSO-}d_6$  data a hydroxyl ( $\delta_{\text{H}}$  4.46).

A COSY correlation between  $\text{H-13'}$  and  $\text{H-14'}$  provided evidence for this substructure, HMBC correlations from  $\text{H-13'}$  to  $\text{C-14'}$ ,  $\text{H-14'}$  to  $\text{C-13'}$  strengthened this relationship. Lastly from the  $\text{DMSO-}d_6$  data there is a COSY correlation from the hydroxyl proton on  $\text{C-13'}$  linking the OH to  $\text{H-13'}$ , and there are HMBC correlations from the OH to  $\text{C-13'}$ , and OH to  $\text{C-14'}$ .

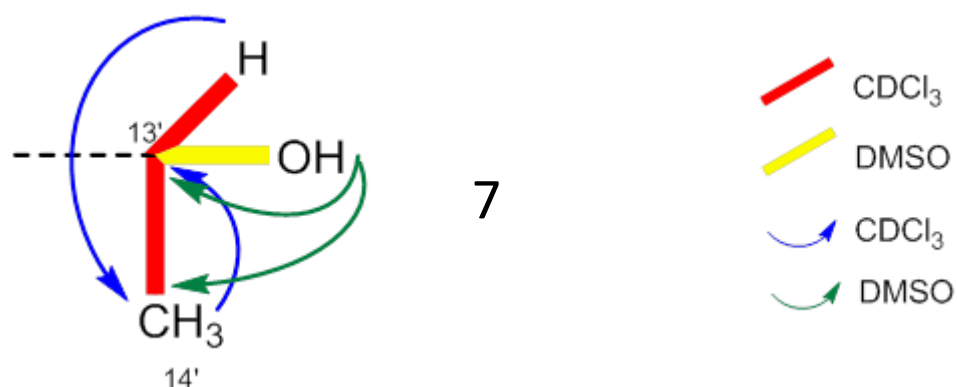


Figure 39 - COSY and HMBC correlations establishing substructure 7 of satratoxin H.

The substructures 1-4 can be linked through HMBC correlations between them, these correlations in addition to HMBC correlations from isolated carbon moieties that could not be linked into substructures enabled these fragments to be assembled into the trichothecene core (Figure 40).

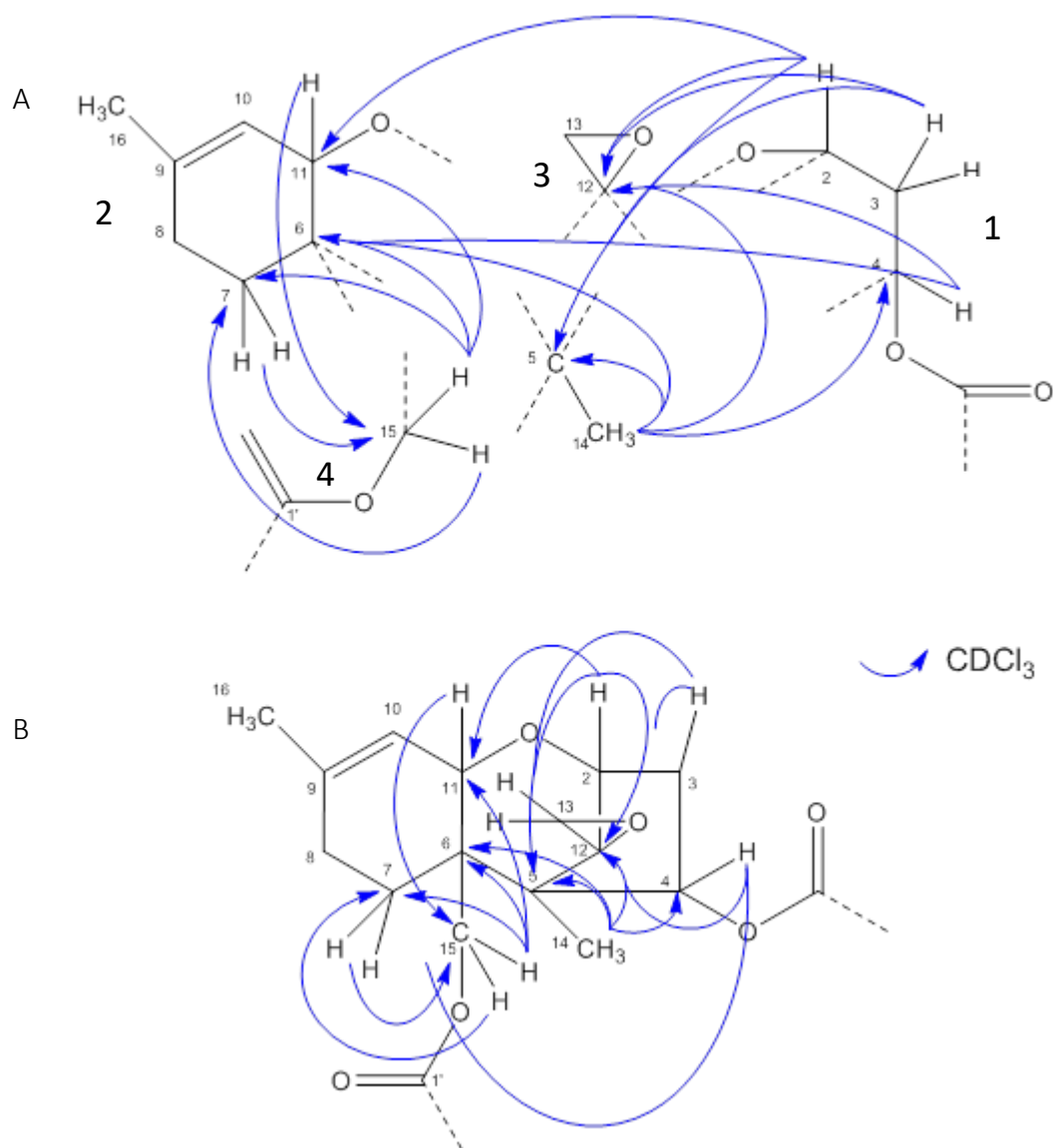


Figure 40 - A) HMBC correlations between substructures 1-4 and isolated carbon moieties that establish the connectivity between them to form the trichothecene core of satratoxin G, B) Substructures 1-4 and isolated carbon moieties organised into the trichothecene core of satratoxin H.

Substructures 5-7 can be linked through HMBC correlations between them, these correlations in addition to HMBC correlations from isolated carbon moieties that could not be linked into substructures enabled these fragments to be assembled into the macrocyclic ring of satratoxin H (Figure 41).

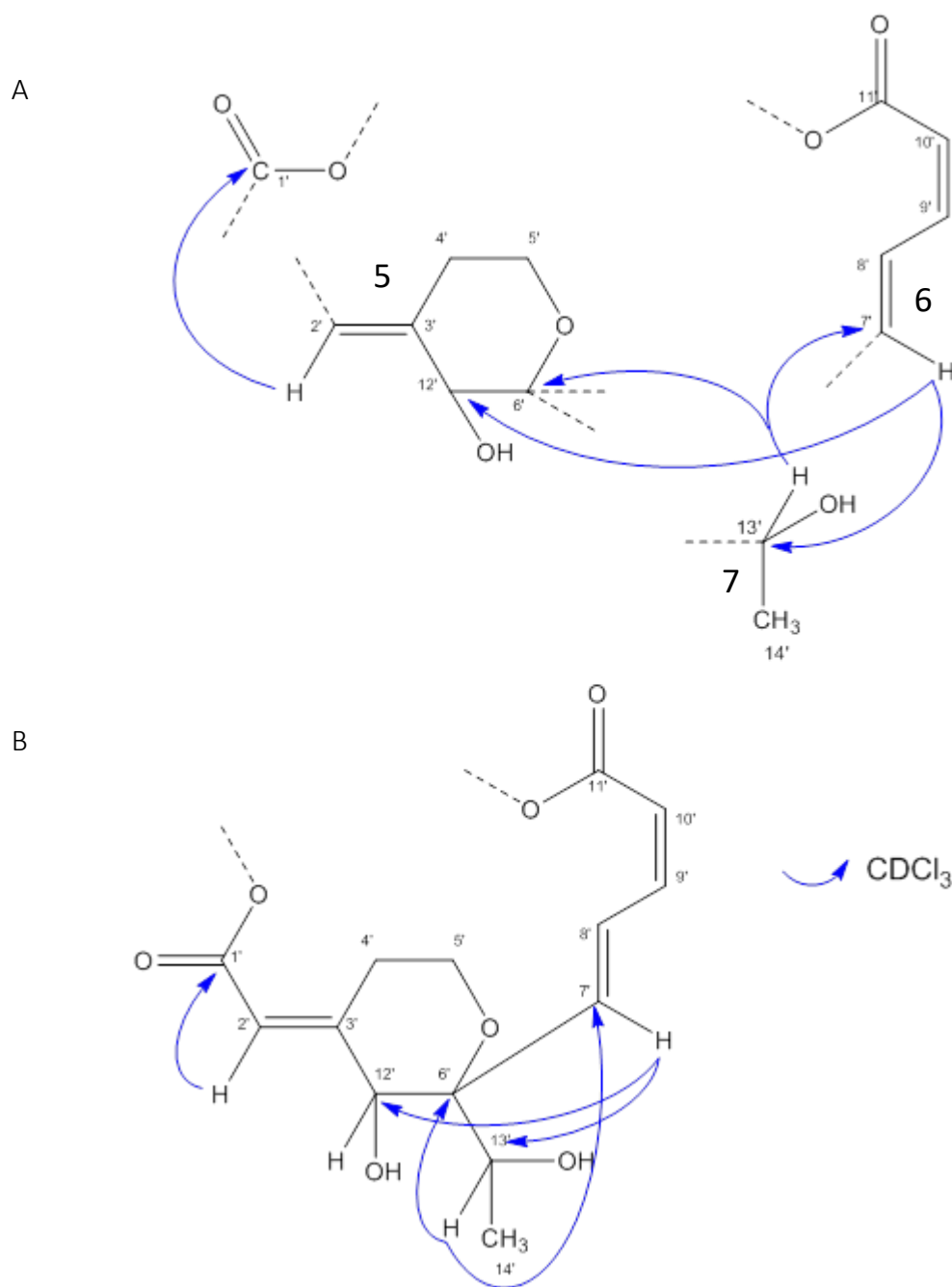


Figure 41 - A) HMBC correlations between substructures 5-7 and isolated carbon moieties that establish the connectivity between them to form the macrocyclic ring of satratoxin H. B) Substructures 4-6 and isolated carbon moieties organised into the macrocyclic ring of satratoxin H.

The HMBC correlation between H<sub>2</sub>-15 to C-1' provides a link between the trichothecene core and the macrocyclic ring through the ester forming the complete satratoxin H structure (Figure 42).

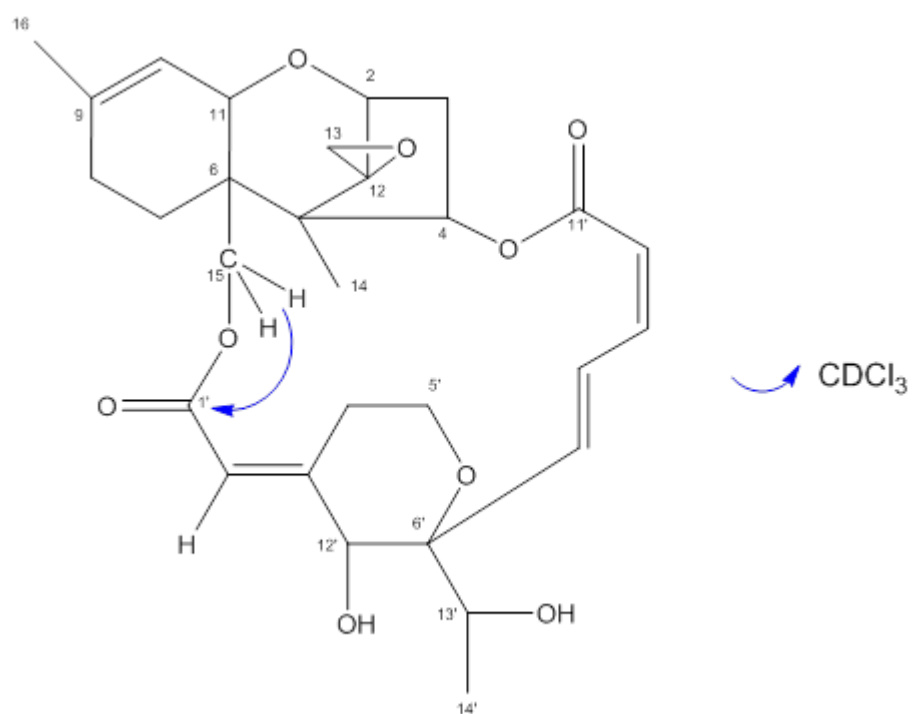


Figure 42 - The completed satratoxin H structure with the HMBC correlation that link the trichothecene core and the macrocyclic ring.

Table 5 - Satratoxin H (7) NMR data in CDCl<sub>3</sub>.

Satratoxin H - CDCl <sub>3</sub>								
Position	<sup>13</sup> C	DEPT	HSQC	<sup>1</sup> H Peak	<i>J</i> = Hz	<i>n</i> H	HMBC	COSY
2	79.1	CH	3.82	d	(4.8)	1	C-5, C-11, C-12	H-3b
3	34.4	CH <sub>2</sub>	2.42	dd	(15.3, 8.5)	1	C-2, C-5, C-12	H-3b, H-4
			2.18	dt	(15.2, 5.0)	2	C-4	H-2, H-3a, H-4
4	74.1	CH	5.88	dd	(8.5, 5.2)	1	C-4, C-6, C-12	H <sub>2</sub> -3
5	48.9	C						
6	43.4	C						
7	20.3	CH <sub>2</sub>	1.88	m		2	C-6, C-15	H-8a
8	27.6	CH <sub>2</sub>	2.02	m		2	C-7, C-9	H <sub>2</sub> -7, H-16
9	140.3	C						
10	118.9	CH	5.42	dq	(5.3, 1.6)	1	C-6, C-8, C-16	H-11, H-16
11	68.2	CH	3.58	d	(5.3)	1	C-7, C-9, C-10, C-15	H-10, H-16
12	65.5	C						
13	48.1	CH <sub>2</sub>	3.11	d	(4.0)	1	C-12	H-13b
			2.80	d	(4.0)	1	C-12	H-13a
14	7.6	CH <sub>3</sub>	0.80	s		3	C-4, C-5, C-6, C-12	
15	64.2	CH <sub>2</sub>	4.54	dd	(12.7, 1.4)	1	C-6, C-7, C-11, C-1'	H-15b
			3.84	d	(12.7)	1	C-7	H-15a
16	23.3	CH <sub>3</sub>	1.70	s		3	C-8, C-9, C-10	H-8a, H-10, H-11
1'	166.2	C						
2'	119.1	CH	5.82	d	(2.6)	1	C-1', C-4', C-12'	
3'	154.9	C						
4'	25.3	CH <sub>2</sub>	3.86	m		1	C-2', C-3'	H-2', H-4'b, H-5'b
			2.64	m		1	C-3', C-5'	H-2', H-4'a, H-5'b
5'	60.5	CH <sub>2</sub>	3.88	m		1	C-4', C-6'	H-5'b
			3.73	td	(11.8, 3.3)	1		H <sub>2</sub> -4', H-5a
6'	81.3	C						
7'	132.0	CH	6.05	d	(17.0)	1	C-8', C-9', C-12', C-13'	H-8'
8'	134.2	CH	7.32	ddd	(17.2, 10.0, 1.1)	1	C-9', C-10'	H-7', H-9'
9'	142.9	CH	6.58	ddd	(11.0, 10.0, 0.9)	1	C-7', C-11'	H-8', H-10'
10'	120.4	CH	5.87	dd	(10.9, 1.5)	1	C-8', C-11'	H-9'
11'	167.1	C						
12'	73.6	CH	3.96	d	(6.1)	1	C-2', C-3', C-4'	12'-OH
13'	69.7	CH	4.33	q	(6.4)	1	C-6', C-7', C-14'	H-14'
14'	15.7	CH <sub>3</sub>	1.14	d	(6.5)	3	C-6', C-13'	H-13'
12'-OH			2.27	d	(6.6)	1		H-12'



Table 6 - Satratoxin H (7) NMR data in DMSO-*d*<sub>6</sub>.

Satratoxin H - DMSO- <i>d</i> <sub>6</sub>								
Position	<sup>13</sup> C	DEPT	HSQC	<sup>1</sup> H Peak	<i>J</i> = Hz	<i>n</i> H	HMBC	COSY
2	78.0	CH	3.68	d	(3.3)	1	C-4, C-11, C-12	H-3b
3	34.0	CH <sub>2</sub>	2.44	ddd	(14.9, 8.4)	1	C-2, C-5, C-12	H-3b, H-4
			1.95	m		1		H-2, H-3a, H-4
4	74.0	CH	5.88	m		1	C-6, C-12	H <sub>2</sub> -3
5	48.3	C						
6	42.8	C						
7	19.7	CH <sub>2</sub>	1.82	dd	(13.3, 5.3)	1	C-16	H-7b, H <sub>2</sub> -8
			1.74	td	(12.4, 6.9)	1		H-7a, H <sub>2</sub> -8
8	27.0	CH <sub>2</sub>	1.96	m		2		H <sub>2</sub> -7
9	138.4	C						
10	119.4	CH	5.34	dq	(5.0, 1.5)	1		H-11, H-16
11	66.9	CH	3.71	d	(5.5)	1	C-9, C-10	H-10
12	65.4	C						
13	47.2	CH <sub>2</sub>	3.05	d	(4.1)	1	C-12, C-12	H-13b
			2.78	d	(4.1)	1	C-12	H-13a
14	7.3	CH <sub>3</sub>	0.70	s		3	C-6, C-5, C-12, C-4	
15	63.9	CH <sub>2</sub>	4.43	d	(12.5)	1	C-5	H-15b
			3.67	d	(10.6)	1		H-15a
16	22.8	CH <sub>3</sub>	1.67	s		3	C-8, C-9, C-10	H-10, H-11
1'	165.8	C						
2'	117.1	CH	5.74	d	(2.4)	1	C-4', C-12'	H-4'b
3'	156.8	C						
4'	25.4	CH <sub>2</sub>	3.57	dt	(14.8, 2.4)	1		H-4'b, H <sub>2</sub> -5'
			2.56	m		1		H-2', H-4'a, H <sub>2</sub> -5'
5'	59.0	CH <sub>2</sub>	3.76	ddd	(11.4, 6.7, 1.9)	1		H <sub>2</sub> -4', H-5'b
			3.47	td	(11.5, 3.2)	1		H <sub>2</sub> -4', H-5'a
6'	81.0	C						
7'	132.4	CH	7.24	ddd	(17.0, 10.4, 1.1)	1	C-6', C-9', C-10'	H-8', H-9'
8'	134.4	CH	6.12	d	(17.2)	1	C-6', C-9', C-12', C-13'	H-7'
9'	143.6	CH	6.73	td	(10.6, 0.9)	1	C-8', C-11'	H-7', H-10'
10'	119.1	CH	5.90	dt	(11.1, 0.9)	1	C-7', C-11'	H-9'
11'	166.5	C						
12'	72.1	CH	3.81	d	(5.3)	1	C-2', C-3', C-4'	OH
13'	67.9	CH	4.15	qd	(6.5, 3.8)	1	C-6', C-8', C-14'	H-14', OH
14'	17.1	CH <sub>3</sub>	0.97	d	(6.5)	3	C-6', C-13'	H-13'
12'-OH			5.32	d	(5.3)	1	C-6', C-12'	H-12'
13'-OH			4.46	d	(3.9)	1	C-13', C-14'	H-13'

### 3.4 Comparison with Literature

The original  $^1\text{H}$  and  $^{13}\text{C}$   $\text{CDCl}_3$  NMR data and proposed structure for satratoxin H was published in 1977.<sup>46</sup> In 2017,  $^1\text{H}$  and  $^{13}\text{C}$  NMR data for satratoxin H recorded in  $\text{DMSO}-d_6$  was published with a structure that conformed to the original.<sup>50</sup> The data here provides

Table 7 - Comparison data for satratoxin H in  $\text{CDCl}_3$ .

Satratoxin H - $\text{CDCl}_3$						
Literature and Experimental Differences						
Position	Experimental		Eppley (1977)		Differences	
	$^{13}\text{C}$	$^1\text{H}$	$^{13}\text{C}$	$^1\text{H}$	$^{13}\text{C}$	$^1\text{H}$
					$\geq \pm 1.0$	$\geq \pm 0.2$
2	79.1	3.82	79.1	3.90	0.0	0.08
3	34.4	2.42	34.4	2.45	0.0	0.03
		2.18		2.20		0.02
4	74.1	5.88	74.2	5.90	0.1	0.02
5	48.9		49.0		0.1	
6	43.4		43.4		0.0	
7	20.3	1.88	20.4	1.90	0.1	0.02
8	27.6	2.02	27.6	2.10	0.0	0.08
9	140.3		140.2		-0.1	
10	118.9	5.42	119.0	5.46	0.1	0.04
11	68.2	3.58	68.2	3.62	0.0	0.04
12	65.5		65.4		0.0	
13	48.1	3.11	48.0	2.98	-0.1	-0.13
		2.80		2.98		0.18
14	7.6	0.80	7.6	0.83	0.0	0.03
15	64.2	4.54	64.2	4.22	0.0	-0.32
		3.84		4.22		0.38
16	23.3	1.70	23.3	1.74	0.0	0.04
1'	166.2		166.2		0.0	0.00
2'	119.1	5.82	119.0	5.85	-0.1	0.03
3'	154.9		155.1		0.2	
4'	25.3	3.86	25.3	3.74	0.0	-0.12
		2.64		2.60		-0.04
5'	60.5	3.88	60.4	3.90	-0.1	0.02
		3.73		3.90		0.17
6'	81.3		81.4		0.1	
7'	132.0	6.05	132.2	6.09	0.2	0.04
8'	134.2	7.32	134.2	7.36	0.0	0.04
9'	142.9	6.58	143.0	6.63	0.1	0.05
10'	120.4	5.87	120.4	5.91	0.0	0.04
11'	167.1		167.0		-0.1	
12'	73.6	3.96	73.7	3.97	0.1	0.01
13'	69.7	4.33	69.7	4.38	0.0	0.05
14'	15.7	1.14	15.7	1.16	0.0	0.02

some inconsistencies with the data from both articles, Table 7 for CDCl<sub>3</sub> and Table 8 for DMSO-*d*<sub>6</sub>. This appears to be mainly due to where the solvent peak was referenced and, in some cases, when both protons were able to be distinguished on methylene groups. The DMSO-*d*<sub>6</sub> used for these NMR experiments also contains a water peak, this moisture also appears to have influenced the chemical shifts.

Table 8 - Comparison data for satratoxin H in DMSO-*d*<sub>6</sub>.

Satratoxin H - DMSO- <i>d</i> <sub>6</sub>						
Literature and Experimental Differences						
Position	Experimental		Li, Y (2017)		Differences	
	<sup>13</sup> C	<sup>1</sup> H	<sup>13</sup> C	<sup>1</sup> H	<sup>13</sup> C	<sup>1</sup> H
					≥ ±1.0	≥ ±0.2
2	78.0	3.68	78.5	3.69	0.5	0.01
3	34.0	2.44	34.5	2.45	0.5	0.01
		1.95		1.95		0.00
4	74.0	5.88	74.5	5.89	0.5	0.01
5	48.3		48.9		0.6	
6	42.8		43.3		0.5	
7	19.7	1.82	20.2	1.78	0.5	-0.04
		1.74		1.78		0.04
8	27.0	1.96	27.5	1.97	0.5	0.01
9	138.4		139.0		0.6	
10	119.4	5.34	119.9	5.34	0.5	0.00
11	66.9	3.71	67.4	3.72	0.5	0.01
12	65.4		65.9		0.5	
13	47.2	3.05	47.7	3.06	0.5	0.01
		2.78		2.78		0.00
14	7.3	0.70	7.82	0.71	0.5	0.01
15	63.9	4.43	64.1	4.43	0.2	0.00
		3.67		4.43		0.76
16	22.8	1.67	23.4	1.67	0.6	0.00
1'	165.8		166.3		0.5	
2'	117.1	5.74	117.6	5.75	0.5	0.01
3'	156.8		157.3		0.6	
4'	25.4	3.57	26.0	3.55	0.6	-0.02
		2.56		3.55		0.99
5'	59.0	3.76	59.5	3.76	0.5	0.00
		3.47		3.48		0.01
6'	81.0		81.5		0.5	
7'	132.4	7.24	132.9	7.26	0.5	0.02
8'	134.4	6.12	135.0	6.15	0.6	0.03
9'	143.6	6.73	144.1	6.74	0.5	0.01
10'	119.1	5.90	119.6	5.89	0.5	-0.01
11'	166.5		167.0		0.5	
12'	72.1	3.81	72.6	3.82	0.5	0.01
13'	67.9	4.15	68.4	4.17	0.5	0.02
14'	17.1	0.97	17.6	0.97	0.5	0.00

The original  $^1\text{H}$  and  $^{13}\text{C}$   $\text{CDCl}_3$  NMR data and proposed structure for satratoxin G was published in 1980.<sup>47</sup> In 2017,  $^1\text{H}$  and  $^{13}\text{C}$  NMR data in  $\text{DMSO}-d_6$  and a crystal structure for satratoxin G was published with a structure that conformed to the original. There are some significant differences in the spectral data between the data reported here and the data reported in these two articles. In regard to the  $\text{CDCl}_3$  data (Table 9) most of the differences

Table 9 - Comparison data for satratoxin G in  $\text{CDCl}_3$ .

Satratoxin G - $\text{CDCl}_3$						
Literature and Experimental Differences						
Position	Experimental		Eppley (1980)		Differences	
	$^{13}\text{C}$	$^1\text{H}$	$^{13}\text{C}$	$^1\text{H}$	$^{13}\text{C}$	$^1\text{H}$
					$\geq \pm 1.0$	$\geq \pm 0.2$
2	79.2	3.83	79.3	3.90	0.1	0.07
3	34.4	2.20	34.4	2.00	0.0	-0.20
		2.44		2.50		0.06
4	73.7	5.91	73.7	6.00	0.0	0.09
5	49.2		49.3		0.1	
6	43.2		43.3		0.1	
7	20.1	1.87	20.2	2.00	0.1	0.13
8	27.5	2.04	27.5	2.00	0.0	-0.04
		2.00		2.00		0.00
9	140.4		140.3		-0.1	
10	118.7	5.42	118.8	5.46	0.1	0.04
11	68.1	3.58	68.1	3.61	0.0	0.03
12	65.4		65.4		0.0	
13	48.1	3.13	48.1	2.98	0.0	-0.15
		2.81		2.98		0.17
14	8.0	0.83	8.0	0.87	0.0	0.04
15	64.9	4.38	64.9	4.02	0.0	-0.36
		4.11		4.02		-0.09
16	23.3	1.71	23.3	1.74	0.0	0.03
1'	166.9		166.9		0.0	
2'	61.0	3.41	61.0	3.43	0.0	0.02
3'	65.4		65.4		0.0	
4'	22.6	2.42	22.7	2.50	0.1	0.08
5'	60.1	3.99	60.3	3.90	0.2	-0.09
		3.93		3.90		-0.03
6'	81.4		81.5		0.1	
7'	131.9	5.88	132.0	5.90	0.1	0.02
8'	131.5	6.95	131.5	7.00	0.1	0.05
9'	144.2	6.65	144.2	6.68	0.0	0.03
10'	119.9	5.90	120.0	5.93	0.1	0.03
11'	166.9		166.9		0.0	
12'	72.4	3.26	72.6	4.35	0.2	1.09
13'	70.0	4.35	70.1	4.45	0.1	0.10
14'	16.0	1.10	16.1	1.12	0.1	0.02

appear to be attributable to where the solvent peak was referenced in the  $^1\text{H}$  NMR spectra, however there are still two very large differences at H-4' and H-12'.

The majority of the differences found between the experimental data and the literature data for the NMR spectra obtained in  $\text{DMSO}-d_6$  are not explainable by changes in solvent peak referencing. There are several large differences in both the  $^{13}\text{C}$  and  $^1\text{H}$  spectral data (Table 10).

Table 10 - Comparison data for satratoxin G in  $\text{DMSO}-d_6$ .

Satratoxin G - $\text{DMSO}-d_6$						
Literature and Experimental Differences						
Position	Experimental		Li, Y (2017)		Differences	
	$^{13}\text{C}$	$^1\text{H}$	$^{13}\text{C}$	$^1\text{H}$	$^{13}\text{C}$	$^1\text{H}$
					$\geq \pm 1.0$	$\geq \pm 0.2$
2	78.1	3.70	78.6	3.71	0.5	0.01
3	34.0	2.44	34.6	2.43	0.6	-0.01
4	73.6	5.95	74.3	5.97	0.7	0.02
5	48.7		49.5		0.8	
6	42.6		43.3		0.7	
7	19.4	1.76	19.8	1.72	0.4	-0.04
8	26.8	1.97	27.4	1.94	0.6	-0.03
9	138.4		139.0		0.6	
10	119.2	5.32	119.7	5.33	0.5	0.01
11	66.8	3.74	67.0	3.73	0.2	-0.01
12	65.4		65.8		0.4	
13	47.2	3.07	47.7	3.08	0.5	0.01
		2.80		2.79		-0.01
14	7.9	0.77	8.3	0.72	0.4	-0.05
15	64.4	4.26	64.5	4.12	0.1	-0.14
		3.96		4.12		0.16
16	22.7	1.66	23.4	1.66	0.7	0.00
1'	167.6		169.0		1.4	
2'	58.3	3.58	54.0	3.61	-4.3	0.03
3'	64.6		65.4		0.8	
4'	22.8	1.97	28.0	2.14	5.2	0.17
5'	59.2	3.81	60.2	3.83	1.1	0.02
		3.77		3.83		0.06
6'	82.2		82.6		0.4	
7'	132.8	5.84	135.7	5.78	2.9	-0.06
8'	130.2	6.78	128.7	6.89	-1.5	0.11
9'	145.2	6.78	145.1	6.78	-0.1	
10'	118.8	5.89	119.4	5.89	0.6	
11'	166.2		166.9		0.8	
12'	68.7	4.09	67.1	4.27	-1.6	0.18
13'	70.9	4.09	70.2	3.70	-0.7	-0.39
14'	17.3	0.92	17.5	1.08	0.3	0.16

Upon closer examination of the crystal structure (Figure 43) provided by Li *et al.*<sup>50</sup> it first appeared that they may have mistakenly isolated and crystallised the lesser known satratoxin F (**8**) (Figure 44), rather than satratoxin G. This was due to the presence of a ketone at the C-13' positions in satratoxin F as opposed to a hydroxyl found at the C-13' position in satratoxin G. Further inspection though showed that the crystal structure also lacked the double bond from 7' to 8' which both satratoxins contain in their macrocyclic ring. The lack of this double bond instead makes the crystallised compound myotoxin A (**9**) (Figure 45), which Li *et al.* also isolated.

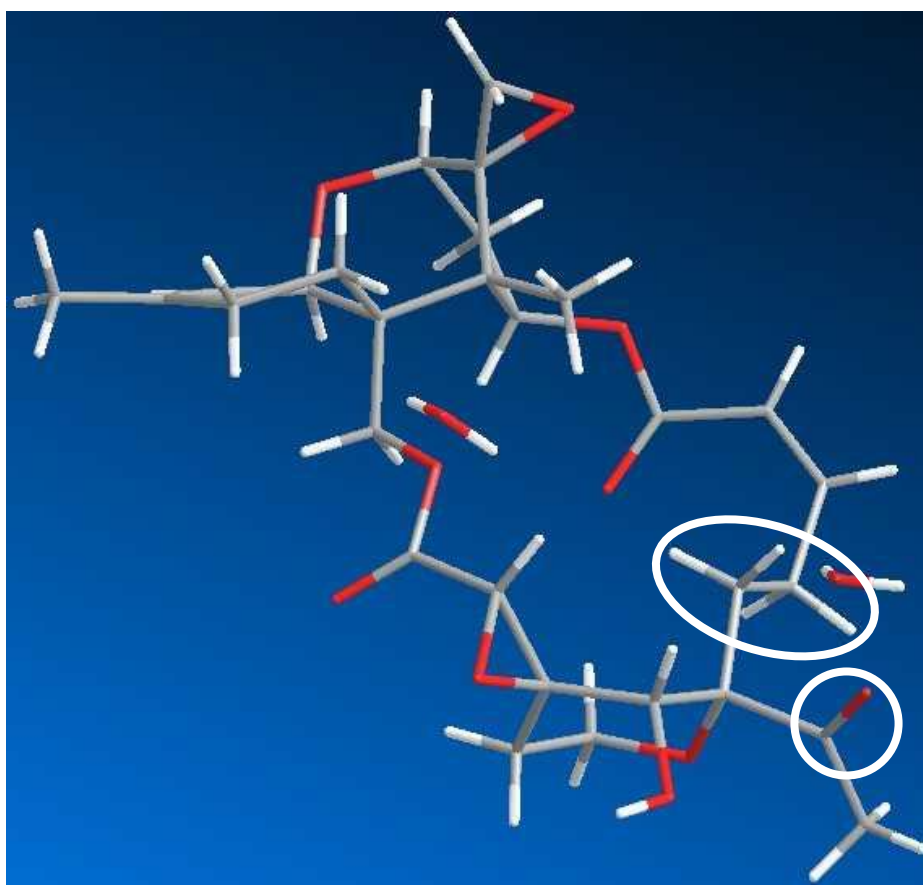


Figure 43 - Crystal structure obtained by Li, Y *et al.* (2017) that appears to have been mischaracterised as satratoxin G when it is myotoxin A. The circle highlights the presence of a ketone at position C-13' rather than a hydroxyl group, and the oval highlights the missing double bond at the 7' to 8' position.

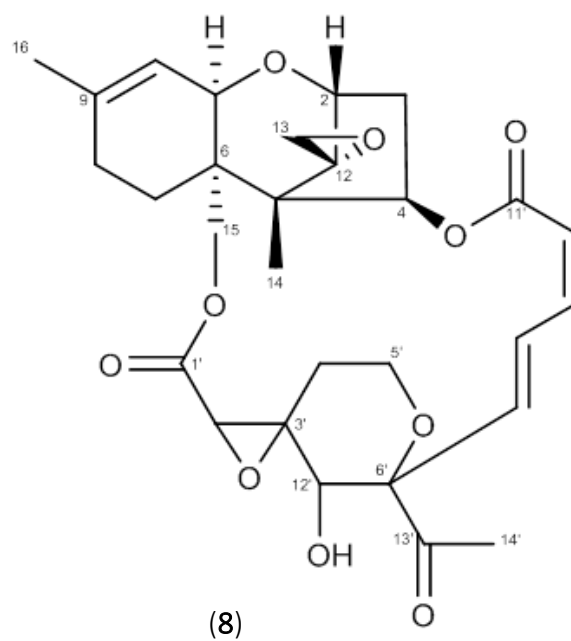


Figure 44 - Structure of satratoxin F (8).

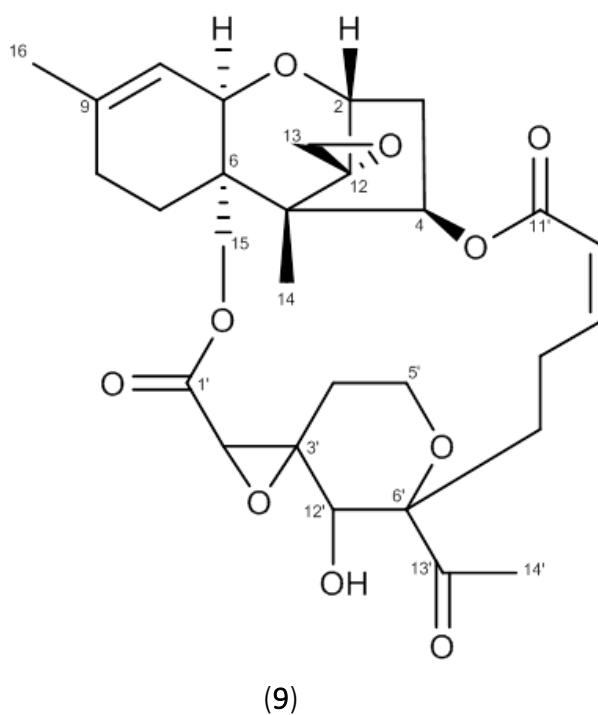


Figure 45 - Structure of myotoxin A (9), the compound that Li et al. actually crystallised.

### 3.5 Related Structures

The trichothecenes are produced by several genera of fungi other than *Stachybotrys*, such as *Fusarium*, *Myrothecium*, *Trichoderma* and *Trichothecium*.<sup>74, 75</sup> Macrocytic trichothecenes are considered to be some of the most toxic trichothecenes and are generally more toxic than simple trichothecenes.<sup>44, 76</sup> There are several subtypes of macrocytic trichothecenes other than the satratoxins, including roridins and verrucarins, and are grouped based upon structural similarity.<sup>36</sup>

Roridins A (**10**), D (**11**), and E (**12**) are macrocytic trichothecenes produced by *Myrothecium* and *Stachybotrys* species, and show a lower level of toxicity compared to the satratoxins.<sup>44</sup> *M. verrucaria* has been observed to produce multiple different roridins,<sup>77</sup> *S. chartarum* has been observed to produce roridin E.<sup>48</sup> These roridins are differentiated based upon the functional group found at the 2'-3' position, similar to where the difference between satratoxin G and H is found however, roridins do not contain the ring structure in their macrocyclic ring.

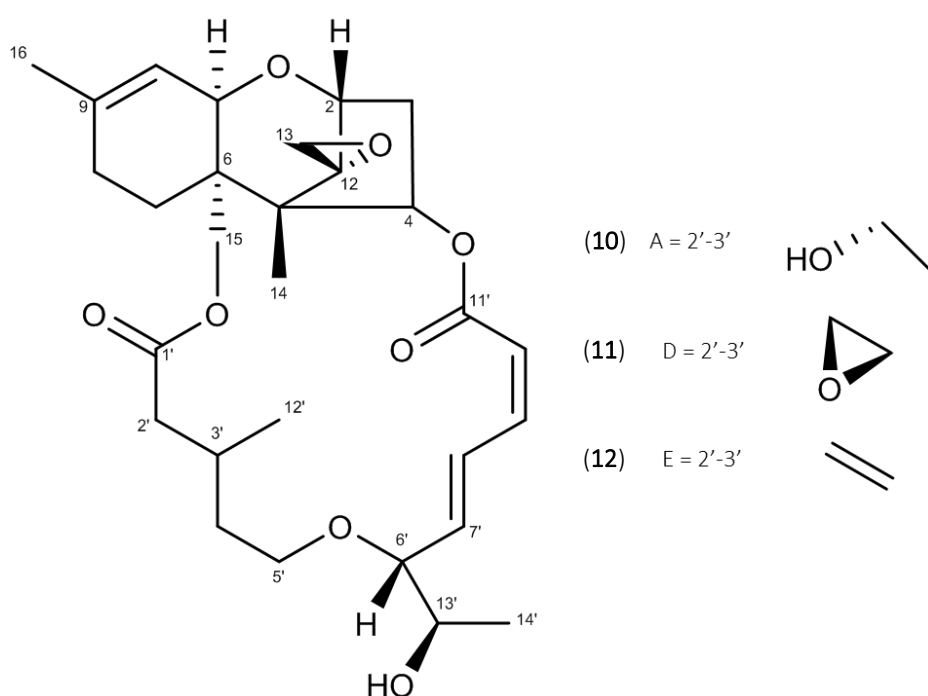
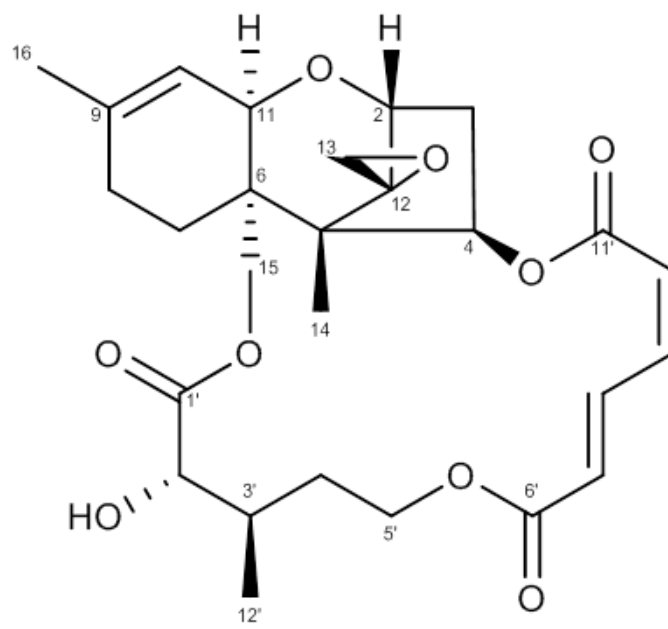


Figure 46 - Structures of roridin A (**10**), D (**11**), and E (**12**).



Verrucarin A (**13**), produced by *M. verrucaria*,<sup>78</sup> is macrocyclic trichothecene differing from others by containing a carbonyl at C-6' rather than a carbon side chain. Verrucarin A is one of the least toxic macrocyclic trichothecenes.<sup>76</sup>



(13)

Figure 47 - Verrucarin A (**13**).

## 4. Conclusion

For decades mould contamination found in homes and offices has been associated with adverse respiratory health effects suffered by inhabitants. *S. chartarum* which is often referred to as toxic black mould has been singled out as a common offender. The built environment produces a very complex combination of conditions and each building can be unique. The understanding of how fungi interact with the built environment and their inhabitants is still poorly understood. Mycotoxins, in particular trichothecenes, are a strong contender as a causative agent for adverse respiratory health conditions.

Due to the high prevalence of poor respiratory health and low-quality buildings with mould contamination in New Zealand this research was undertaken to examine the trichothecenes produced by *S. chartarum*. The isolation and characterisation of two trichothecenes satratoxins G and H, from the macrocyclic trichothecene subgroup, was a primary focus.

This study began with an investigation of *S. chartarum* strains found in New Zealand. Four strains of *S. chartarum* isolated from different New Zealand environments were cultured to determine their phenotype and chemotype. The cultures were found to have vastly different growth characteristics and production of trichothecenes. MS analysis provided the information about the production of metabolites and trichothecenes by the different strains. Importantly it revealed which strains were macrocyclic trichothecene producers enabling them to be utilised in future investigations.

The investigation of *S. chartarum* was planned to include a genetic screening process to identify their ITS and Tri5 information. This would have revealed important information about their abilities to produce trichothecenes without the need for time consuming culturing and isolation experiments. Unfortunately, this was not able to take place but through a combination of information provided by the ICMP database and MSMS analysis several strong conclusions were able to be drawn. Genetic screening will be crucial for any future experimentation with environmental samples.

NMR characterisation confirmed the structures reported in historical and recent literature, however there were several differences in the chemical shifts in our data, in particular with

the proton spectra. The results here are reported using CDCl<sub>3</sub> and DMSO-*d*<sub>6</sub> and full spectral information has been provided for comparison with all past and future data.

Several challenges arose during the experimentation involved in this study. Notably the separation of the satratoxins G and H which only differ by a double bond versus an epoxide at the 2' to 3' position in the macrocyclic ring. Often steps in the isolation procedure had to be repeated several times to obtain pure fractions.

The epidemic levels of respiratory health disorders both globally and within New Zealand are driving increased interest and research into this area. Much of the research being done is epidemiological, without complete understanding of the moulds involved and how their structures and metabolites might affect human health, the causation of these disorders will not be found. The present study was undertaken to address this essential point.

## 5. Experimental

### 5.1 General Experimental

#### 5.1.1 NMR Analysis

Compounds were dissolved in two different deuterated solvents:  $\text{CDCl}_3$  and  $\text{DMSO-}d_6$ , and spectra were collected at 30 °C with chemical shifts referenced to the relevant solvent peak. For  $\text{CDCl}_3$ :  $^1\text{H}$   $\delta$  7.24 ppm and  $^{13}\text{C}$   $\delta$  77.23 ppm; for  $\text{DMSO}$ :  $^1\text{H}$   $\delta$  2.50 ppm and  $^{13}\text{C}$   $\delta$  39.51 ppm. NMR spectra were obtained using a three-channel Bruker 500 MHz machine. Proton frequency was 500 MHz and 125 MHz for  $^{13}\text{C}$ . The 51-mm Oxford Instruments, 11.74 Tesla, superconducting magnet (ca. 1992) was equipped with TMC antivibration legs and a Bruker 60 sample autosampler. Spectra were processed using MestReNova software (version 12.0.1).

#### 5.1.2 Chromatography

TLC analysis was performed using silica gel 60 sheets. The TLC plates were visualised under UV light ( $\lambda = 254$  nm) then dipped in a vanillin staining solution (0.1% vanillin/5%  $\text{H}_2\text{SO}_4/\text{EtOH}$ ) and heated to visualise spots. One of the following four mobile phases were used throughout:

1. MeOH in DCM
2. MeOH in  $\text{CHCl}_3$
3. MeOH in PE and DCM
4. PE in EtOAc

Flash chromatography was carried out using regular 35-75  $\mu\text{m}$  silica or PEI silica depending on the purification stage. The solvent systems discussed in section 2.6 were used for all silica-based chromatography. For PEI chromatography the methods described by Jarvis and Hinkley were followed.<sup>43</sup> Preparation of PEI silica was prepared by following the method detailed by Jarvis.<sup>73</sup> In brief, silica was suspended in a 10% (w/v) solution of PEI in a 250 ml Erlenmeyer flask. The mixture was sonicated for 1 h, degassed under vacuum, then

sonicated for a further 30 min. The silica was washed with MeOH (2 x 50 mL) and DCM (2 x 50 mL), and then dried overnight at 50 °C.

For flash chromatography the ratio of silica to sample was altered depending on the purity of the sample and went from 20:1 silica:sample for crude extracts up to 100:1 silica:sample for high level purification. This required a variety of columns to be used to contain the total volume of silica and sample. In brief the column was filled with a silica slurry made with the chosen solvent system. The sample was dissolved in the same solvent system and loaded onto the top of the column in a thin even band. The column was eluted with gravity or pressurised air depending on the desired speed of elution. The volume of fractions was dependent on the stage of purification; larger bulk fractions were collected for crude separation, for higher level purification multiple fractions of 1 mL or less were collected.

HPLC was performed using a ThermoScientific UltiMate 3000 UHPLC and an Agilent Technologies 1260 Infinity HPLC. As discussed in sections 2.3 and 2.7 HPLC methods were developed and adapted from the ones described by Hinkley (2001).<sup>43</sup> All HPLC was performed using a 100 x 3 mm Kinetex reversed-phase C18 column, and detection was done with UV/Vis at the wavelengths 225, 260, 280, and 300 nm. Column heater was set to 40 °C and 1 µL injection volumes were used for all samples. Solvents used for HPLC were all HPLC grade and mixtures are reported as % v/v unless otherwise stated, the solvents in use were: A (deionised water), and B (ACN); each with 0.1% formic acid.

Two HPLC programmes were used.

1. Gradient from 25% to 80% B from 0 to 30 min, then ramp to 100% B from 30 to 31 min, hold at 100% B until 40 min, ramp down to 25% B from 40 to 42 min, hold at 25% B until 55 min for column re-equilibration. Turn off data acquisition at 40 min, flow rate was constant at 0.2 mL/min, maximum operating pressure set to 250 Bar
2. Gradient from 25% to 80% B from 0 to 15 min, then ramp to 100% B from 15 to 16 min, hold at 100% B until 25 min, ramp down to 25% B from 26 to 28 min, hold at 25% B until 35 min for column re-equilibration. Turn off data acquisition at 25 min, flow rate was constant at 0.4 or 0.5 mL/min dependent on pressure levels, maximum operating pressure set to 600 Bar.

LCMS was performed using an Agilent LCMS. All LCMS was performed using a 50 x 3 mm Kinetex reversed-phase C18 column. Detection was done with UV/Vis at the wavelengths 225, 260, and 300 nm. Mass spectra were obtained through electron spray, recording was done from 200 to 1,000, Single Ion Monitoring recorded for protonated, sodiated, and loss of water species. Column heater was set to 40 °C and 1 µL injection volumes were used for all samples. Solvents used for LCMS were all HPLC grade and mixtures are reported as % v/v unless otherwise stated, the solvents in use were: A (deionised water with 0.1% formic acid), and B (MeOH); each with 0.1% formic acid. An isocratic programme was used for LCMS runs: 45% A, 55% B for 10 min. Flow rate constant at 0.5 mL/min, maximum operating pressure set to 1,000 Bar.

## 5.2 *Stachybotrys chartarum* Strains

### 5.2.1 Cultures

The New Zealand *Stachybotrys chartarum* species used were purchased from Landcare Research. They were part of the ICMP culture collection. Cultures were grown on PDA at 25 °C in the dark until growth was sufficient for spore harvesting. Spores were harvested by covering cultures with a 20% Tween20 solution and the agar plates were scrapped clean. This spore suspension was used to inoculate rice cultures. Trichothecenes were produced on rice by modifying previously described methods.<sup>66, 67</sup> In brief, 250 g parboiled rice was soaked in 250 mL distilled water for 2 hours in 2.0 L Erlenmeyer flasks before being autoclaved. After cooling, flasks were inoculated with the previously obtained *S. chartarum* spores and incubated at 25 °C in the dark for a minimum of 4 weeks. Rice cultures were checked and shaken every 2-3 days to break up clumps of rice, ensuring maximal growth and toxin production.

### 5.2.2 Extraction of Metabolites

Rice cultures were extracted following methods modified from those described by Jarvis *et al.* (1998).<sup>67</sup> Following incubation, rice cultures were soaked in an extraction solvent mixture overnight. The extract solvent mixture was 1:1 chloroform:methanol and rice was soaked at a ratio of 1:3 rice:solvent. The solvent was decanted, and cultures were again

soaked in fresh extraction solvent overnight. Extracts were pooled and vacuum-filtered twice through Whatman's filter paper. Solvent was removed under vacuum by rotary evaporation at 40°C. The resultant residue was dissolved in DCM and the solution vacuum filtered through Whatman's filter paper before rotary evaporation at 40 °C to dryness. This process yielded approximately 15 g of a dark flaky material.

## 5.3 Purification of the Satratoxins

Following the process outlined in section 2.6 and further explained in section 5.1.2 crude extracts were subjected to repeated rounds of flash chromatography until sufficient purity was achieved. Eluting compounds were concentrated based on TLC data (vanillin spray) and taking a very narrow selection, highly-purified satratoxin samples were obtained.

### 5.3.1 *Satratoxin G*

A pure fraction of 14 mg was collected for NMR characterisation. The pure fractions of satratoxin G yielded a colourless material. For NMR data refer to chapter 3, table 3 (CDCl<sub>3</sub>) and table 4 (DMSO-*d*<sub>6</sub>). Spectra of all NMR experiments are provided for reference in appendix A.

### 5.3.2 *Satratoxin H*

A pure fraction of 8 mg was collected for NMR characterisation. The pure fractions of satratoxin H yielded a colourless material. For NMR data refer to chapter 3, table 5 (CDCl<sub>3</sub>) and table 6 (DMSO-*d*<sub>6</sub>). Spectra of all NMR experiments are provided for reference in appendix B.

## 5.4 Genetic Analysis

As stated in section 2.5 the genetic screening did not take place, below is a summary of the PCR primers and method of analysis that would have been used.

#### 5.4.1 PCR Primers

The primers selected for species identification were based upon the standard ITS region primers for fungal identification; ITS1F and ITS4.<sup>79</sup> The primers selected for chemotype identification amplified an allele containing *Tri5* gene region.<sup>80</sup>

Table 11 - PCR primers

Primer	Sequence
ITS1F	CTT GGT CAT TTA GAG GAA GTA A
ITS4	TCC TCC GCT TAT TGA TAT GC
<i>Tri5</i> Forward	CAT CAA TCC AAC AGT TTC AC
<i>Tri5</i> Reverse	GTT ATC AGA AAC TTC CAA CG

#### 5.4.2 Analysis

PCR planning and primer design was done using Geneious (version 8.1.8, Biomatters Ltd, NZ). If sequence had been obtained forward and reverse sequences would have been assembled and analysed also using Geneious. The sequences would have been checked with a Basic Local Alignment Search Tool (BLAST) search to identify their species and chemotype status.



## References

1. Bent, S., *Herbal medicine in the United States: review of efficacy, safety, and regulation: grand rounds at University of California, San Francisco Medical Center*. J Gen Intern Med, 2008. **23**(6): p. 854-9.
2. Verdine, G.L., *The combinatorial chemistry of nature*. Nature, 1996. **384**(6604 Suppl): p. 11-3.
3. Rodrigues, T., et al., *Counting on natural products for drug design*. Nat Chem, 2016. **8**(6): p. 531-41.
4. Mahdi, J.G., et al., *The historical analysis of aspirin discovery, its relation to the willow tree and antiproliferative and anticancer potential*. Cell Prolif, 2006. **39**(2): p. 147-55.
5. Achan, J., et al., *Quinine, an old anti-malarial drug in a modern world: role in the treatment of malaria*. Malar J, 2011. **10**: p. 144.
6. Weaver, B.A., *How Taxol/paclitaxel kills cancer cells*. Mol Biol Cell, 2014. **25**(18): p. 2677-81.
7. Tan, S.Y. and Y. Tatsumura, *Alexander Fleming (1881-1955): Discoverer of penicillin*. Singapore Med J, 2015. **56**(7): p. 366-7.
8. Demain, A.L., *Antibiotics: natural products essential to human health*. Med Res Rev, 2009. **29**(6): p. 821-42.
9. Butler, M.S., *The role of natural product chemistry in drug discovery*. J Nat Prod, 2004. **67**(12): p. 2141-53.
10. Newman, D.J. and G.M. Cragg, *Natural Products as Sources of New Drugs from 1981 to 2014*. J Nat Prod, 2016. **79**(3): p. 629-61.
11. Yocum, R.R., J.R. Rasmussen, and J.L. Strominger, *The mechanism of action of penicillin. Penicillin acylates the active site of Bacillus stearothermophilus D-alanine carboxypeptidase*. J Biol Chem, 1980. **255**(9): p. 3977-86.
12. Peraica, M., et al., *Toxic effects of mycotoxins in humans*. Bull World Health Organ, 1999. **77**(9): p. 754-66.

13. Betcher, A.M., *The civilizing of curare: a history of its development and introduction into anesthesiology*. Anesth Analg, 1977. **56**(2): p. 305-19.
14. Hennekinne, J.A., M.L. De Buyser, and S. Dragacci, *Staphylococcus aureus and its food poisoning toxins: characterization and outbreak investigation*. FEMS Microbiol Rev, 2012. **36**(4): p. 815-36.
15. Kim, J.B., et al., *Food poisoning associated with emetic-type of Bacillus cereus in Korea*. Foodborne Pathog Dis, 2010. **7**(5): p. 555-63.
16. Kumar, P., et al., *Aflatoxins: A Global Concern for Food Safety, Human Health and Their Management*. Front Microbiol, 2016. **7**: p. 2170.
17. Adams, R.I., et al., *Ten questions concerning the microbiomes of buildings*. Building and Environment, 2016. **109**: p. 224-234.
18. Andersen, B., K.F. Nielsen, and B.B. Jarvis, *Characterization of Stachybotrys from water-damaged buildings based on morphology, growth, and metabolite production*. Mycologia, 2002. **94**(3): p. 392-403.
19. Shorter, C., et al., *Indoor visible mold and mold odor are associated with new-onset childhood wheeze in a dose-dependent manner*. Indoor Air, 2018. **28**(1): p. 6-15.
20. Pekkanen, J., et al., *Moisture damage and childhood asthma: a population-based incident case-control study*. Eur Respir J, 2007. **29**(3): p. 509-15.
21. Mendell, M.J., et al., *Respiratory and allergic health effects of dampness, mold, and dampness-related agents: a review of the epidemiologic evidence*. Environ Health Perspect, 2011. **119**(6): p. 748-56.
22. Korkalainen, M., et al., *Synergistic proinflammatory interactions of microbial toxins and structural components characteristic to moisture-damaged buildings*. Indoor Air, 2017. **27**(1): p. 13-23.
23. Kirjavainen, P.V., et al., *Microbial secondary metabolites in homes in association with moisture damage and asthma*. Indoor Air, 2016. **26**(3): p. 448-56.
24. Zhang, L.T.B.J., *The impact of respiratory disease in New Zealand: 2016 update*. 2016, Asthma and Respiratory Foundation NZ: Wellington.

25. Isaacs, N. and M. Donn, *Health and housing--seasonality in New Zealand mortality*. Aust J Public Health, 1993. **17**(1): p. 68-70.
26. Jarvis, B.B., *Stachybotrys chartarum: a fungus for our time*. Phytochemistry, 2003. **64**(1): p. 53-60.
27. Miller, J.D., T.G. Rand, and B.B. Jarvis, *Stachybotrys chartarum: cause of human disease or media darling?* Med Mycol, 2003. **41**(4): p. 271-91.
28. Wang, Y., et al., *Overview of Stachybotrys (Memnoniella) and current species status*. Fungal Diversity, 2015. **71**(1): p. 17-83.
29. Straus, D.C., *Molds, mycotoxins, and sick building syndrome*. Toxicol Ind Health, 2009. **25**(9-10): p. 617-35.
30. Thrasher, J.D. and S. Crawley, *The biocontaminants and complexity of damp indoor spaces: more than what meets the eyes*. Toxicol Ind Health, 2009. **25**(9-10): p. 583-615.
31. Kuhn, D.M. and M.A. Ghannoum, *Indoor mold, toxigenic fungi, and Stachybotrys chartarum: infectious disease perspective*. Clin Microbiol Rev, 2003. **16**(1): p. 144-72.
32. Bitnun, A. and R.M. Nosal, *Stachybotrys chartarum (atra) contamination of the indoor environment: Health implications*. Paediatr Child Health, 1999. **4**(2): p. 125-9.
33. Etzel, R.A., et al., *Acute pulmonary hemorrhage in infants associated with exposure to Stachybotrys atra and other fungi*. Arch Pediatr Adolesc Med, 1998. **152**(8): p. 757-62.
34. Hodgson, M.J., et al., *Building-associated pulmonary disease from exposure to Stachybotrys chartarum and Aspergillus versicolor*. J Occup Environ Med, 1998. **40**(3): p. 241-9.
35. Pestka, J.J., et al., *Stachybotrys chartarum, trichothecene mycotoxins, and damp building-related illness: new insights into a public health enigma*. Toxicol Sci, 2008. **104**(1): p. 4-26.

36. McCormick, S.P., et al., *Trichothecenes: from simple to complex mycotoxins*. Toxins (Basel), 2011. **3**(7): p. 802-14.
37. Andersen, B., et al., *Molecular and phenotypic descriptions of Stachybotrys chlorohalonata sp. nov. and two chemotypes of Stachybotrys chartarum found in water-damaged buildings*. Mycologia, 2003. **95**(6): p. 1227-38.
38. Semeiks, J., et al., *Comparative genome sequencing reveals chemotype-specific gene clusters in the toxigenic black mold Stachybotrys*. BMC Genomics, 2014. **15**: p. 590.
39. Schoch, C.L., et al., *Nuclear ribosomal internal transcribed spacer (ITS) region as a universal DNA barcode marker for Fungi*. Proc Natl Acad Sci U S A, 2012. **109**(16): p. 6241-6.
40. Raja, H.A., et al., *Fungal Identification Using Molecular Tools: A Primer for the Natural Products Research Community*. J Nat Prod, 2017. **80**(3): p. 756-770.
41. Schoch, C.L., et al., *Finding needles in haystacks: linking scientific names, reference specimens and molecular data for Fungi*. Database (Oxford), 2014. **2014**.
42. Hossain, M.A., M.S. Ahmed, and M.A. Ghannoum, *Attributes of Stachybotrys chartarum and its association with human disease*. J Allergy Clin Immunol, 2004. **113**(2): p. 200-8; quiz 209.
43. Hinkley, S.F. and B.B. Jarvis, *Chromatographic method for Stachybotrys toxins*. Methods Mol Biol, 2001. **157**: p. 173-94.
44. Islam, Z., et al., *Purification and comparative neurotoxicity of the trichothecenes satratoxin G and roridin L2 from Stachybotrys chartarum*. J Toxicol Environ Health A, 2009. **72**(20): p. 1242-51.
45. Aleksic, B., et al., *Production of four macrocyclic trichothecenes by Stachybotrys chartarum during its development on different building materials as measured by UPLC-MS/MS*. Building and Environment, 2016. **106**: p. 265-273.
46. Eppley, R.M., et al., *Structure of Satratoxin H, a metabolite of Stachybotrys atra. Application of proton and carbon-13 nuclear magnetic resonance*. The Journal of Organic Chemistry, 1977. **42**(2): p. 240-243.

47. Eppley, R.M., et al., *Structures of satratoxin F and satratoxin G, metabolites of Stachybotrys atra: application of proton and carbon-13 nuclear magnetic resonance spectroscopy*. The Journal of Organic Chemistry, 1980. **45**(12): p. 2522-2523.
48. Ridge, C.D., et al., *Isolation and characterization of roridin E*. Magn Reson Chem, 2016.
49. Liu, Y., et al., *Preparative Separation and Purification of Trichothecene Mycotoxins from the Marine Fungus Fusarium sp. LS68 by High-Speed Countercurrent Chromatography in Stepwise Elution Mode*. Mar Drugs, 2018. **16**(2).
50. Li, Y., et al., *Cytotoxic trichothecene-type sesquiterpenes from the sponge-derived fungus Stachybotrys chartarum with tyrosine kinase inhibition*. Rsc Advances, 2017. **7**(12): p. 7259-7267.
51. Shank, R.A., et al., *Current and future experimental strategies for structural analysis of trichothecene mycotoxins--a prospectus*. Toxins (Basel), 2011. **3**(12): p. 1518-53.
52. Tang, P.W., et al., *A Review of Gene Knockout Strategies for Microbial Cells*. Recent Pat Biotechnol, 2015. **9**(3): p. 176-97.
53. Hanada, K., et al., *Functional compensation of primary and secondary metabolites by duplicate genes in Arabidopsis thaliana*. Mol Biol Evol, 2011. **28**(1): p. 377-82.
54. Nielsen, M.L., et al., *Genes Linked to Production of Secondary Metabolites in Talaromyces atrovirens Revealed Using CRISPR-Cas9*. PLoS One, 2017. **12**(1): p. e0169712.
55. Loke, K.K., et al., *RNA-seq analysis for secondary metabolite pathway gene discovery in Polygonum minus*. Genom Data, 2016. **7**: p. 12-3.
56. Puri, K.D., et al., *RNA-Seq Revealed Differences in Transcriptomes between 3ADON and 15ADON Populations of Fusarium graminearum In Vitro and In Planta*. PLoS One, 2016. **11**(10): p. e0163803.
57. Kimura, M., et al., *Molecular and genetic studies of fusarium trichothecene biosynthesis: pathways, genes, and evolution*. Biosci Biotechnol Biochem, 2007. **71**(9): p. 2105-23.

58. Ye, W., et al., *De Novo Transcriptome Analysis of Plant Pathogenic Fungus Myrothecium roridum and Identification of Genes Associated with Trichothecene Mycotoxin Biosynthesis*. Int J Mol Sci, 2017. **18**(3).
59. Forgacs, J., et al., *Toxicity of Stachybotrys atra for animals*. Trans N Y Acad Sci, 1958. **20**(8): p. 787-808.
60. Jie, C.Y., et al., *Stachybotrys from soil in China, identified by morphology and molecular phylogeny*. Mycological Progress, 2013. **12**(4): p. 693-698.
61. Gareis, M. and C. Gottschalk, *Stachybotrys spp. and the guttation phenomenon*. Mycotoxin Res, 2014. **30**(3): p. 151-9.
62. Andersen, B., et al., *Pre-contamination of new gypsum wallboard with potentially harmful fungal species*. Indoor Air, 2017. **27**(1): p. 6-12.
63. Nelson, B.D., *Stachybotrys chartarum: the toxic indoor mold*. APSnet Features. Online. doi, <http://www.apsnet.org/publications/apsnetfeatures/Pages/Stachybotrys.aspx>, 2001. **10**.
64. Cunningham, M., et al., *A Pilot Study to Characterise the Biocontaminant Cloud while Decladding "Leaky Buildings"*. BRANZ Ltd, Judgeford, New Zealand, 2013(Study Report SR 296).
65. Ltd, B. *Remediation details: mould*. 2016 31/10/2016 [cited 2018 20/04/2018]; Available from: <https://www.weathertight.org.nz/fixing-leaky-buildings/remediation-detailing-solutions/remediation-details-mould/#h3-1>.
66. Jarvis, B.B., et al., *Trichothecenes produced by Stachybotrys atra from Eastern Europe*. Appl Environ Microbiol, 1986. **51**(5): p. 915-8.
67. Jarvis, B.B., et al., *Study of toxin production by isolates of Stachybotrys chartarum and Memnoniella echinata isolated during a study of pulmonary hemosiderosis in infants*. Appl Environ Microbiol, 1998. **64**(10): p. 3620-5.
68. Sulyok, M., *Methods of Stachybotrys chartarum culture for the generation of satratoxins*. 2016, Personal Communication.

69. Service, U.A.R. *Controlling Kudzu With Naturally Occurring Fungus*. 2009 [cited 2018 April 05, 2018]; Available from: [www.sciencedaily.com/releases/2009/07/090719185107.htm](http://www.sciencedaily.com/releases/2009/07/090719185107.htm).
70. Wu, B., et al., *Spirocyclic drimanes from the marine fungus Stachybotrys sp. strain MF347*. Mar Drugs, 2014. **12**(4): p. 1924-38.
71. Deng, W.P., et al., *Total synthesis and structure revision of stachybotrys spiro lactams*. J Org Chem, 2003. **68**(19): p. 7422-7.
72. Islam, Z., J.R. Harkema, and J.J. Pestka, *Satratoxin G from the black mold Stachybotrys chartarum evokes olfactory sensory neuron loss and inflammation in the murine nose and brain*. Environ Health Perspect, 2006. **114**(7): p. 1099-107.
73. Jarvis, B.B., *Macrocyclic trichothecenes from brazilian Baccharis species: From microanalysis to large-scale isolation*. Phytochemical Analysis, 1992. **3**(6): p. 241-249.
74. Omar, H.E.M., N.M. El Sawi, and A.R.M.A. Meki, *Acute toxicity of the mycotoxin roridin E on liver and kidney of rats*. Journal of Applied Animal Research, 1997. **12**(2): p. 145-152.
75. Haschek, W.M. and K.A. Voss, *Mycotoxins*, in *Haschek and Rousseaux's Handbook of Toxicologic Pathology (third ed.)*. 2013, Academic Press: Boston. p. 1187-1258.
76. Pestka, J.J. and J.H. Forsell, *Inhibition of human lymphocyte transformation by the macrocyclic trichothecenes roridin A and verrucarins A*. Toxicol Lett, 1988. **41**(3): p. 215-22.
77. Jarvis, B.B., et al., *Isolation and Characterization of the Trichoverroids and New Roridins and Verrucarins*. Journal of Organic Chemistry, 1982. **47**(6): p. 1117-1124.
78. Yan, F., et al., *Identification of verrucarins as a potent and selective steroid receptor coactivator-3 small molecule inhibitor*. PLoS One, 2014. **9**(4): p. e95243.
79. Martin, K.J. and P.T. Rygiewicz, *Fungal-specific PCR primers developed for analysis of the ITS region of environmental DNA extracts*. BMC Microbiol, 2005. **5**: p. 28.
80. Ulrich, S., et al., *Identification of Stachybotrys spp. by MALDI-TOF mass spectrometry*. Anal Bioanal Chem, 2016. **408**(27): p. 7565-7581.

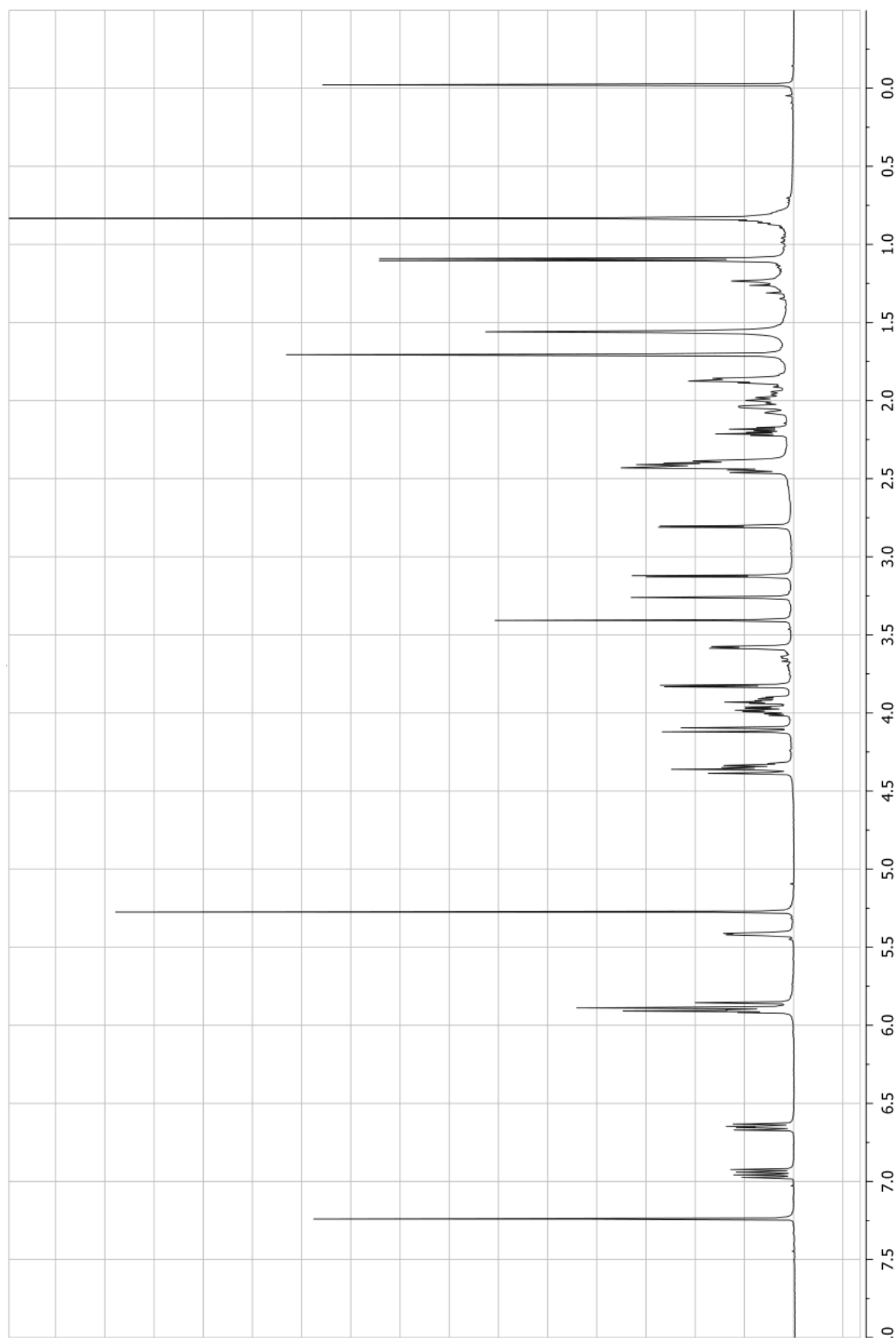


Figure 48 -  $^1\text{H}$  NMR spectrum of satratoxin G (6) in  $\text{CDCl}_3$  (500 MHz).



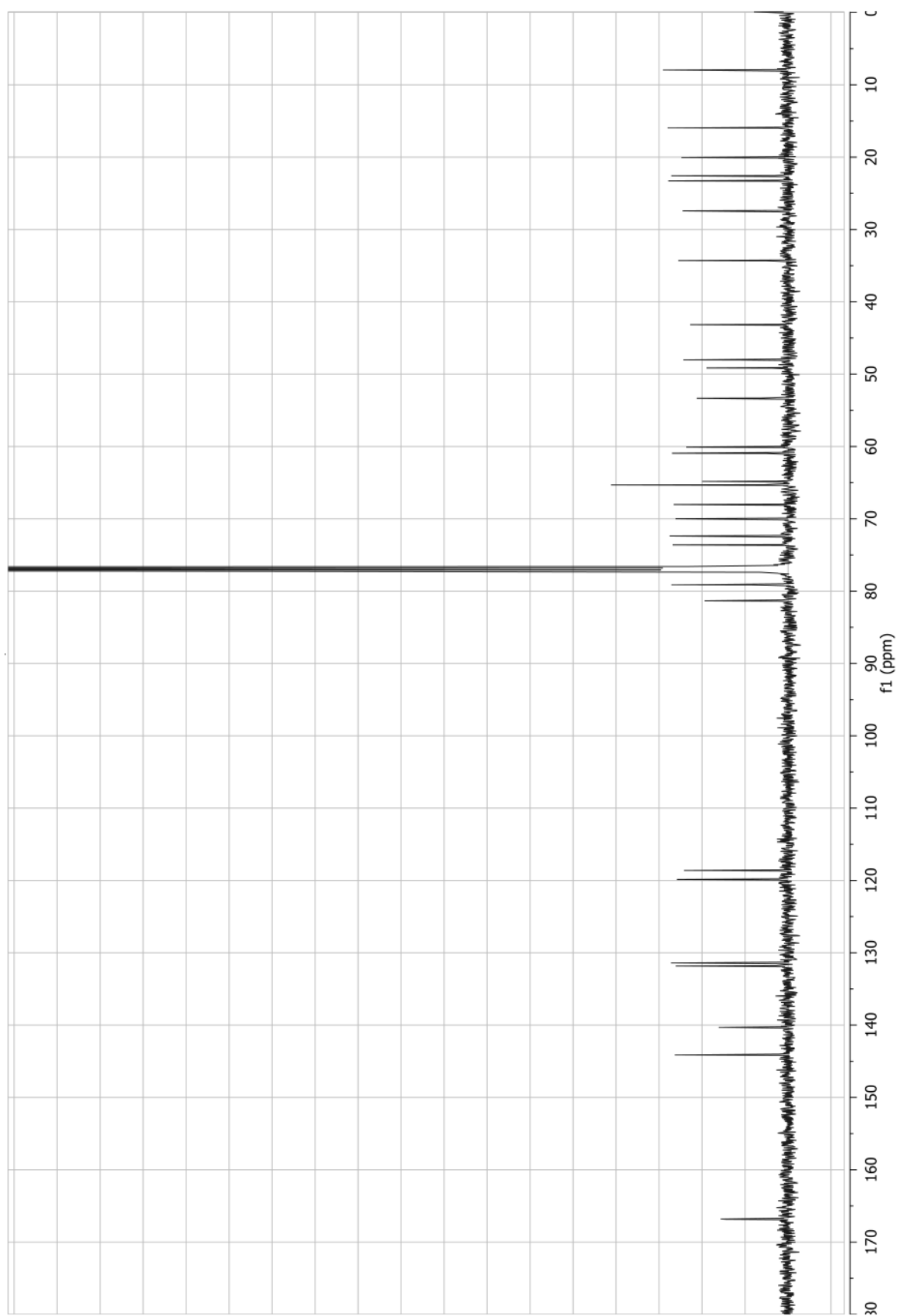


Figure 49 -  $^{13}\text{C}$  NMR spectrum of satratoxin G (6) in  $\text{CDCl}_3$  (125 MHz).

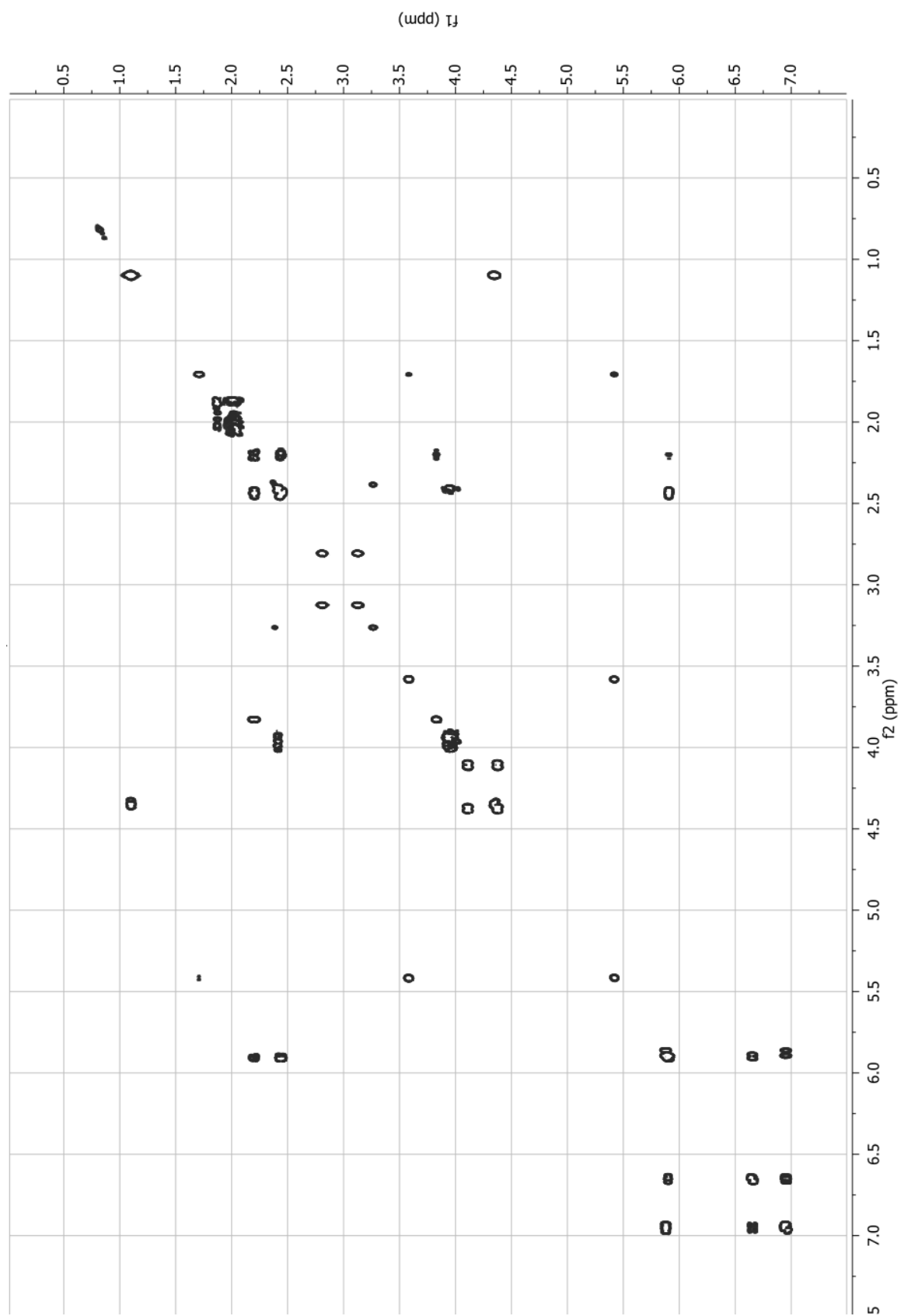


Figure 50 - COSY NMR spectrum of satratoxin G (6) in  $\text{CDCl}_3$ .

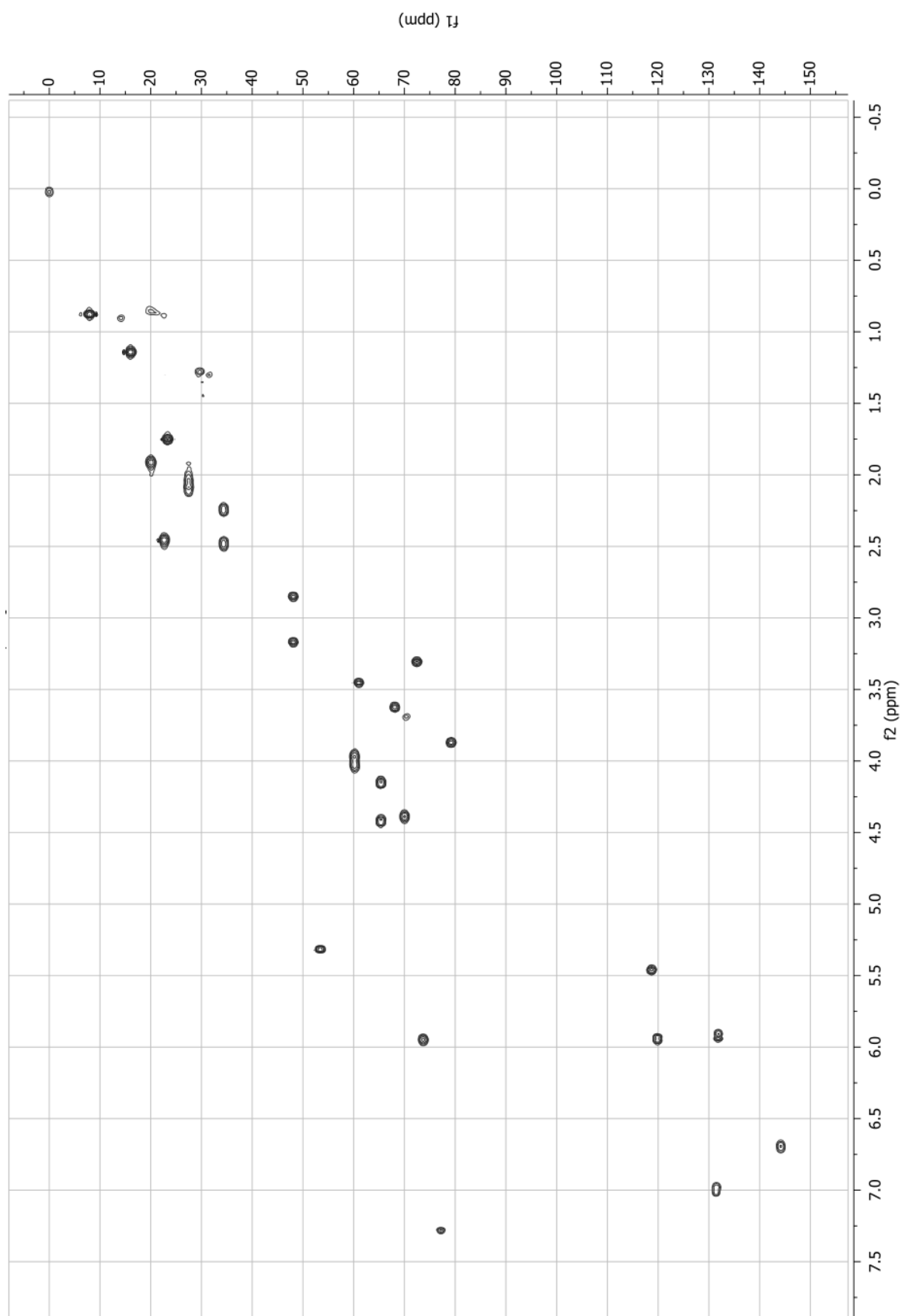


Figure S1 - HSQC NMR spectrum of satratoxin G (6) in CDCl<sub>3</sub>.

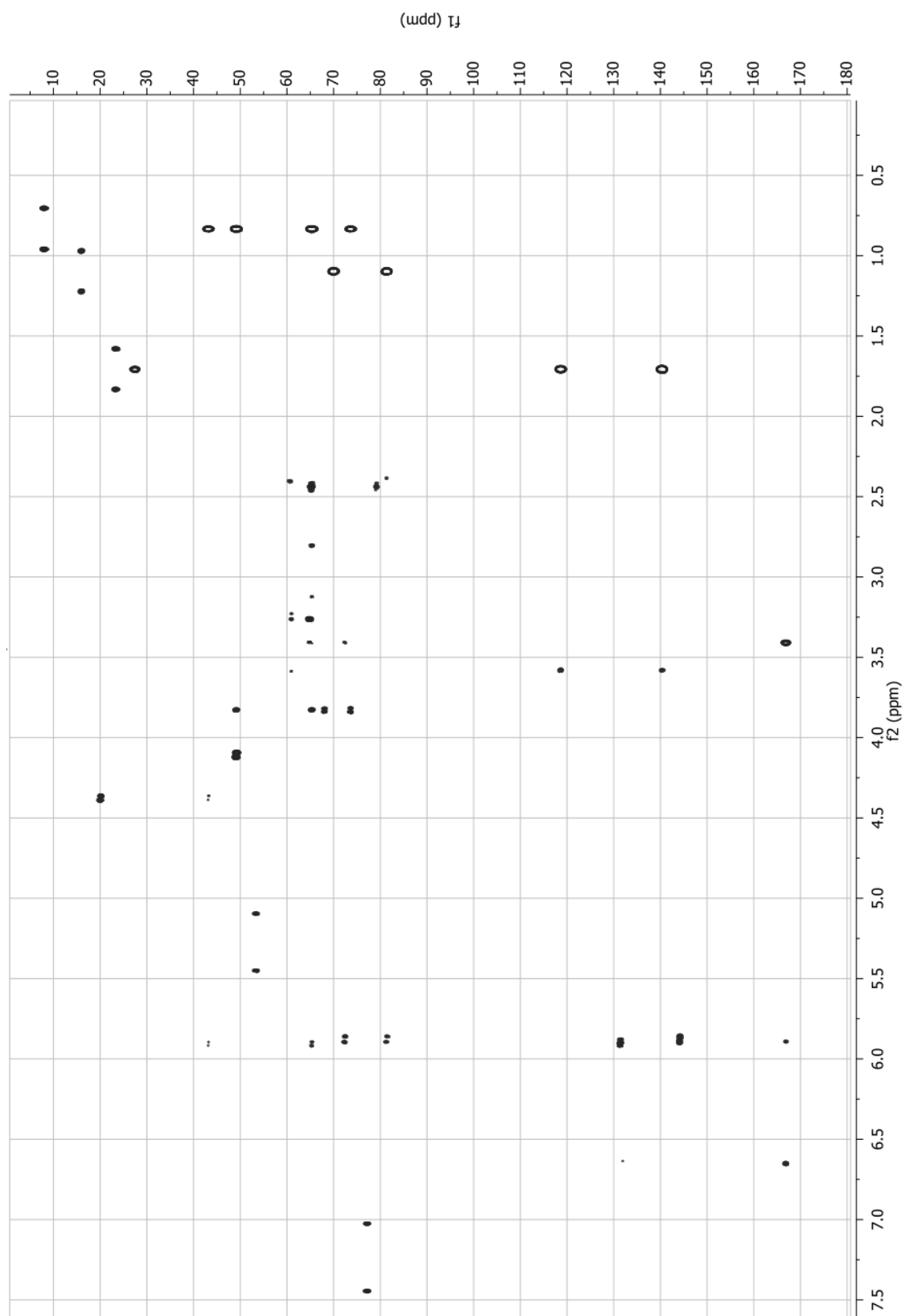
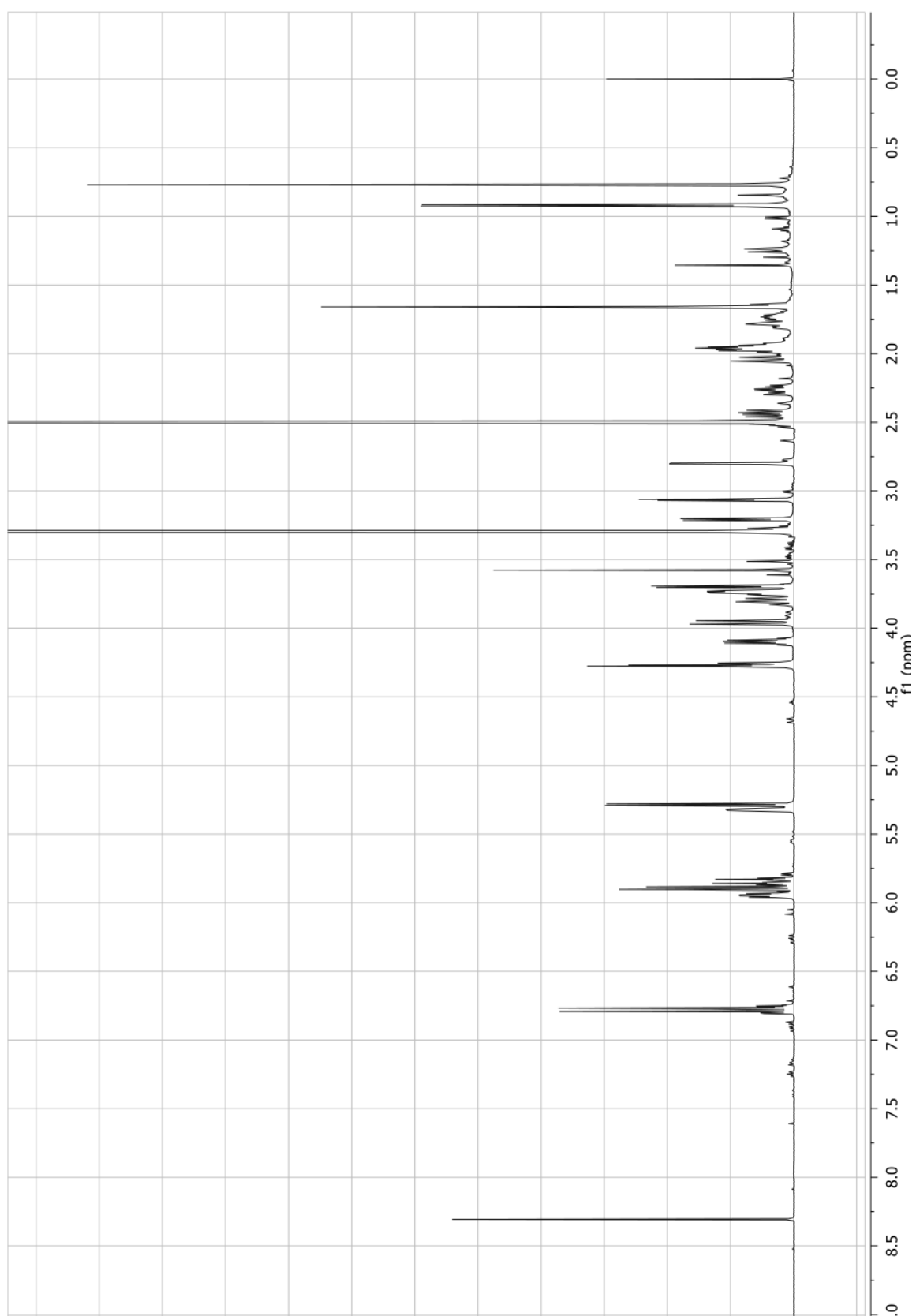


Figure S2 - HMBC NMR spectrum of satratoxin G (**6**) in  $\text{CDCl}_3$ .



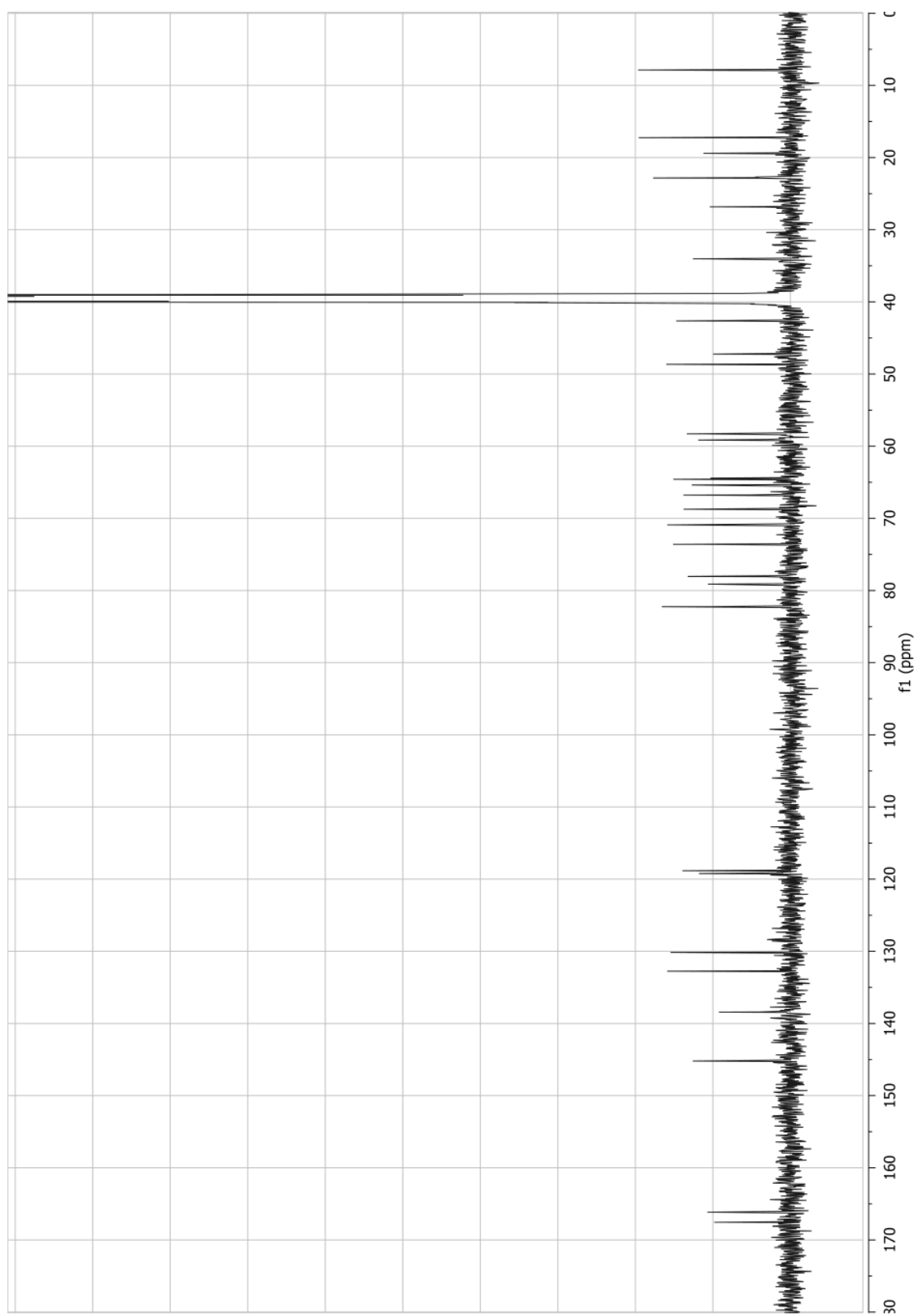


Figure 54 -  $^{13}\text{C}$  NMR spectrum of satratoxin G (6) in  $\text{DMSO-d}_6$  (125 MHz).

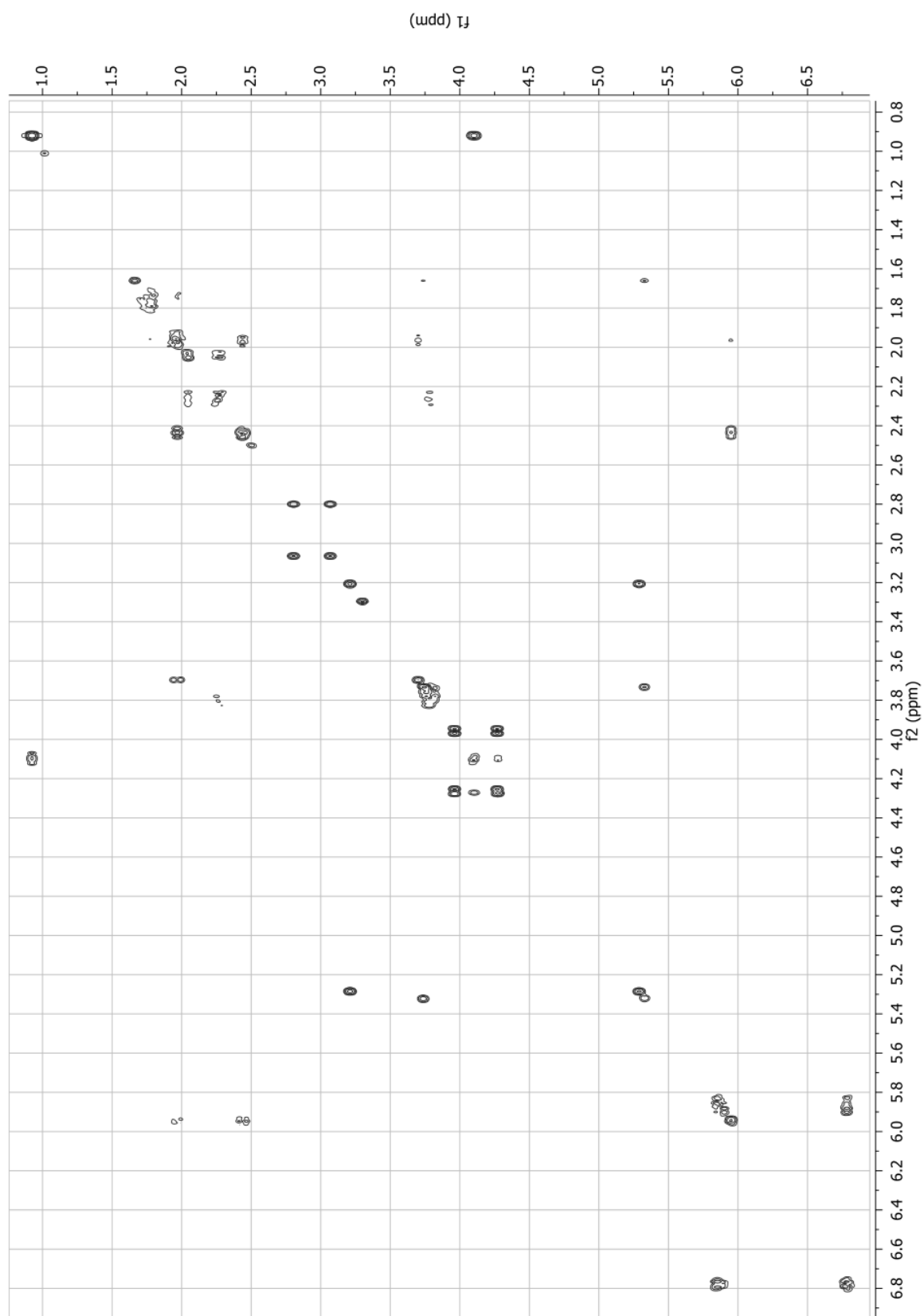


Figure 55 - COSY NMR spectrum of satratoxin G (6) in DMSO- $d_6$ .

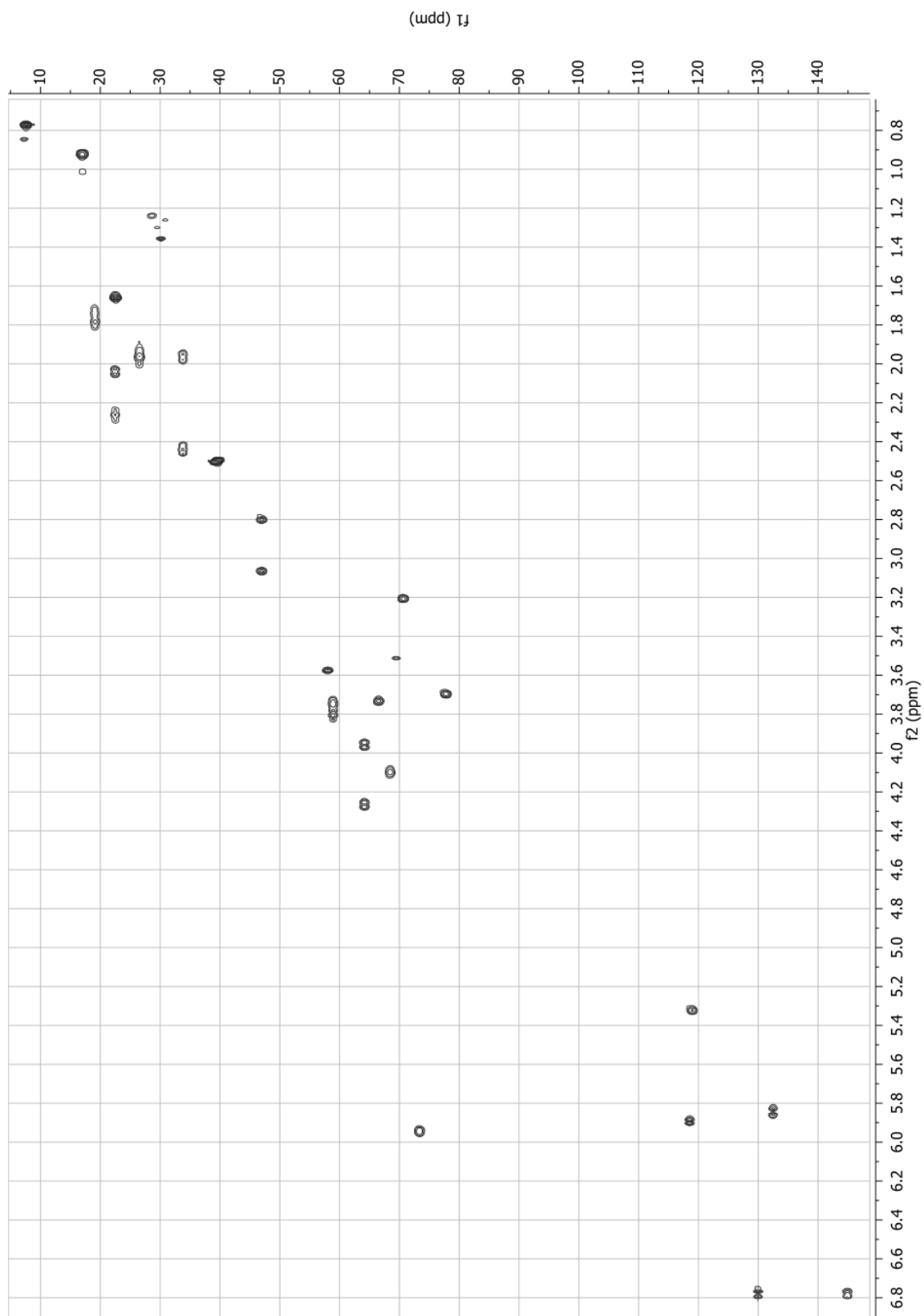


Figure S6 - HSQC NMR spectrum of satratoxin G (6) in DMSO- $d_6$ .



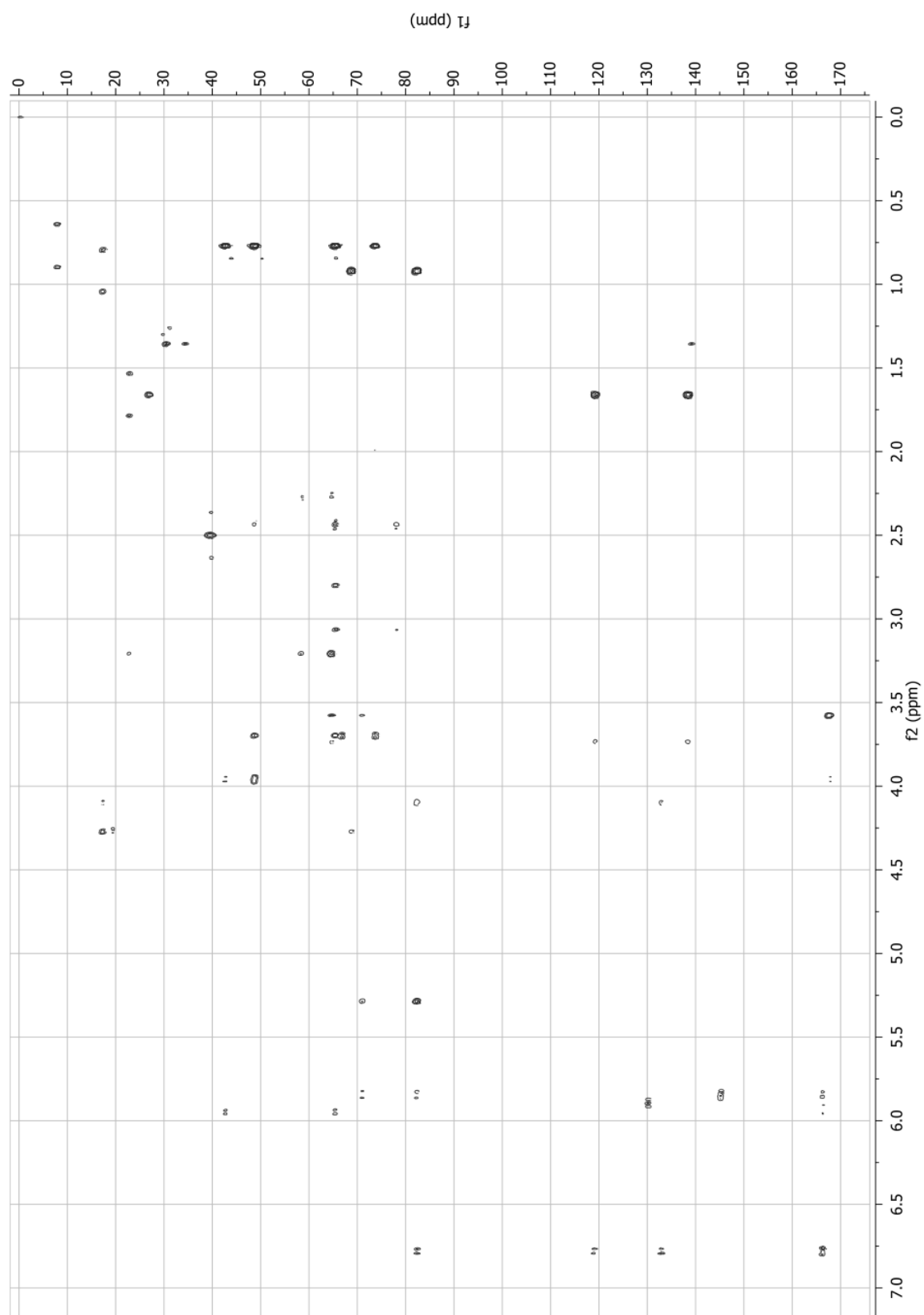


Figure 57 - HMBC NMR spectrum of satratoxin G (**6**) in DMSO- $d_6$ .

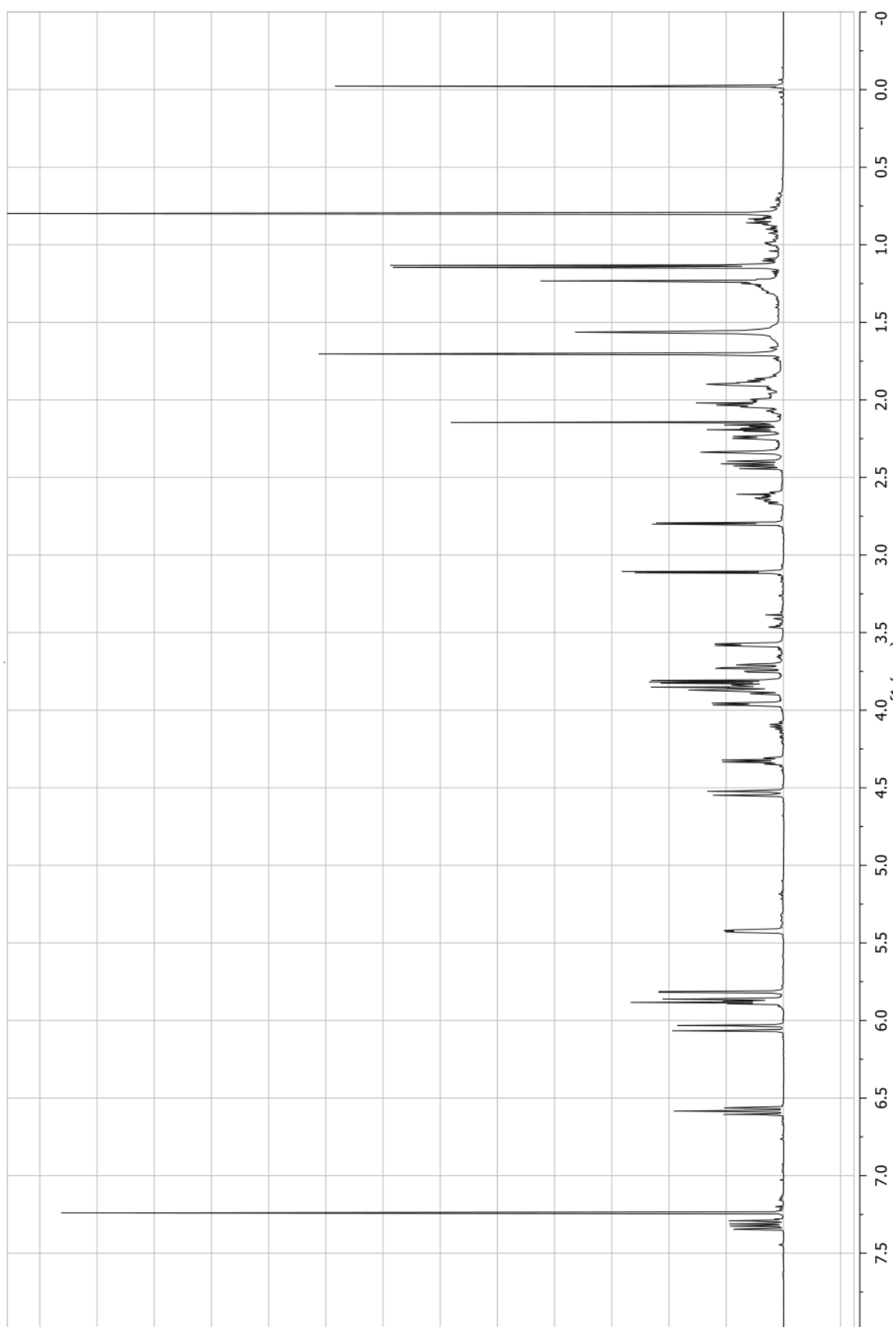


Figure 58 -  $^1\text{H}$  NMR spectrum of satratoxin H (7) in  $\text{CDCl}_3$  (500 MHz).

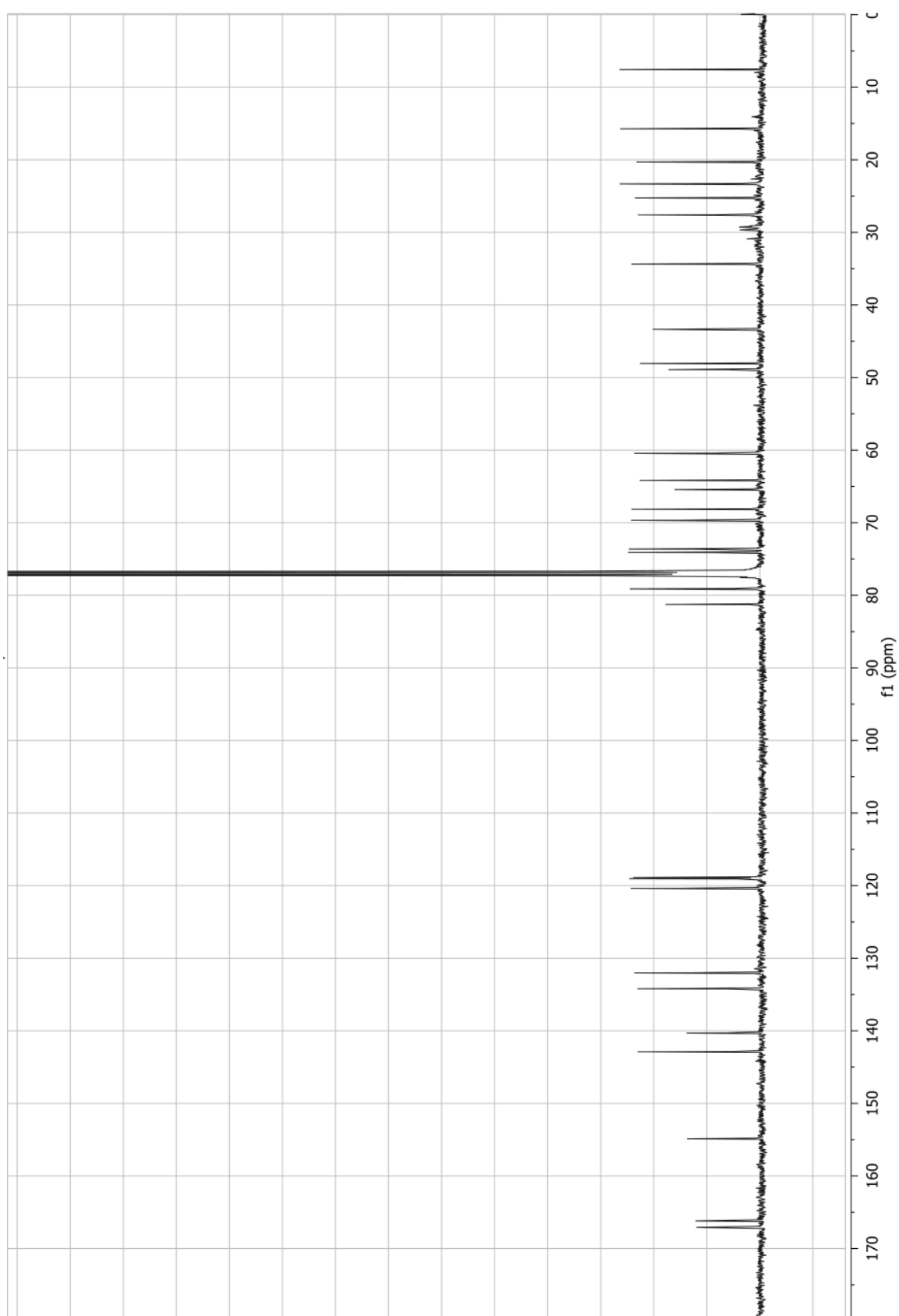


Figure 59 -  $^{13}\text{C}$  NMR spectrum of satratoxin H (7) in  $\text{CDCl}_3$  (125 MHz).



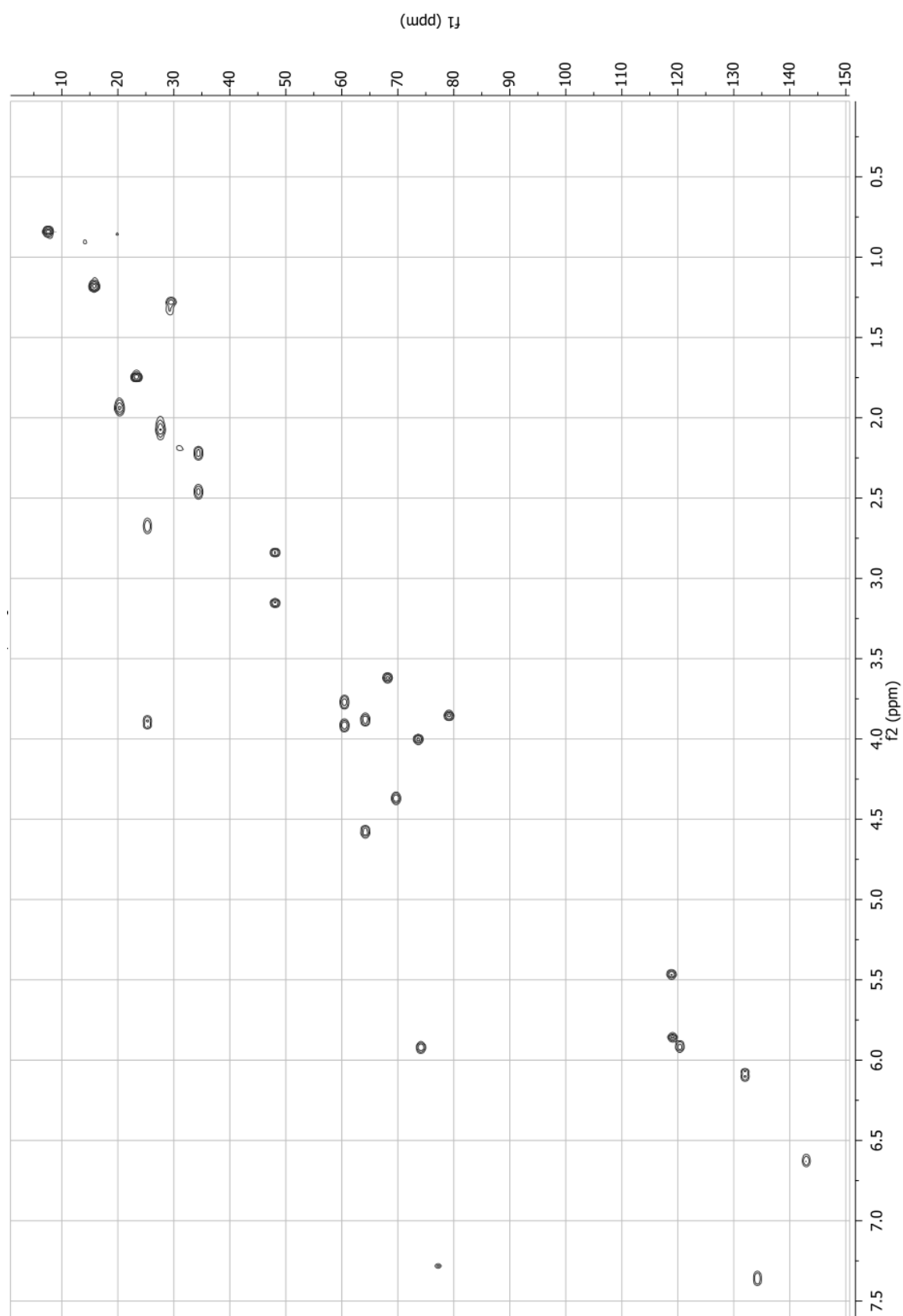


Figure 61 - HSQC NMR spectrum of satratoxin H (7) in  $\text{CDCl}_3$ .

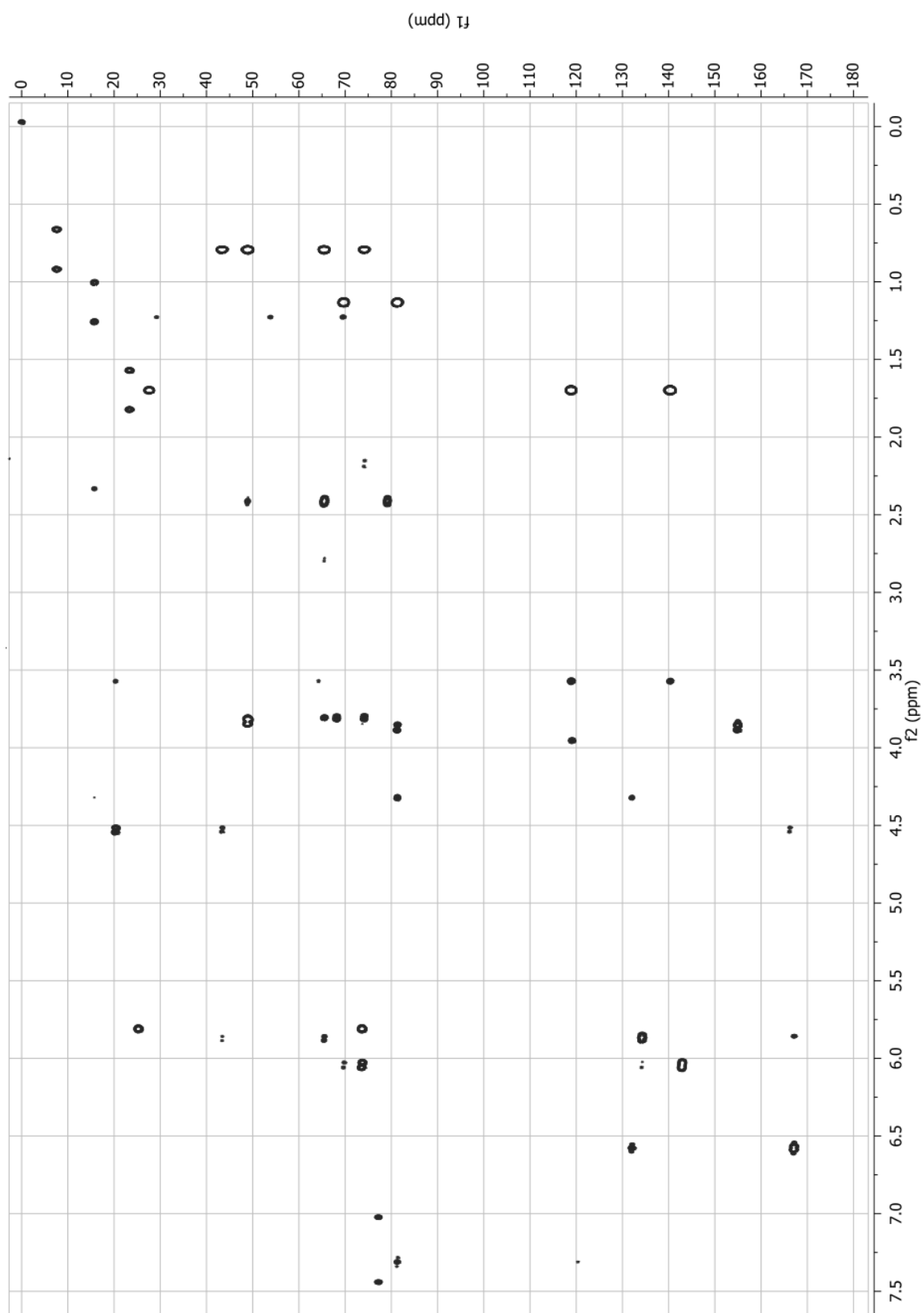


Figure 62 - HMBC NMR spectrum of satratoxin H (7) in  $\text{CDCl}_3$ .

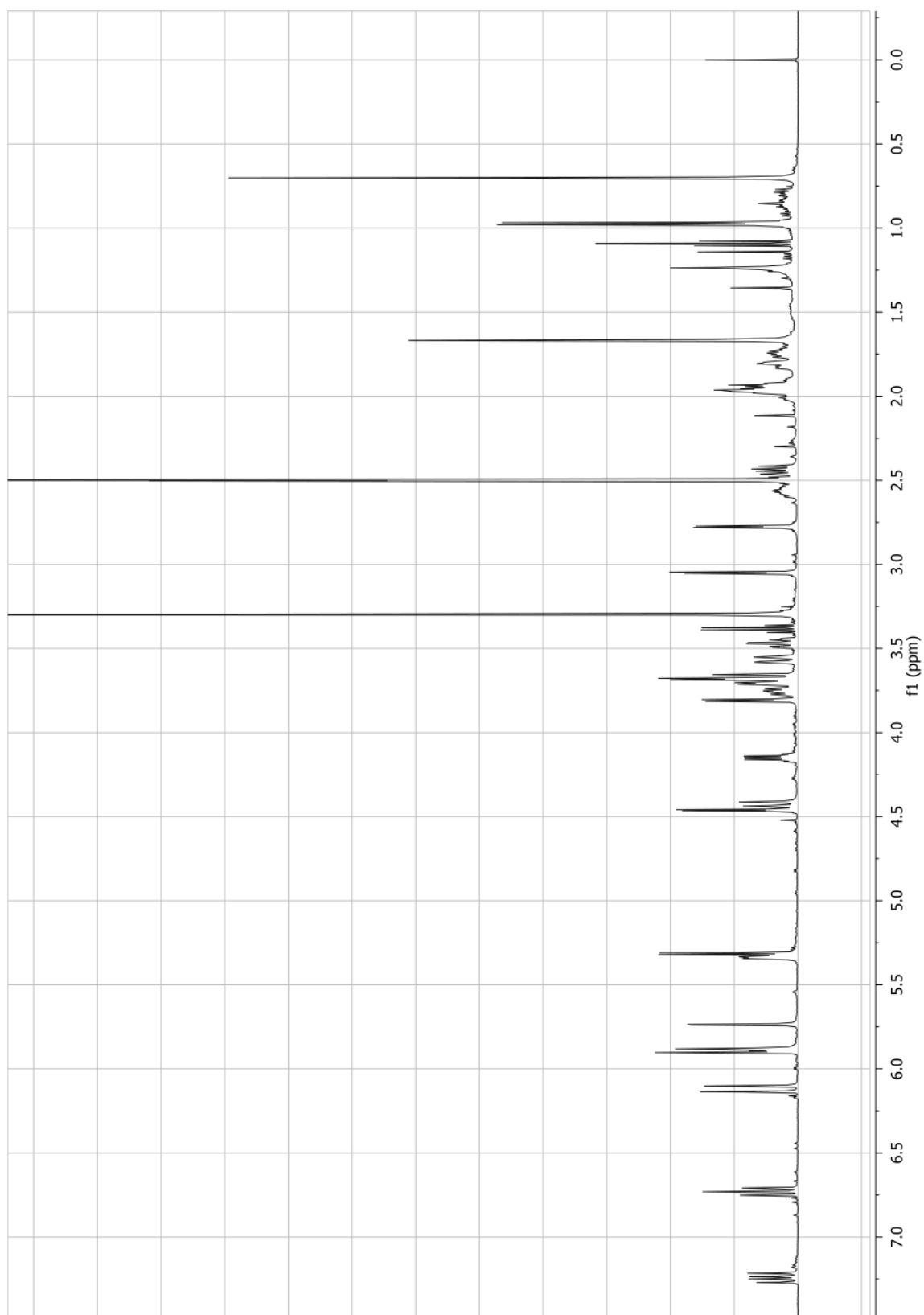


Figure 63 -  $^1\text{H}$  NMR spectrum of satratoxin H (7) in  $\text{DMSO}-d_6$  (500 MHz).

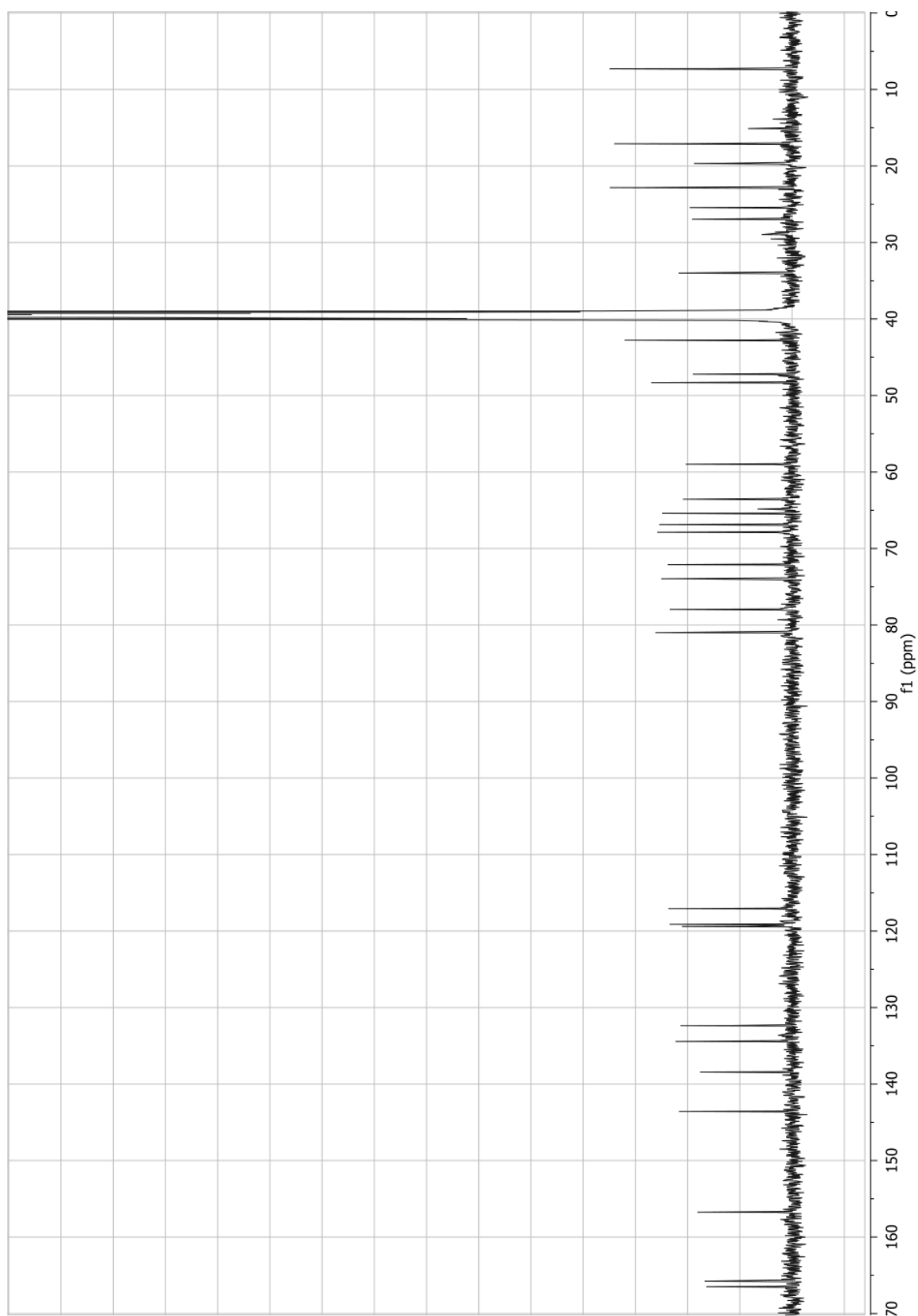


Figure 64 -  $^{13}\text{C}$  NMR spectrum of satratoxin H (7) in  $\text{DMSO-d}_6$  (125 MHz).



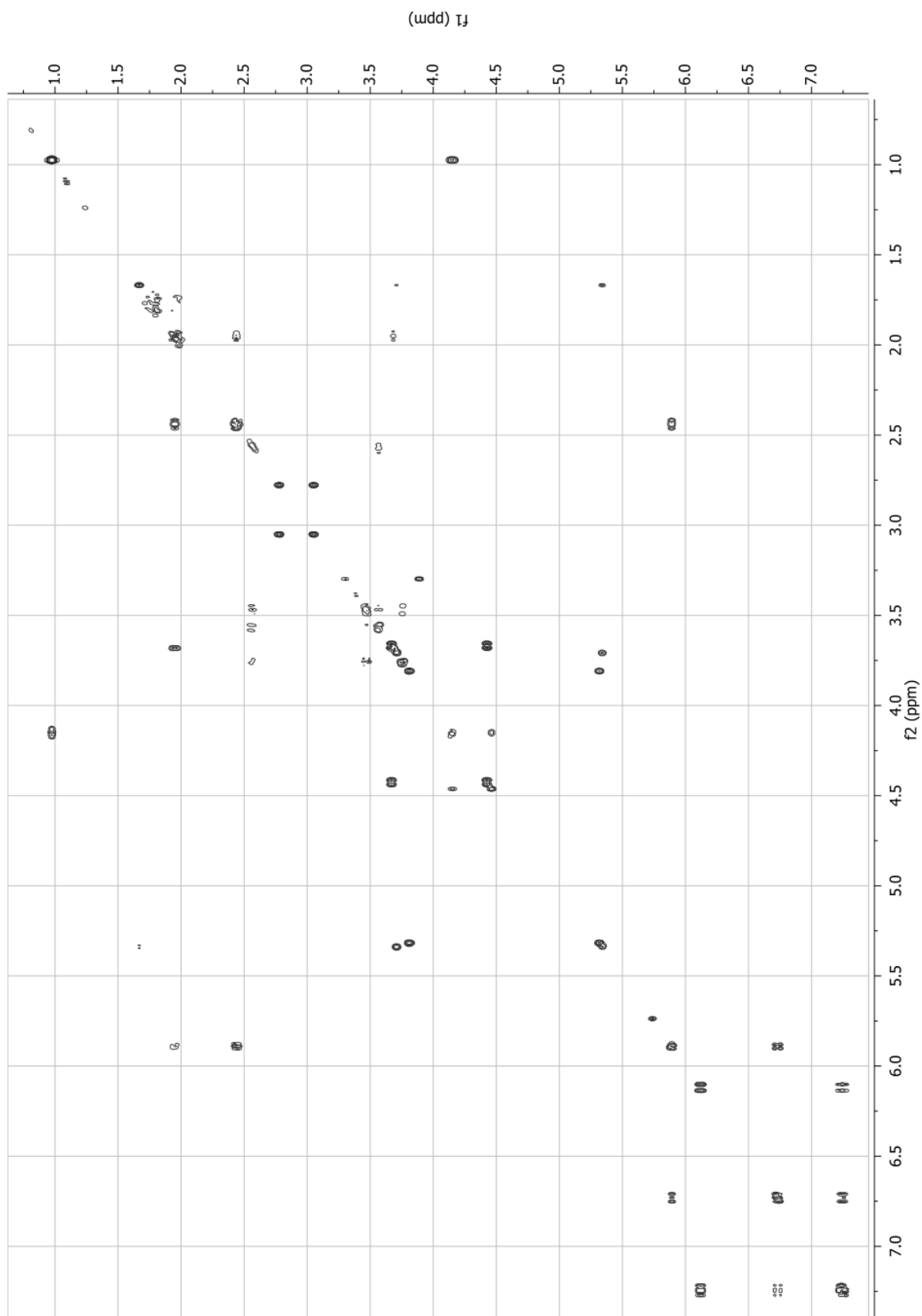


Figure 65 - COSY NMR spectrum of satratoxin H (7) in DMSO- $d_6$ .

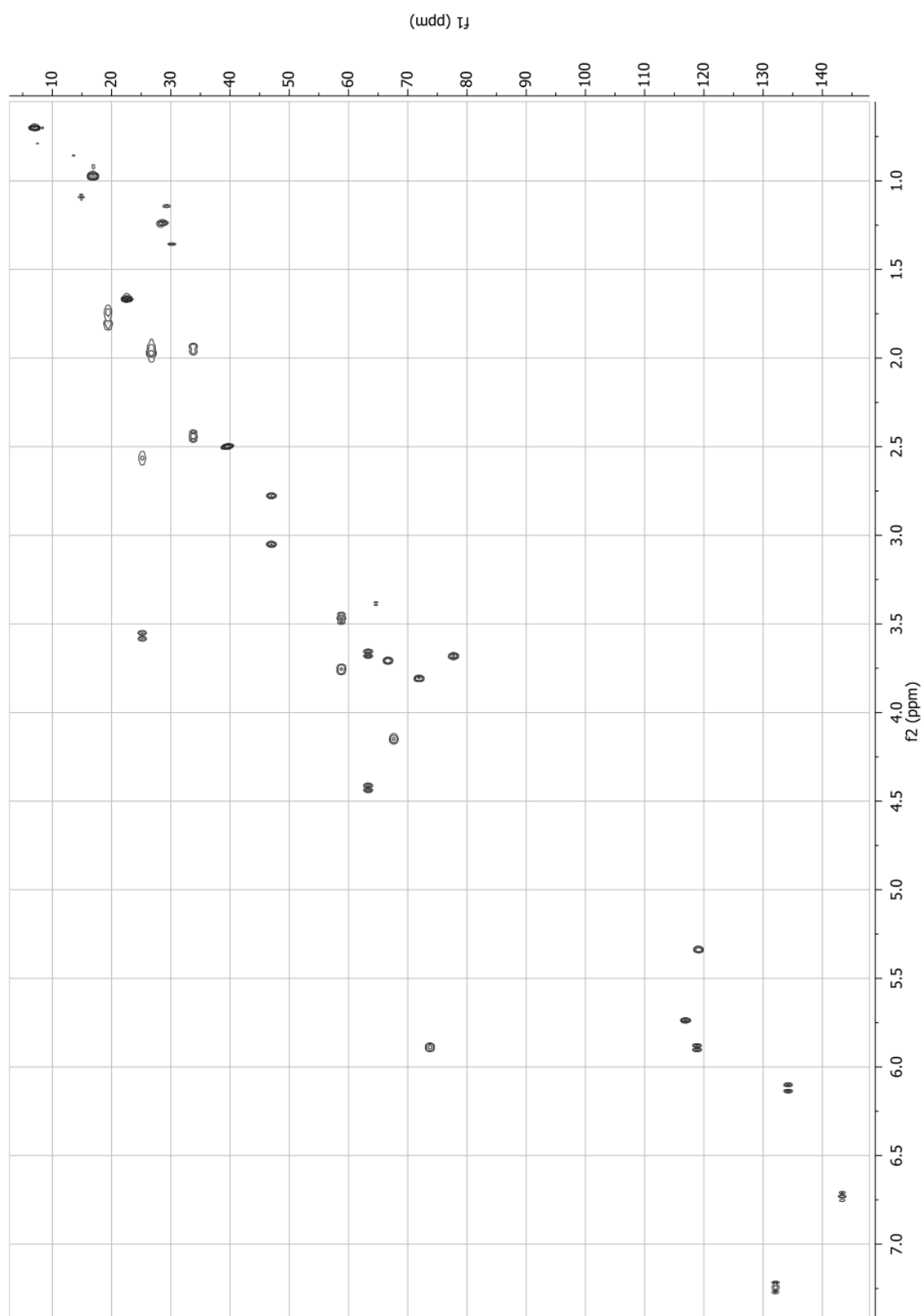


Figure 66 - HSQC NMR spectrum of satratoxin H (7) in DMSO-d<sub>6</sub>.

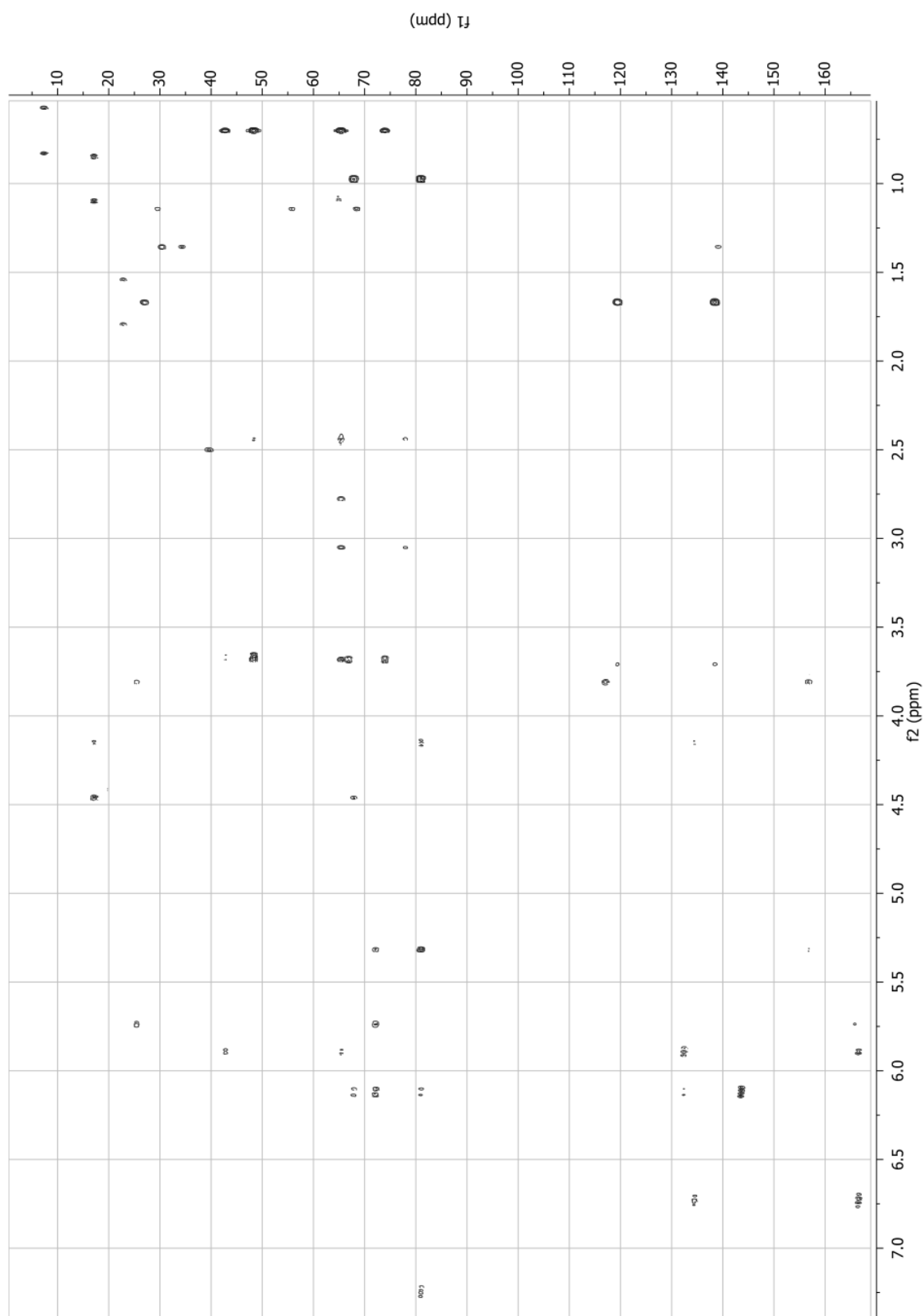


Figure 67 - HMBC NMR spectrum of satratoxin H (7) in DMSO-d<sub>6</sub>.